Regulation of Decidual $CD8^+$ T cells in Preeclampsia

Dissertation
zur Erlangung des Doktorgrades
der Biomedizinischen Wissenschaften
(Dr. rer. physiol.)

der
Fakultät für Medizin
der Universität Regensburg

vorgelegt von
Wenqin Shi

im Jahr
2025

FREISEITE

Regulation of Decidual $CD8^+$ T cells in Preeclampsia

Dissertation
zur Erlangung des Doktorgrades
der Biomedizinischen Wissenschaften
(Dr. rer. physiol.)

der
Fakultät für Medizin
der Universität Regensburg

vorgelegt von
Wenqin Shi

im Jahr
2025

Dekan: Prof. Dr. Dirk Hellwig

Betreuer/in: Prof. Dr. Maria Emilia Solano

Tag der mündlichen Prüfung: 09. 02. 2026

1. Introduction

1.1 Decidua: The Maternal-Fetal Immune Interface During Pregnancy

Pregnancy is a complex physiological process, which begins with the attachment of the blastocyst to the uterine endometrium, initiating the critical process of implantation (1,2). Following implantation, the endometrium undergoes a remarkable transformation into a specialized, immune-rich tissue known as the decidua. This process is called decidualization (3). The decidua serves as the primary site of direct contact between maternal tissues and invading fetal trophoblast cells (4). This region is therefore considered the maternal-fetal interface, a unique immunological environment that is crucial for establishing maternal tolerance to the semi-allogeneic fetus and ensuring a successful pregnancy (5,6). The majority of human pregnancies are singleton pregnancies, which have a single placenta and decidua (Figure 1B). In the case of human twin pregnancies, these could develop either with separate placentas (dichorionic) or a shared placenta (monochorionic).

1.1.1 Human Uterine Physiology and Remodeling

The human uterus is a remarkably dynamic organ, undergoing profound cyclical and developmental transformations. For example, throughout the menstrual cycle, the endometrium cycles through phases of proliferation, secretion, and shedding in response to fluctuating ovarian hormones, primarily estrogens and progesterone (7). This tightly regulated process prepares the uterine environment for potential embryo implantation (7). During pregnancy, the role of the uterus expands dramatically as it accommodates the growing fetus, provides vital nutrients and oxygen, and ultimately facilitates delivery through powerful peristaltic contractions (8). Pregnancy is accompanied by profound changes in uterine tissue, including cellular differentiation and tissue enlargement (9). These features highlight the dynamic nature of the uterus, both in the non-pregnant state and throughout pregnancy.

Anatomically, the uterus is a multi-layered organ engineered for these complex functions, composed of three distinct layers: the inner endometrium, the central myometrium, and the

outer serosa (8). The structural design of these layers facilitates the massive growth required during gestation. As pregnancy progresses, the uterus expands to 500-1,000 times its non-pregnant volume, with a nearly 24-fold increase in weight (10). This enlargement is primarily driven by the hypertrophy and elongation of myometrial smooth muscle cells (10).

1.1.1.1 Human Embryo Implantation and Decidualization

The journey of pregnancy begins with implantation, the process by which the blastocyst attaches to and embeds within the receptive endometrium, typically 6 to 7 days after fertilization (11). This critical event unfolds in three sequential stages: apposition, where the blastocyst makes initial contact; adhesion, where it firmly attaches; and finally, invasion, where embryonic trophoblast cells penetrate the endometrial tissue until the blastocyst is fully embedded (12) (Figure 1).

Following successful implantation, the endometrium undergoes a final, profound transformation known as decidualization. This process involves the extensive remodeling of endometrial stromal cells into highly specialized decidual cells, creating a new layer, the decidua (13). The decidua is functionally divided into three regions: the decidua basalis, which forms the maternal component of the placenta; the decidua capsularis, which covers the growing embryo; and the decidua parietalis, which lines the uterine cavity, not directly involved in implantation (14,15).

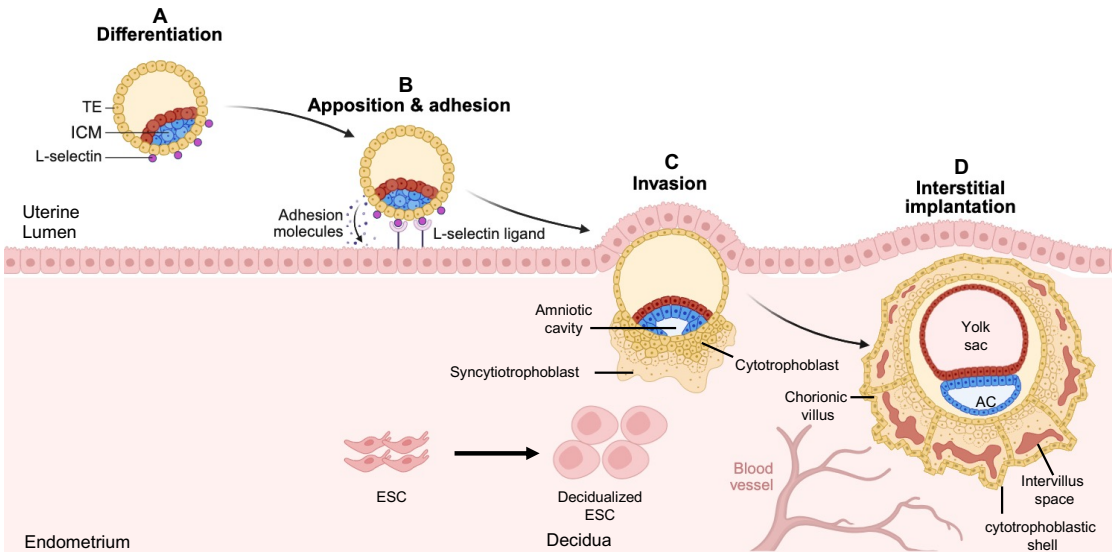

Figure 1. Overview of the Human Embryo Implantation. This figure demonstrates the key cellular events of embryo implantation. Following firm attachment to the uterine epithelium, embryonic trophectoderm cells fuse to form the invasive, multinucleated syncytiotrophoblast (STB), which embeds the blastocyst into the maternal decidua. Proliferative cytotrophoblasts (CTB) underlying the STB form columns, creating primary villi. These columns then expand and fuse laterally to establish the cytotrophoblast shell, which anchors the conceptus. TE: trophectoderm, ICM: inner cell mass, ESC: endometrium stroma cell. The figure was created with Biorender.

1.1.2 Development of the Placenta

The placenta is a unique, transient organ, primarily of fetal origin. Its proper formation requires an interaction between embryonic trophoblast lineages and the maternal endometrium, including its extensive vascular system (16). Once established, the placenta performs a suite of functions essential for a successful pregnancy. It engineers the fetoplacental circulation, which serves as the foundation for nutrient, gas, and waste exchange between mother and fetus (17). Beyond this vital transport role, the placenta acts as a major endocrine organ, producing a variety of hormones, enzymes, and cytokines that maintain the gravid state (17,18). Furthermore, it forms a crucial protective barrier, selectively regulating the passage of substances to shield the developing fetus from harm (19).

1.1.2.1 The Process of Human Placenta Development

In humans, the foundation for the placenta starts around day 5 to 6 post-fertilization (20,21). As the blastocyst makes stable contact with the uterine epithelium, the trophectoderm cells begin to merge, forming a multinucleated, highly invasive structure known as the primary syncytium, or syncytiotrophoblast (22,23). This syncytium acts as the engine of invasion, penetrating the uterine epithelium and embedding the embryo into the endometrium, which transfers into the decidua (24). By day 14, the blastocyst is fully implanted (25).

Unlike the syncytium, the cytotrophoblast cells beneath it remain in an individual, non-merged state. Around day 12 post-fertilization, these cells begin to form column-like structures that extend into the syncytiotrophoblast. Within a short time, they reach the tops of the trabeculae, break through the syncytiotrophoblast, and spread laterally, merging with neighboring cells (26). Eventually, a continuous cytotrophoblast shell forms between the villi and the decidua,

enclosing the embryonic structure. At the same time, the primary villi consisting of a core of cytotrophoblast cells surrounded by an outer layer of syncytiotrophoblast also formed (27).

The final stage of placental construction involves the maturation and vascularization of the villi. Around day 17 post-fertilization, extraembryonic mesenchymal cells invade the core of the primary villi, transforming them into secondary villi. By day 18, fetal capillaries differentiate within this mesenchymal core, marking the development of tertiary villi and the establishment of the fetal vascular network (27,28). In parallel, a distinct population of cytotrophoblast cells, the extravillous trophoblasts (EVT), detaches from the anchoring shell and invades deeply into the decidua and the maternal spiral arteries. By the end of the first trimester, this complex interplay of cellular invasion, proliferation, and differentiation results in a fully formed and functional placenta (Figure 2).

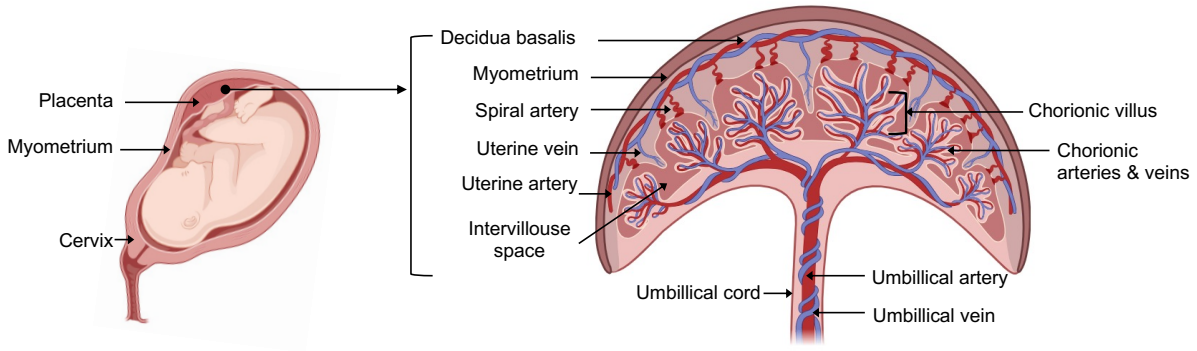

Figure 2. Overview of the Human Placenta. The figure demonstrates the details of a human placenta, including the maternal part and fetal part. Maternal part: decidua, spiral artery, uterine artery and vein, and intervillous space. Fetal parts: chorionic villus, chorionic artery and vein, umbilical cord, umbilical artery and vein. The figure was created with Biorender.

1.1.3 Spiral Artery Remodeling

In humans, the establishment of a functional uteroplacental circulation is fundamental for maternal-fetal exchange and a critical factor for a successful pregnancy. Uterine spiral arteries, which originate from the uterine arteries, supply blood to the placental intervillous space and maintain adequate uteroplacental perfusion throughout pregnancy, providing essential nutrients and oxygen to the fetus (29–31).

As pregnancy progresses, blood flow to the uterus and placenta increases dramatically. This dynamic rise in perfusion provides a robust foundation for meeting the metabolic demands of the growing fetus and is essential for normal placental function (29). This hemodynamic shift is achieved through the process of uterine spiral artery remodeling, which involves the invasion of EVTs into the arterial wall. EVT invasion is preceded by initial vascular changes in the decidua, such as endothelial vacuolization and edema of vascular smooth muscle cells (VSMCs). Following these modifications, invading trophoblasts infiltrate and progressively replace the native VSMCs and endothelial cells, ultimately transforming the uterine spiral arteries into high-capacitance, low-resistance vessels (32,33). This profound structural alteration ensures a continuous and stable high-volume supply of oxygenated blood to the placenta throughout pregnancy. However, the defective uterine spiral artery remodeling can lead to pregnancy complications, such as preeclampsia and fetal growth restriction (34). In humans, EVTs deeply invade into the inner third of the myometrium (35).

1.2 Preeclampsia

Preeclampsia is a pregnancy-related disorder that affects multiple organs, characterized by high blood pressure, deregulation in angiogenic factors, and impaired placental angiogenesis (36). Affecting 2-10% of pregnancies worldwide, preeclampsia is a leading cause of perinatal morbidity and mortality and significantly increases the long-term risk of cardiovascular disease for both mother and child (37–39).

1.2.1 Diagnosis

According to “Hypertensive Disorders in Pregnancy: Diagnostics and Therapy,” published by the German, Austrian, and Swiss Societies for Gynecology and Obstetrics in 2024 (40), preeclampsia is diagnosed as gestational or chronic hypertension with the involvement of at least one organ dysfunction that arises during pregnancy and without any pre-existing condition. The organs typically affected include the placenta (manifesting as fetal growth restriction), kidneys, liver, lungs, central nervous system, and hematologic system. This guideline is used as a diagnostic criterion in our study.

Further, preeclampsia can be classified into two major subtypes based on the gestational age at diagnosis (41). Late-onset preeclampsia (LOPE), diagnosed at or after 34 weeks of gestation, is the predominant form, accounting for approximately 80-95% of cases globally (42). In contrast, early-onset preeclampsia (EOPE), diagnosed before 34 weeks, is less common but is associated with more severe placental dysfunction and significantly higher rates of maternal and neonatal morbidity and mortality (41).

1.2.2 Pathophysiology of Preeclampsia

1.2.2.1 The Classical Two-Stage Model

The cause of preeclampsia remains unclear, but a foundational concept emerged as early as 1967 when Robertson and Brosens linked preeclampsia to poor placentation, characterized by defective remodeling of the uteroplacental spiral arteries (43). This concept was included in the classical "two-stage model" of preeclampsia (44). In this framework, Stage 1 is defective placentation, which leads to Stage 2, the subsequent maternal clinical syndrome. A central concept of this model was that poor placentation was a common pathogenic mechanism for all forms of preeclampsia.

However, this assumption has been challenged. The observation that most cases of late-onset preeclampsia are not associated with fetal growth restriction is inconsistent with severe placental insufficiency. Therefore, the classical two-stage model is now primarily considered linked to early-onset preeclampsia, while evidence for this mechanism is lacking in late-onset preeclampsia (34,45,46).

1.2.2.2 A Revised Model: Different Placental Origins for One Maternal Syndrome

In 2019, building upon the concept of poor placentation, Staff et al. proposed that several etiologies involving distinct mechanisms may ultimately converge on the same maternal syndrome and manifest preeclampsia (45). The first etiology remains the classical defective

placentation pathway, typically leading to early-onset preeclampsia. The second, newly proposed etiology, suggests uteroplacental malperfusion occurring in late pregnancy, without evidence of impaired placentation. It arises when the placenta outgrows the capacity of the uterus, leading to compression of the terminal villi and subsequent impairment of intervillous perfusion. This results in syncytiotrophoblast hypoxia and stress, which leads to the aberrant release of pro-inflammatory cytokines, reactive oxygen species, extracellular vesicles, and soluble FLT1 (sFLT1) into the maternal circulation (34,47,48). The accumulation of these factors contributes to widespread maternal endothelial dysfunction, initiating the second stage of the disorder, which is characterized by impaired vasodilation, systemic inflammation, and a prothrombotic state (39). Although the timing and underlying causes of this pathway differ from defective spiral artery remodeling, they both result in comparable maternal responses, such as hypertension and organ damage. A third etiology is proposed to account for cases not explained by the first two, such as placental aging or senescence (49). The revised two-stage model of preeclampsia thus explains why fetal growth restriction (FGR) is more commonly associated with early-onset than late-onset preeclampsia.

1.2.2.3 sFLT1 in The Pathophysiology and Clinical Assessment of Preeclampsia

The pathophysiology of preeclampsia is centrally driven by an imbalance in circulating angiogenic factors (50). Vascular endothelial growth factor (VEGF) family members, which include VEGF-A, VEGF-B, VEGF-C, VEGF-D, and placental growth factor (PlGF), play a key role in angiogenesis. These ligands exert their biological functions by binding to three tyrosine kinase receptors: VEGFR1, VEGFR2, and VEGFR3. Among them, VEGF-A, VEGF-B, and PlGF are known to bind to VEGFR1 (51). VEGFR1 signals through the phosphorylation of key intracellular tyrosine residues that recruit downstream effectors. Notably, phosphorylated tyrosine 794 binds PLCγ1 to activate endothelial nitric oxide synthase (eNOS) and promote tubular formation, while phosphorylated tyrosines 1169 and 1213 could drive cell survival and proliferation (52).

sFLT1, a soluble isoform of VEGFR1 found in the circulation, acts as a decoy receptor by competitively binding with VEGF-A, VEGF-B, and PlGF. Because it lacks the intracellular

domain required for signal transduction, this inhibition ultimately exacerbates angiogenic dysfunction and vasoconstriction (53), impairs vascular remodeling (54), and reduces vascular permeability (55,56) (Figure 3).

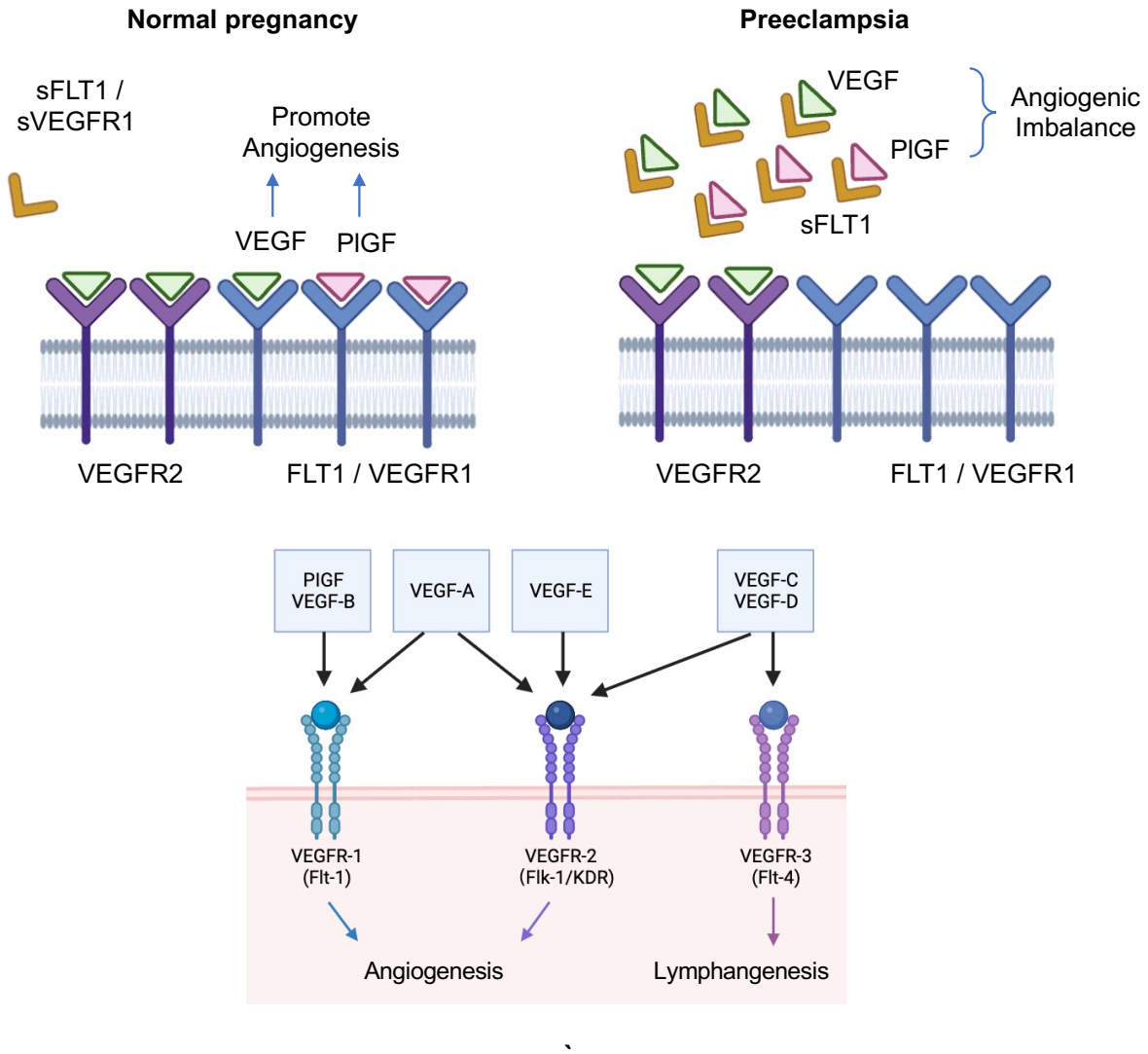

Figure 3. The Anti-Angiogenic State in Preeclampsia Mediated by Excess sFLT1. Schematic illustrating the mechanism by which excess sFLT1 disrupts physiological angiogenic signaling in preeclampsia and the mechanism of growth factors and receptors within the VEGF family. The figure was created with Biorender.

1.2.2.3.1 The sFlt1/PlGF Ratio as a Clinical Biomarker

Numerous large-scale clinical trials have validated the serum sFlt1/PlGF ratio as a powerful tool for the short-term prediction of preeclampsia in women with suspected disease. Studies

by Zeisler et al. have validated the clinical utility of the sFlt1/PlGF ratio in preeclampsia prediction. A ratio of ≤38 is highly effective for ruling out the condition, with a negative predictive value of 99.3% for one week and 94.3% for up to four weeks. Conversely, a ratio of >38 helps predict the onset of preeclampsia within four weeks, offering a positive predictive value of 36.7% and demonstrating superiority over standard clinical variables (57,58).

Women with an sFlt1/PlGF ratio over 85 in cases of early-onset preeclampsia or over 110 in late-onset preeclampsia are recommended to undergo individualized monitoring or inpatient management (59). Nonetheless, Costa et al. suggested that the sFlt1/PlGF ratio should be used only as a predictor for preeclampsia between 20 and 36 weeks of gestation (60), aiming for early detection, timely intervention, and proactive monitoring. However, its clinical utility extends beyond this predictive window into after 36 weeks. In this context, it may help with the differential diagnosis of different types of hypertension(61,62), assessing disease severity and short-term prognosis (63,64), and informing clinical decision-making regarding the optimal timing of delivery (63).

1.2.3 Comorbidities and Clinical Risk Factors Associated with Preeclampsia

Preeclampsia is associated with a variety of pre-existing comorbidities. Among the most significant of these, chronic hypertension, pre-gestational and gestational diabetes mellitus, and obesity play crucial roles in elevating the risk of developing the disorder (65). Similarly, chronic kidney disease is a potent risk factor, as impaired renal function is linked to the endothelial dysfunction that often precedes the clinical onset of preeclampsia (66). The comorbidities associated with preeclampsia extend well beyond these, the presence of which may suggest a maternal state less able to adapt to the profound cardiovascular and metabolic demands of pregnancy, thereby increasing susceptibility to the placental and systemic abnormalities.

Currently, the international guidelines from the International Society for the Study of Hypertension in Pregnancy (ISSHP) and the American College of Obstetricians and Gynecologists (ACOG) largely agree on several key high-risk factors, but some differences

exist as well (67,68) (Table 1). The classification of risk factors in the 'Hypertensive Disorders in Pregnancy: Diagnostics and Therapy' guideline (40) used for this study shares significant overlap with those proposed by the ISSHP and ACOG (Table 2).

Table 1. Comparison of the risk factors for preeclampsia from ISSHP and AC

	ISSHP	ACOG
High-risk factors	Previous preeclampsia	Previous preeclampsia
	Chronic renal disease	Chronic renal disease
	Chronic hypertension	Chronic hypertension
	Diabetes mellitus	Diabetes mellitus
	SLE or APS	SLE or APS
	BMI ≥30kg/m^2	/
	Assisted reproductive therapy	/
	/	Multiple pregnancy
Moderate-risk factors	First pregnancy	First pregnancy
	Age ≥40 years	Age ≥40 years
	Multifetal pregnancy	/
	Prior placental abruption	/
	Prior stillbirth	/
	Prior fetal growth restriction	/
	/	BMI≥35kg/m^2
	/	Inter-pregnancy interval>10 years
	/	Family history of preeclampsia

ISSHP, International Society for the Study of Hypertension in Pregnancy. ACOG, American College of Obstetricians and Gynecologists. APS, antiphospholipid syndrome, SLE: systemic lupus erythematosus, BMI: body mass index.

Table 2. Classification of Risk Factors for Preeclampsia as Defined by the 2024 Hypertensive Disorders in Pregnancy: Diagnostics and Therapy Guideline

	Hypertensive Disorders in Pregnancy: Diagnostics and Therapy Guideline
Risk factors	High maternal age
	High maternal BMI
	Ethnicity (Caucasian < African < South Asian)

Positive family history; mother with preeclampsia
Primiparity
Previous pregnancy with preeclampsia
Conception (Assisted reproductive technology, especially cryo-cycle and oocyte donation)
Multiple pregnancy
Chronic hypertension
Diabetes mellitus (Type I / Type II)
SLE
APS
Smoking

1.2.3.1 Overweight and Obesity: A Pre-pregnancy Risk Factor for Pathological Pregnancy Outcomes

BMI is an important indicator for assessing women's nutritional and health status. According to the World Health Organization (WHO), a BMI between 25.0 and 29.9 kg/m² is classified as overweight, while a BMI of 30.0 kg/m² or greater is defined as obesity (69).

Numerous studies have demonstrated that elevated pre-pregnancy BMI is closely associated with adverse pregnancy outcomes, including stillbirth, macrosomia, gestational diabetes mellitus, neonatal mortality, and preterm birth (70–72). Moreover, increasing evidence indicates that higher pre-pregnancy BMI significantly elevates the risk of pre-eclampsia (73).

Endothelial dysfunction, a feature of preeclampsia, is worsened progressively by obesity (74). Obesity can lead to endothelial nitric oxide synthase uncoupling in perivascular adipose tissue, reducing nitric oxide (NO) production from endothelial cells (75). Concurrently, the high levels of free fatty acids characteristic of obesity also synergistically impair this process (76), thereby impairing vasodilation that depends on endothelial function. In addition, chronic systemic inflammation of obesity further contributes to endothelial impairment by decreasing the levels of anti-inflammatory adiponectin and promoting the accumulation of pro-inflammatory mediators (74).

In individuals with overweight and obesity, adipocytes release fibrinogen and plasminogen activator inhibitor-1 (PAI-1), which contribute to increased blood viscosity (77). This is compounded by endothelial dysfunction leading to vasoconstriction and the accumulation of perivascular adipose tissue, causing increased vascular stiffness, which represents a complex vascular pathology driven by a combination of structural and functional changes. Structural alterations, such as vascular smooth muscle cell change and fibrosis, are coupled with functional impairments, which lead to microvascular dysfunction and subsequent end-organ damage (78). Together, these factors elevate peripheral vascular resistance and predispose the individual to hypertension (74,79). The resulting hypertension, in turn, further exacerbates vascular resistance and stiffness, creating a vicious cycle.

Obesity is associated with elevated oxidative stress (80), which in turn exacerbates endothelial injury. The accumulation of oxidized low-density lipoprotein (oxLDL) and excessive production of reactive oxygen species in obesity contribute significantly to increased oxidative stress levels (74). Moreover, the hypercoagulable state associated with obesity (81) and disturbances in lipid metabolism are also key contributors to endothelial dysfunction (82).

Furthermore, overweight and obesity can also induce a series of metabolic disturbances during pregnancy, which can lead to several pathological consequences (83–85). For example, during pregnancy, the reduction in insulin sensitivity is a physiological phenomenon (86), but this is more severe in overweight and obese women (83). A state of physiological hyperlipidemia is also a normal adaptation of maternal metabolism during pregnancy. However, in pregnancies with overweight and obesity, the lipid elevation is often pathologically exacerbated, especially with higher levels of total cholesterol and low-density lipoprotein cholesterol (85). Maternal overweight and obesity drive a persistent state of chronic, low-grade inflammation (87–89). This inflammatory milieu, in turn, promotes the production of ROS (89), which can lead to several adverse pregnancy outcomes (90).

Taken together, chronic systemic inflammation, oxidative stress, and endothelial dysfunction interact in the context of overweight and obesity, forming a complex network of pathophysiological disturbances. These factors are also potential contributors to the development of preeclampsia, suggesting shared mechanistic pathways between overweight/obesity-related metabolic disturbances and preeclampsia (91). This pre-existing pathophysiological network, driven by excess body weight, has been shown to increase the risk of adverse pregnancy outcomes. Furthermore, the impact of maternal overweight and obesity extends throughout the gestational period (84,92) and can even have long-term consequences for the health of the offspring (83).

1.2.4 Gaining Mechanistic Cues of Pregnancy Pathology: Advantages and Limitations of the Murine Model of Human Pregnancy

Due to the high potential risk of performing exploratory and therapeutic interventions in human pregnancy, animal models and particularly the mouse pregnancy model have become an essential tool in reproductive research.

1.2.4.1 Mouse Uterine Physiology and Uterine Remodeling

The mouse uterus provides a powerful model for studying pregnancy, featuring a distinct bipolar anatomy with a mesometrial and an anti-mesometrial side that dictates the spatial and temporal events of implantation. The myometrium is comprised of an outer longitudinal layer, an inner circular layer, and a mesh-like middle layer (93). Given fundamental differences in uterine anatomy, mouse and human pregnancies exhibit different implantation patterns. The mouse uterus allows for multiple, separated implantations along the uterine horns, each forming an independent decidua and placenta (Figure 4, A). In contrast, the majority of human pregnancies are singleton pregnancies, which have a single placenta and decidua (Figure 4, B).

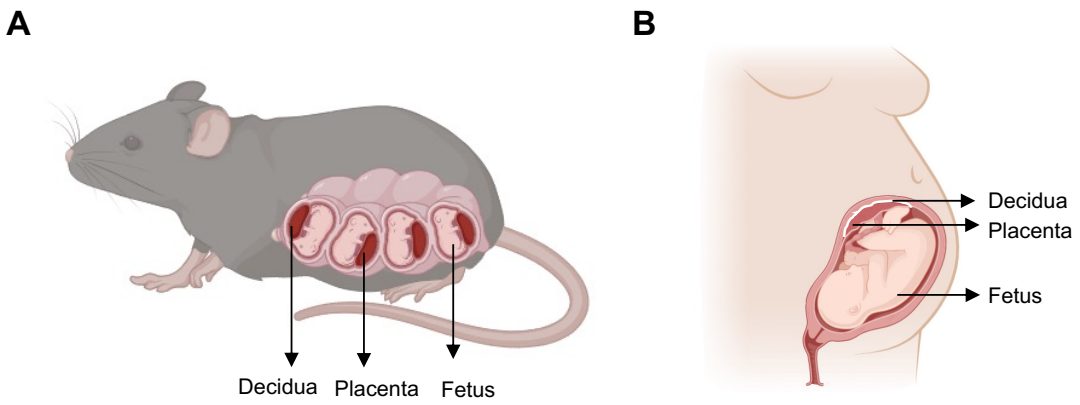

Figure 4. Distinct uterus and implantation patterns in multiparous mouse versus uniparous human pregnancy. A: In mouse pregnancy, a multiparous mouse with multiple implantations, each implantation consists of a fetus, placenta, and fetal membranes. B: Human pregnancy, uniparous with a single implantation, containing one fetus and placenta within the uterine cavity. The figure was created with Biorender.

Both human and mouse present a hemochorial placentation, with embryo-derived trophoblast cells that invade into the maternal uterine tissue, which is a process that is conserved across the two species (94,95). In the mouse, implantation initiates around gestational day (GD) 4.5 and becomes visible by GD 6.5 (96). Following this, embryo implantation expands laterally until it reaches the mesometrial side, where the decidua basalis is established (96). Around GD 8.5, the antimesometrial decidua begins to regress and eventually becomes a thin residual layer, whereas the decidua basalis persists and continues to function (96).

This anatomical specialization also leads to the formation of unique immunological structures. Notably, around GD 8.5, a structure named mesometrial lymphoid aggregate of pregnancy (MLAp) forms between two layers of mouse uterine myometrium, which is with a dense accumulation of uterine Natural Killer (uNK) cells. With the formation of the MLAp, the inner myometrial layer on the mesometrial side gradually disappears. The MLAp and the associated muscular layers on the mesometrial side are collectively referred to as the mesometrium, directly adjacent to the underlying endometrial tissue (97). Decidua, together with MLAp, is the site where the critical processes of immune tolerance and angiogenesis are orchestrated to support a successful pregnancy (98,99).

1.2.4.2 The Process of Mouse Placenta Development

Unlike the single placenta in humans, mouse placental development is a unique two-stage process (100), involving an initial, more primitive placenta that is later replaced by a definitive, mature one. After the embryo fully embeds in the endometrium by GD 6, it is first nourished by the choriovitelline placenta. This temporary structure serves as the primary source of nutrition from approximately GD 6 to GD 10-11 (101,102). Subsequently, the definitive chorioallantoic placenta becomes structurally and functionally mature around GD 11, taking over this vital role for the remainder of the pregnancy (101,103).

The outermost layer of the placenta is the maternal decidua. This compartment primarily consists of decidual cells and maternal immune cells such as uNK, invading trophoblast cells, and the maternal vasculature (15). Adjacent to the decidua lies a thin layer composed of large, invasive, polyploid cells referred to as parietal trophoblast giant cells (P-TGCs) (104). Beneath this layer is the spongiotrophoblast layer, which consists primarily of spongiotrophoblast cells (SpT) and glycogen trophoblast cells (GlyT). Together, the P-TGC and SpT layers constitute the “junctional zone”. The innermost compartment is the labyrinth, where maternal and fetal exchange of nutrients, oxygen, and metabolic waste occurs (105) (Figure 5). In contrast to humans, extravillous trophoblast invasion is much shallower in mice (106), with primarily interstitial invasion, restricted to the mesometrial decidua (107).

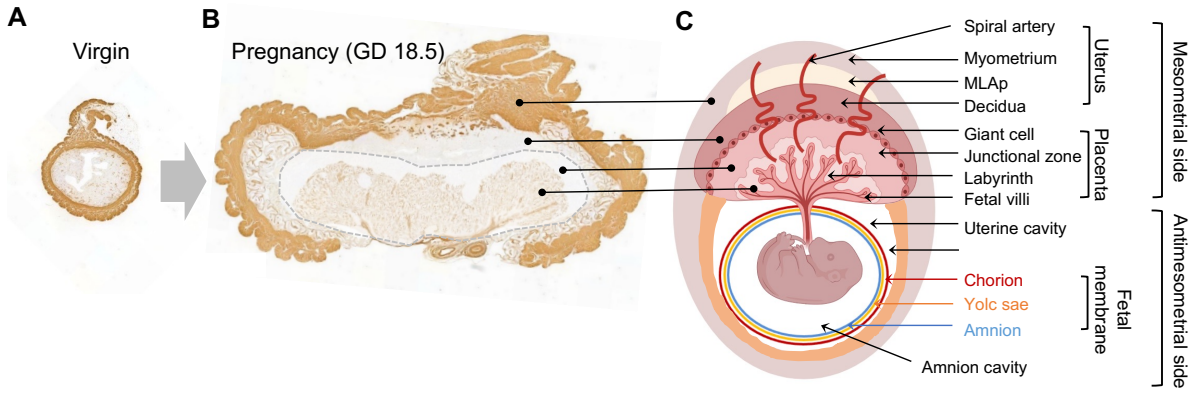

Figure 5. Overview of the Pregnant Mouse Uterus. A and B: The figures demonstrate the dramatic growth of the mouse uterus from the virgin state to GD 18.5. C: A detailed single implantation site is shown, including the mesometrial and anti-mesometrial compartments, the distinct uterine layers, the

placental zones (including the decidua, junctional zone, and labyrinth), and the relative location of the fetus and its fetal membranes. The figure was created with Biorender.

Immunologically, inbred mouse strains lack the genetic variability and, therefore, the maternal-fetal mismatches normally present in human pregnancy. However, selecting different mouse strains allows for the generation of allogeneic mouse models that closely mimic human pregnancy.

Overall, the conserved biology between human and mouse pregnancies, combined with practical advantages such as a short gestation period, large litter sizes, and cost-effectiveness, has solidified the mouse's role in human reproductive research (96,108). However, the short duration of murine gestation remains a key difference from human pregnancy. Therefore, understanding the developmental equivalence between mice and humans, as well as the translational relevance of murine models, is important (Figure 6).

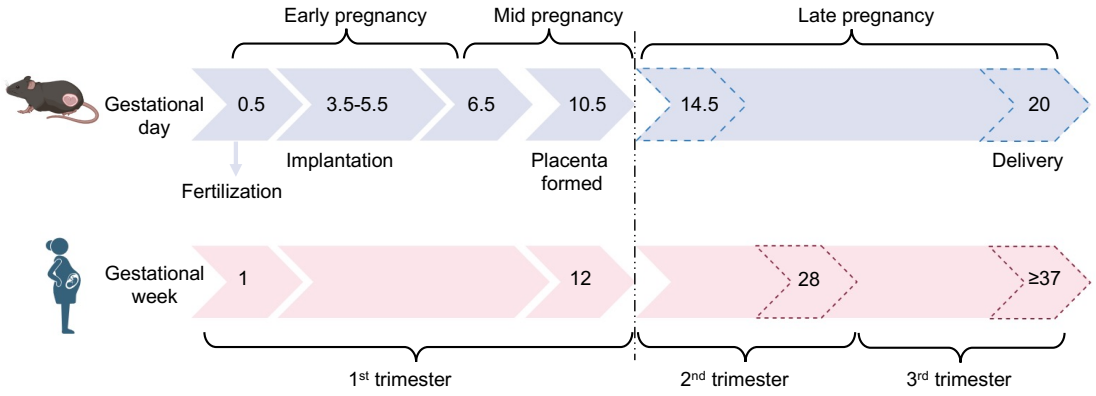

Figure 6. Comparative timeline of key pregnancy points in mice and humans. This figure compares the gestational timelines of the mouse (top) and human (bottom). Key developmental points of the mouse, including fertilization, implantation, placental formation, and delivery, are all indicated. Early, mid, and late pregnancy in mice versus first, second, and third trimesters in humans are aligned for comparison (109). The figure was created with BioRender .

1.2.4.3 Preeclampsia-like Mouse Model

To better understand the immune changes in human preeclampsia, mouse models of preeclampsia have been developed. In the present thesis, we took advantage of a mouse model that closely mimics the features of preeclampsia syndrome through the overexpression

of human sFLT1 (hsFLT1). Overexpression of hsFLT1 induced significant hypertension in this mouse model, which was accompanied by systemic vascular remodeling, including a reduction in the maternal aortic lumen, thickening of the aortic wall, and an increase in *Hif1α.* Furthermore, renal histology revealed features characteristic of preeclampsia, such as reduced endothelial cell marker Cd31, endothelial cell swelling, capillary lumen occlusion, more pronounced fibrosis, and a compromised glomerular filtration barrier. Collectively, these manifestations closely recapitulated the clinical and pathological features of human preeclampsia.

The model consists of double-transgenic dams expressing hsFLT1 under the control of a doxycycline-induced reverse tetracycline-controlled trans-activator (rtTA) (54). Starting at GD10.5, dams receive doxycycline in the drinking water to induce hsFLT1 overexpression and trigger preeclampsia-like symptoms. These females are normally compared to littermate pregnant females, which received sucrose-only drinking water and therefore do not express hsFLT1 (53).

1.3 $CD8^+$ T Cell in Healthy Pregnancy and Preeclampsia

1.3.1 Major Immune Cells of the Maternal-Fetal Interface in Healthy Pregnancy

The maternal-fetal interface is the site of a fundamental immunological paradox. Here, embryo-derived trophoblasts, which express paternal antigens and are thus semi-allogeneic, come into intimate contact with the maternal immune system (110). In any other context, this would trigger a rejection response. However, during pregnancy, the fetus and placenta are not only tolerated but are actively supported for many months. This remarkable feat is orchestrated by a unique and highly specialized population of immune cells that accumulates in the decidua, creating a local environment of profound immune regulation (111). These cells are critical for tissue homeostasis, uterine spiral artery remodeling, and the overall success of pregnancy (112).

Decidual natural killer (dNK) cells are the most abundant leukocytes (50–70%) in the decidua (113). They adopt a unique pro-angiogenic and non-cytotoxic phenotype, actively promoting trophoblast invasion and spiral artery remodeling (112,114). This crucial function is mediated by specialized receptors recognizing fetal human leukocyte antigen (HLA) molecules (3), for example, the interaction between KIR2D and fetal HLA-C, which directly regulates NK cells to influence trophoblast migration and spiral artery remodeling (115,116).

Decidual macrophages, are the second most abundant leukocyte population (10-20%) (117). They predominantly exhibit an anti-inflammatory M2-like phenotype, which is essential for creating a tolerogenic environment (117,118). Their key functions include secreting enzymes like MMP-7 and MMP-9 to enable trophoblast invasion (119) and promoting angiogenesis (120). This M2 polarization also contributes to local immune suppression, for example, through interactions with regulatory T cells (119). Consequently, an imbalance between pro-inflammatory M1-like and M2-like is associated with pregnancy pathologies such as preeclampsia (121).

T cells constitute another major immune population in the decidua, with an enrichment of $CD8^+$ T cells over $CD4^+$ T cells (122). These traditionally cytotoxic cells are functionally modulated through the co-expression of various immune checkpoint molecules, which contribute to the local tolerogenic environment (123,124).

1.3.2 The Immune Compartment at the Maternal-Fetal Interface is Affected in Preeclampsia

In contrast to the immune tolerance of a healthy pregnancy, preeclampsia has been characterized by a dysregulation of the immune environment at the maternal-fetal interface (125). In preeclampsia, decidual NK cells undergo a critical functional dysregulation, shifting from a pro-angiogenic to a more cytotoxic phenotype (126). This shift involves an increase in both their number and interferon-γ (IFN-γ) -mediated cytotoxicity, which inhibits trophoblast invasion and migration (127). Additionally, the secretion of tumor necrosis factor (TNF) is

reduced from dNK, affecting artery remodeling (128), while their production of key angiogenic factors like VEGF and PlGF is also impaired (129).

This dysregulation is observed in decidual macrophages as well, which shift from the anti-inflammatory M2-like to a pro-inflammatory M1-like phenotype. The secretion of pro-inflammatory cytokines by these M1-like cells is thought to underlie acute atherosclerosis and impair spiral artery remodeling, ultimately compromising placental blood circulation (130).

As described in detail below, the decidual T cell compartment also undergoes changes in preeclampsia, such as an increase in pro-inflammatory Th17 cells and a decrease in programmed cell death protein 1 (PD-1) expression on $CD8^+$ effector memory T cells (131). These shift from regulation to effector function contributes to the local immune dysfunction in preeclampsia.

1.3.3 $CD8^+$ T Cell of Maternal-Fetal Interface

1.3.3.1 Fundamental Characteristics of $CD8^+$ T Cells

$CD8^+$ T cells are not only cytotoxic in function, but they are also the most abundant T cell population at the maternal-fetal interface (132). They can differentiate into various memory T cell subsets, thereby establishing a pool of cells poised for a rapid response upon re-exposure to the same antigen. These subsets include central memory T cells (Tcm), effector memory T cells (Tem), tissue-resident memory T cells (Trm), and peripheral memory T cells (Tpm).

The long-term persistence of the $CD8^+$ memory T cell pool is not only dependent on antigen stimulation. Still, it is also actively sustained through a process of antigen-independent homeostatic proliferation and survival (133). This process is primarily driven by homeostatic cytokines, most notably Interleukin-7 (IL-7) and Interleukin-15 (IL-15) (134). While IL-7 provides essential pro-survival signals that prevent the $CD8^+$ T cells from undergoing apoptosis, IL-15 can maintain $CD8^+$ T cells long-term by a low level of proliferation (133). Furthermore,

TNF and IFN-γ also play a crucial role in promoting $CD8^+$ T cell proliferation in the context of an inflammatory immune response (135,136).

Activated effector $CD8^+$ T cells are key executors of the adaptive immune response, capable of eliminating infected or malignant cells throughout the body (137). To accomplish this task, they must be able to precisely enter target organs (138). However, the capacity for migration is not restricted to effector $CD8^+$ T cells. Memory $CD8^+$ T cells also retain this ability, which allows them to patrol in circulation and various tissues, thereby ensuring long-term immunological surveillance and homeostasis.

The migration of $CD8^+$ T cells from the circulation into tissue is a precisely orchestrated, multi-step cascade. The process initiates with rolling and adhesion, where selectins mediate the initial capture, followed by the firm binding of integrins like lymphocyte function-associated antigen-1 (LFA-1) and very late antigen-4 (VLA-4) to their endothelial ligands, intercellular adhesion molecule 1 (ICAM-1) and vascular cell adhesion molecule 1 (VCAM-1) (139–141). The final step, extravasation, is dependent on guidance from local chemokine gradients. For instance, the C-X-C motif chemokine ligand 10 and C-X-C motif chemokine receptor 3 (CXCL10-CXCR3) signaling axis serves as a pivotal control point for immune cell trafficking at the maternal-fetal interface, the tight regulation of which is essential for pregnancy success. Nancy et al. indicated that in a healthy pregnancy, decidual stromal cells establish an immune-privileged environment precisely by silencing the genes for T-cell-attracting chemokines, thereby actively limiting effector T cell access to protect the fetus (142). Conversely, when this protective silencing is breached, such as during infection, the same CXCL10-CXCR3 pathway can drive a harmful influx of pathogenic T cells. In such cases, the therapeutic blockade of CXCR3 is protective, preventing infection-induced fetal wastage (143).

1.3.3.2 $CD8^+$ T cells Support a Healthy Pregnancy

A central paradox in pregnancy is how the maternal adaptive immune system maintains tolerance towards the semi-allogeneic fetus. So far, it is known that $CD8^+$ effector memory T cells, a main subset at the maternal-fetal interface, display a reduced expression of cytolytic

proteins like perforin and granzyme B, indicating a suppression of their cytotoxic function (144). Beyond the general restraint observed in memory populations, the decidua is also enriched with specialized $CD8^+$ regulatory T cell (Treg) subsets, which actively suppress immune responses (124), for example, in humans, KIR^+CD8^+ T cells are considered as a regulatory subsets, which is functionally equivalent of murine $Ly49^+CD8^+$ T cells, the frequency of which is significantly elevated in the decidua (145), which play a critical role in promoting maternal–fetal immune tolerance and preventing immune dysregulation during pregnancy (146).

In mice, $CD8^+$ Tregs have been proven to be essential for a successful pregnancy through two distinct functions: ensuring immune tolerance and actively promoting placental development. Their importance in preventing fetal rejection is highlighted by the reduced frequency of decidual $Tim3^+CTLA4^+$ $CD8^+$ Tregs in abortion-prone mice (147) and the increased fetal loss following Tim-3/PD-1 blockade in healthy pregnancies (148). Beyond this protective role, the $CD8^+CD122^+$ T cell subsets can ameliorate stress-induced intrauterine growth restriction (IUGR) by enhancing placental angiogenesis and function (149).

1.3.3.3 $CD8^+$ T Cells in Preeclampsia

Research on CD8+ T cells in the context of preeclampsia has been relatively limited, yielding contrasting findings (Table 3). Early work reported changes in decidual $CD8^+$ T cells (150–154), or particular subsets, e.g., increased $CD28^+CD8^+$ T cells (155), or reduced fraction of $PD1^+$ effector memory $CD8^+$ T cells (156). Intriguingly, more recent observations unequivocally underscored an overall reduced frequency of decidual $CD8^+$ T cells in preeclampsia pregnancies (157–160). The inconsistent findings regarding the altered $CD8^+$ T cell compartment in preeclampsia leave open questions of how and why. This knowledge gap forms the central rationale for the work presented in this thesis.

Table 3. Summary of Studies on $CD8^+$ T Cells in the Decidua of Preeclampsia.

Decidual $CD8^+$ T Cells in Preeclampsia	Title	Author, year

↑ $CD8^+$ /CD28+	Lymphocyte subset distribution and cytokine secretion in third trimester decidua in normal pregnancy and preeclampsia	Wilczyński et al., 2003
↓ $CD8^+$ T cells	Specific subsets of immune cells in human decidua differ between normal pregnancy and preeclampsia	Rieger et al., 2009
↓ $CD8^+$ T cells	Altered decidual leucocyte populations in the placental bed in pre-eclampsia and fetal growth restriction	Williams et al., 2009
↑ $CD8^+$ T cells	The unique pathophysiology of early-onset severe preeclampsia: role of decidual T regulatory cells	Quinn et al., 2011
↓ $CD8^+$ T cells	Impairment of the accumulation of decidual T cells, NK cells, and monocytes, and the poor vascular remodeling of spiral arteries, were observed in oocyte donation cases	Nakabayashi et al., 2016
↑ $CD8^+$ T cells in spiral artery wall with AA lesion	Lymphocyte characterization of decidua basalis spiral arteries with acute atherosis in preeclamptic and normotensive pregnancies	Johnsen et al., 2019
↑ $CD8^+$ T cells	T lymphocytes in the third trimester decidua in preeclampsia	Milosevic-Stevanovic et al., 2019
↓PD-1 in dedicual $CD8^+$ EM cells	Analysis of TCR Repertoire and PD-1 Expression in Decidual and Peripheral CD8+ T Cells Reveals Distinct Immune Mechanisms in Miscarriage and Preeclampsia	Morita et al., 2020
↓ $CD8^+$ memory cells in parietalis, ↓ activated CD8+ memory T cells in basalis	Decidual memory T-cell subsets and memory T-cell stimulatory cytokines in early- and late-onset preeclampsia	Kieffer et al., 2020
↓ $CD8^+$ T cells	Decreased Expression of Cytotoxic Proteins in Decidual CD8+ T Cells in Preeclampsia	Soljic et al., 2021
↓ cytotoxic T lymphocyte	Single-cell profiling reveals immune disturbances landscape and HLA-F-mediated immune tolerance at the maternal-fetal interface in preeclampsia	Luo et al., 2023
↓ $CD8^+$ T cells	Phenotypic and functional alteration of CD45+ immune cells in the decidua of preeclampsia patients analyzed by mass cytometry	Min Fu et al., 2023

1.4 The Context-Dependent Role of $CD8^+$ T Cells in Angiogenesis

Angiogenesis, the formation of new blood vessels from a pre-existing vascular network, is a fundamental process essential for embryonic development (161). While often viewed as a process driven by endothelial cells and growth factors, it is now clear that the immune system, particularly T cells, is a potent modulator of vascular growth and remodeling (162).

In diverse contexts ranging from cancer to tissue repair, $CD4^+$ Tregs have been shown to actively promote the formation of new blood vessels (162,163). In contrast to the well-defined role of their $CD4^+$ counterparts, the contribution of $CD8^+$ T cells to angiogenesis is less understood and appears to be highly context-dependent and multifaceted. The limited research available presents a conflicting picture, suggesting that different $CD8^+$ T cell subsets can exert opposing effects on blood vessel formation. On one hand, there is evidence for $CD8^+$ T cells acting as a pro-angiogenic, supportive role in pregnancy (149). On the other hand, pro-inflammatory and cytotoxic $CD8^+$ T cells have been implicated in promoting pathological neovascularization in diseases such as ocular neovascularization (164). This suggests that the functional phenotype of the $CD8^+$ T cell and the tissue context are both key determinants of its effect on angiogenesis.

1.5 Immune Changes in Pregnant Women with Overweight and Obesity

As overweight and obesity are important risk factors for preeclampsia, it is critical to point out that they can also severely influence both physiological and pathological immune responses (Table 4). In pregnancy, such alterations may lead to impaired placental function and an increased risk of pregnancy failure (165). For instance, studies in humans have shown that obesity can lead to reduced numbers of uNK cells, a change that impairs placental artery remodeling (166). Furthermore, the increased expression and activity of the natural cytotoxicity receptor 1 (NCR1) on uNK cells from obese women represents another mechanism that compromises vascular processes (167). Obesity can also favor an inflammatory milieu driven by an accumulation of macrophages at the maternal-fetal interface (168).

Immune changes have been demonstrated in animal models with obesity. For example, diet-induced obesity in murine models of normal gestation is associated with elevated levels of NKp+46 NK cells (the murine homolog of NCR1), MHC II^{high} macrophages, as well as CD4+ and CD8+ T lymphocytes (87).

In contrast, Sureshchandra et al. (169) presented a more complex picture of immune dysregulation in the obese decidua. In this published cohort, obesity had no significant impact on the frequency of decidual NK cells. However, a significant alteration was observed in the T cell compartment, where the proportions of both $CD4^+$ and $CD8^+$ T cells were reduced, yet paradoxically, the frequency of Tregs within the $CD4^+$ population was increased. This study also noted an upregulation in the frequency of HLA-DR^{high} macrophages, which was accompanied by a significant decrease in the expression of key molecules such as TNFα, IL-1β, VEGF-A, and PD-L1 in this specific cell population. This paradoxical finding illustrates how overweight and obesity influence not only the quantity and composition of immune cell populations but also modulate their functional status.

Table 4. Summary of Studies on CD8+ T Cells in the Decidua / Endometrium of the population with BMI ≥25.

Decidual / endometrial $CD8^+$ T cell in women with BMI ≥ 25	Title	Author, Year
↓ $CD8^+$ T cell	Multimodal profiling of term human decidua demonstrates immune adaptations with pregravid obesity	Suhas Sureshchandra et al. 2023
↑ $CD8^+$ T cell with weight loss	The impact of obesity and bariatric surgery on the immune microenvironment of the endometrium	Anie Naqvi et al. 2021
no change	Evaluation of endometrial immune status of polycystic ovary syndrome	Su Liu et al. 2021
no change	Pilot Data Suggest That Obesity and Presence of Malignancy Are Associated with Altered Immune Cell Infiltration in Endometrial Biopsies	Eline Jacques, 2024
↓ $CD8^+$ T cell in high BMI PCOS (compare to high BMI ctrl)	Single-cell profiling of the human endometrium in polycystic ovary syndrome	Gustaw Eriksson, 2025

↓ $CD8^+$ T cell in obese	STAT3 Activation-Induced Fatty Acid Oxidation in $CD8^+$ T Effector Cells Is Critical for Obesity-Promoted Breast Tumor Growth	Chunyan Zhang, 2020

1.6 Hypothesis and Aims

Taken together, research on CD8+ T cells in the context of preeclampsia has been relatively limited, and a clear consensus about their modulation and their relation to preeclampsia manifestations has yet to emerge.

We hypothesize that the abundance of decidual $CD8^+$ T cells is modulated in the context of pregnancies with preeclampsia and altered metabolic status, i.e., increased BMI. In preeclampsia, alterations in the crosstalk between $CD8^+$ T cells and local tissue processes may affect the uterine vasculature. Building on this foundation, this thesis aimed to advance the understanding of the decidual $CD8^+$ T cell regulation in preeclampsia, with a particular focus on the modulatory role of maternal pre-pregnancy BMI. To this end, our study was guided by the following key objectives:

1. The abundance and spatial distribution of $CD8^+$ T cells at the maternal–fetal interface, in normal pregnancy versus preeclampsia and/or pregnancies affected by high BMI.
2. The molecular and cellular factors, including cytokines, chemokines, and migration-related molecules, can modulate $CD8^+$ T cell recruitment, retention, and functional differentiation within decidual and placental tissues, thereby providing further insights into the potential mechanisms underlying the pathogenesis of preeclampsia.
3. The associations among cellular, spatial, and molecular parameters we tested, aiming to integrate multidimensional datasets to obtain a more comprehensive understanding of the role $CD8^+$ T cells may play in the immunopathology of preeclampsia
4. Evaluate the causality of the events in a mouse model of preeclampsia induced by excess hsFLT1.

To address the objectives defined above, we have set the following specific aims:

Objective 1. $CD8^+$ T cell abundance and spatial distribution at the maternal–fetal interface:

- Collect decidual and placental tissue samples from the maternal–fetal interface (normal pregnancies vs. preeclamptic patients, normal BMI vs. high BMI).
- Use IHC/IF to quantify the density and map the spatial distribution of $CD8^+$ T cells relative to blood vessels.
- Study different subsets of $CD8^+$ T cells using flow cytometry.
- Compare the differences in $CD8^+$ T cell quantity and spatial distribution between the normal and preeclamptic groups.

Objective 2. Molecular and cellular factors modulating $CD8^+$ T cells:

- Analyze the expression of relevant cytokines, chemokines, and migration-related molecules in decidual and placental tissues (via qPCR, IHC, IF).
- Investigate the relationship between these molecules and the recruitment, retention, and functional differentiation of $CD8^+$ T cells.

Objective 3. Integrative analysis of cellular, spatial, and molecular parameters:

- Integrate data on $CD8^+$ T cell abundance, spatial distribution, and relevant molecular levels.
- Compare the correlations between parameters among different groups to identify potential pathogenic mechanisms.

Objective 4. Evaluate the causality of the events in a mouse model of preeclampsia induced by excess hsFLT1:

- Quantify the abundance and phenotype of decidual $CD8^+$ T cell subsets in hsFLT1-induced mice to determine if sFLT1 is a direct upstream driver of the cellular deficiency.
- Analyze the decidual expression of key immunomodulatory molecules identified in the human study, such as *Cxcl10*, to establish their position downstream of the sFLT1-driven angiogenic imbalance.

- Compare the overall immunological signature of the mouse model with the human data to validate the translational relevance of the proposed pathogenic mechanism.

2. Materials And Methods

2.1 Material

2.1.1 Mice

The mice used in this dissertation are listed in the following table.

Strain	Breeder
C57BL/6J	Charles River, Sulzfeld, Germany
Balb/c	Charles River, Sulzfeld, Germany
Col1A1tm2(tetO−Flt1∗)Hsc (MGI: 6202353)	Provided by Prof. Dr. Alexandra Gellhaus, University Hospital Essen, Germany

2.1.2 Human Study Population

2.1.2.1 Late-Onset Preeclampsia and Controls

A total of 64 women were enrolled in this study. All patients were treated in the Clinic St. Hedwig of the Order of St. John, Department of Gynecology and Obstetrics, University Hospital Regensburg, Germany, between 2022 and 2024. Late-onset preeclampsia diagnosis followed the guideline “Hypertensive Disorders in Pregnancy: Diagnostics and Therapy” (40). The control group consisted of women with healthy term pregnancies, who were randomly selected from BMI-matched normotensive women. Patients with other pregnancy complications, such as chorioamnionitis, chromosomal and fetal anomalies, were excluded (Table 5). Since flow cytometry study requires cell isolation from fresh tissue, samples for this analysis were collected prospectively, a total of 27 women were enrolled in this study. All patients were treated in the Clinic St. Hedwig of the Order of St. John, Department of Gynecology and Obstetrics, University Hospital Regensburg, Germany, 2025. The inclusion criteria for this patient cohort were identical to those described previously (Appendix 2).

Considering that elevated pre-pregnancy BMI is an independent risk factor for preeclampsia (170,171), we split the participant data according to pre-pregnancy BMI. According to WHO criteria (69), patients were divided into 4 groups: normal BMI control ($18.5 \leq BMI < 25 kg/m^2$,

n=17), normal BMI late-onset preeclampsia (n=16, including one fetal growth restriction case), high BMI control (BMI ≥ 25 kg/m^2, n=15), and high BMI late-onset preeclampsia (n=16, including three fetal growth restriction cases). The study protocol was approved by the Ethics Commission of the University of Regensburg, Germany (21–2427–101).

2.1.2.2 Early-Onset Preeclampsia and Controls

A total of 24 women were enrolled in this study. All patients were treated in the Clinic St. Hedwig of the Order of St. John, Department of Gynecology and Obstetrics, University of Regensburg, Regensburg, Germany, between 2022 and 2024. Preeclampsia diagnosis was followed by the guideline “Hypertensive Disorders in Pregnancy: Diagnostics and Therapy” (40). The gestational age of early-onset preeclampsia is defined as after 20 weeks, while before 34 weeks (41). Women of the control group were randomly selected from those delivered before 34 weeks. Due to the limited availability of eligible specimens, patients were divided into two groups: gestation age-matched control (n=12) and early-onset preeclampsia (n=12). Patients with other pregnancy complications, such as chorioamnionitis, chromosomal and fetal anomalies, were excluded (Table 17). The study protocol was approved by the Ethics Commission of the University of Regensburg, Germany (21–2427–101). All patient data was documented using programs Viewpoint 6.0 (GE Healthcare), SAP, and RedCAP (172,173).

2.1.3 Reagents and Solutions

Reagent	Company	Catalog No.
AbCTMTotal Antibody Compensation Bead Kit	Invitrogen	A10497
Accutase	Sigma-Aldrich	SCR005
Aquatex	SIGMA Life Science	A7030-100G
Bovine Serum Albumin (BSA)	Sigma-Aldrich	C9999
Citrate buffer	Merck/ Sigma-Aldrich	SCR103
Collagenase	Agilent	S3022
DAB Substrate Kit	Carl Roth	K928.4
Dako antibody diluent	Mayer/Sigma-Aldrich	51275

DAPI and Hoechst Nucleic Acid Stains	European Pharmacopoeia Reference Standard	H11115000
eBioscience™ Foxp3 / Transcription Factor Fixation/Permeabilization Concentrate and Diluent	Sigma-Aldrich	1.07209
Ethanol (99.8%)	Life technologies	FB001
Ficoll	PAN Biotech	P30-0101
Hematoxilin	Thermo Fischer	10710C
Hyaluronidase	R&D System	DY005
Hydrogen peroxide 30%	Invitrogen	00-8333-56
IC fixation buffer	eBioscience/Invitrogen	00-4333-57
Normal donkey serum	Invitrogen	AM7021
Normal goat serum	Abcam	ab64269
Normal rat serum	Fisher Scientific	10776834
Normal rabbit serum	Invitrogen	31883
Permeabilization buffer	Biolegend	101320
Qiazol Lysis Reagent	SIGMA Life Science	T8154-100ML
RBC Lysis Buffer	Carl Roth	9713.5
RNA later Soln.	Carl Roth	6640.5
RNeasy Plus Universal Mini Kit (50)	Sigma-Aldrich	9005-64-5
ROTI®Histol	Abcam	ab64238
ROTI®Mount	Thermo Fischer	62249
Streptavidin HRP	Carl Roth	HP68.1
TaqMan™ Universaler Mastermix für PCR, keine AmpErase™ UNG	Thermo Fischer	4324018
TBS (10X)	Merck/ Sigma-Aldrich	1.08562
TruStain FcX™ (anti-mouse CD16/32) Antibody	eBioscience	00-5521
Tryphan Blue solution	Cytiva	17144002
Tween 20	Qiagen	57502096
Xylol (Isomere)	Qiagen	73404
Ponceau S (C.I. 27195)	Sigma Aldrich	6226-79-5
Acid fuchsine	Sigma Aldrich	3244-88-0
Glacial Acetic Acid	Merck	64-19-7
Phosphotungstic Acid Hydrate	Sigma Aldrich	12501-23-4

Orange G (C.I. 16230)	Sigma Aldrich	1936-15-8
Light green (C.I. 42095)	Sigma Aldrich	5141-20-8
water-based mounting medium	VECTOR	ZH0419
Fetal Bovine Serum	Merck	F9665-500ML
Human TruStain FcX™	Biolegend	422302
RPMI-1640-Medium	Sigma Aldrich	R8758-6X500ML
Collagenase IV	Worthington	LS004188
Monensin	BD	554724
Hank's balanced salt solution	Sigma Aldrich	H8264-500mL
NH4Cl (Ammonium Chloride)	Sigma Aldrich	A9434-500G
KHCO3 (potassium bicarbonate)	Sigma Aldrich	237205-100G
EDTA-disodium, dihydrate	Merck	324503-100GM
BD Cytofix/Cytoperm™ Fixation/Permeabilization Kit	BD	554714

2.1.4 Mouse Antibodies for Flow Cytometry

Specificity	Fluorochrome	Clone	Company	Catalog No.
CD4	BUV496	RM4-5	BD	741050
CD44	BUV395	IM7	BD	740215
TCRb	APC	H57-597	BD	553174
CD45.2	APC-Cy7	104	Biolegend	109824
PD1	FITC	J43	Invitrogen	11-9985-82
Ly49	PE	14b11	Biolegend	108208
CD122	PerCP efluor 710	TM-b1	Invitrogen	46-1222-82
CD127	PE-TR	A7R34	Biolegend	135031
CD62L	BV421	MEL-14	Biolegend	104435
CD8a	BV650	53-6.7	Biolegend	100741
CD11b	BV711	M1/70	Biolegend	101241
NK1.1	BV785	PK136	Biolegend	108749
CD45 i.v.	AF700	30-F11	Biolegend	103128
Fixable Viability Dye	efluor 506	/	Invitrogen	65-0866-14
Foxp3	PE-Cy7	FJK-16s	Invitrogen	25-5773-82
CD11c	BUV395	HL3	BD	564080

F4/80	FITC	BM8	Biolegend	123107
CD206	PE-Tx RED (dazzle)	C068C2	Biolegend	141732
CD11b	PE-Cy7	M1/70	Biolegend	552850
FcεRIα	APC	MAR-1	Biolegend	134316
MHCII	BV421	M5/114.15.2	Biolegend	107631
Gr-1	BV650	RB6-8C5	Biolegend	108441
CD117	BV785	2B8	Biolegend	105841
iNOS	PerCP efluor 710	CXNFT	Invitrogen	46-5920-80
Arg1-PE	PE	A1exF5	Invitrogen	12-3697-82
CD45	APC-Cy7	30-F11	BD	557659

2.1.5 Mouse Antibodies and Kits for Immunohistochemistry

Reagent	**Company**	**Cat. No.**
Anti-CD45 antibody	Abcam	ab10558
Anti-Mouse F4/80 antibody	Biorad	MCA497GA
CD8α (D4W2Z) XP® Rabbit mAb	Cell signaling	98941
Goat Anti-Rat IgG H&L (Biotin)	abcam	ab207997
Goat Anti-rabbit IgG H&L (Biotin)	Invitrogen	65-6140
DAB Substrate Kit	Abcam	ab64238
Streptavidin HRP (ready-to-use)	Abcam	ab64269
CEACAM1	Provided by University Medical Center Hamburg- Eppendorf, Germany	

2.1.6 Mouse RNA Isolation, cDNA Synthesis, and qPCR Reagents

Primer Name	**Assay ID**	**Company**
Tnf	Mm00443258_m1	Themo Fisher
Ifng	Mm01168134_m1	
Il7	Mm01295803_m1	
IL5	Mm00434210_m1	
Pecam1	Mm01242576_m1	
Icam1	Mm00516023_m1	
Vcam1	Mm01320970_m1	
Ccl5	Mm01302427_m1	

Cxcl9	Mm00434946_m1
Cxcl10	Mm00445235_m1
Rpl13a	Mm05910660_g1
Rn18s	Mm03928990_g1

Specificity	**Company**	**Cat. No.**
RNeasy Plus Universal Mini Kit (50)	Sigma-Aldrich	9005-64-5
TaqMan™ Universaler Mastermix für PCR, keine AmpErase™ UNG	Thermo Fischer	4324018
QIAwave RNA Plus Mini Kit (50)	Qiagen	74634

2.1.7 Human Antibodies for Flow Cytometry

Specificity	**Fluorochrome**	**Dilution**	**Company**	**Cat. No.**
CD69	BUV496	FN50	BD	750214
CD25	BV785	BC96	Biolegend	302638
CD45RA	BV711	HI100	Biolegend	304138
CD3	BV650	OKT3	Biolegend	317324
KLRG1	BV605	2F1/KLRG1	Biolegend	138419
CD39	PE-Cy7	A1	Biolegend	328212
CD127	PerCP Cy5.5	A019D5	Biolegend	351322
CD103	PE-Dazzle 594	Ber-ACT8	Biolegend	350224
CD4	FITC	SK3	Biolegend	344604
CD27	APC-Cy7	O323	Biolegend	302816
CD8	AF700	HIT8a	Biolegend	300920
γδ TCR	BUV395	11F2	BD	745681
KIR2DL2/L3	BV786	DX27	BD	744650
CD3	BV650	OKT3	Biolegend	317324
KIR3DL1	BV421	DX9	Biolegend	312714
CD8	AF700	HIT8a	Biolegend	300920
PD1	APC,	EH12.2H7	BD	329908
Fixable Viability Dye	Amcyan	/	Invitrogen	65-0866-14

2.1.8 Human Antibodies and Kits for Immunohistochemistry and Immunofluorescence

Reagent	Company	Cat. No.
CD8 Monoclonal Antibody (SP16)	Invitrogen	MA5-14548
CXCL10 Polyclonal Antibody	Invitrogen	PA5-46999
Alpha-Smooth Muscle Actin Monoclonal Antibody (1A4)	Invitrogen	14-9760-82
VCAM-1 (CD106) Recombinant Rabbit Monoclonal Antibody (SA05-04)	Invitrogen	MA5-31965
CD68 (D4B9C) XP® Rabbit mAb	Cell signaling	76437
CD31 Monoclonal Antibody	Invitrogen	MA5-13188
Goat Anti-mouse IgG H&L (Biotin)	Invitrogen	31800
Goat Anti-rabbit IgG H&L (Biotin)	Invitrogen	656140
Donkey anti-Goat IgG (H+L) Secondary Antibody, Biotin	Invitrogen	PA1-28663
Goat Anti-Rabbit IgG H&L (Alexa Fluor® 647) preadsorbed	Abcam	ab150083
Donkey Anti-Mouse IgG H&L (Alexa Fluor® 488)	Abcam	ab150105
DAPI and Hoechst Nucleic Acid Stains	Themo Fisher	62249
DAB Substrate Kit	Abcam	ab64238
Streptavidin HRP (ready-to-use)	Abcam	ab64269
Water-based mounting medium	VECTOR	ZH0419

2.1.9 Human RNA Isolation, cDNA Synthesis, and qPCR Reagents

Primer Name	Assay ID	Company
CEACAM1	Hs05041713_s1	Themo Fisher
HMOX1	Hs01110250_m1	
LYVE1	Hs00272659_m1	
FLT1	Hs01052961_m1	
KDR	Hs00911700_m1	
PGF	Hs00182176_m1	

VEGFA	Hs00900055_m1
IL7	Hs00174202_m1
IL15	Hs01003716_m1
IFNG	Hs00989291_m1
TNF	Hs00174128_m1
AREG	Hs00950669_m1
CCL5	Hs00982282_m1
CXCL9	Hs00171065_m1
CXCL10	Hs00171042_m1
ICAM1	Hs00164932_m1
VCAM1	Hs01003372_m1
PECAM1	Hs01065279_m1
HIF1A	Hs00153153_m1
UBC	Hs05002522_g1
YWHAZ	Hs01122445_g1

Specificity	**Company**	**Cat. No.**
RNeasy Plus Universal Mini Kit (50)	Sigma-Aldrich	9005-64-5
TaqMan™ Universaler Mastermix für PCR, keine AmpErase™ UNG	Thermo Fischer	4324018
QIAwave RNA Plus Mini Kit (50)	Qiagen	74634

2.1.10 Instruments

Equipment	**Conpany**
QuantStudio™ 5 Real-Time PCR System	Themo Fisher
BD LSRFortessaTM cell Analyzer	BD Biosciences
MJ Research PTC 200 Peltier Thermal Cycler	Bio-Rad
Leica RM2125 RTS - The Essential Microtome	Leica
FLUOVIEW FV3000	Olympus
Precellys 24 Tissue Homogenizer	Bertin Technologies

2.1.11 Software

Software	**Company**

Graphpad Prism version 10	GraphPad Software, La Jolla, CA, USA
IBM SPSS Statistics 29.0.0.0	IBM Corp., USA
FlowJo Version 10 for Mac	TreeStar, Asland, OR, USA
SlideViewer 2.6	3DHISTECH, Budapest, Hungary
ImageJ 1.53t	National Institutes of Health (NIH), USA
Qupath v 0.5.1	University of Edinburgh, UK. https://qupath.github.io/
Biorender	Biorender, Toronto, Canada

2.2 Methods

2.2.1 Mouse Handling

The animals were housed at a constant temperature under a 12-hour light/dark cycle with free access to food and water. All animal procedures were performed in accordance with German law for animal protection. Preeclampsia-like mice were used with ethical approvals (No.: G1935/23; G1644/17), and ARRIVE guidelines were followed throughout the whole project. Wildtype mice were used with ethical approval (55.2.2-2532-2-1488) and identified by the internal RUF number (RUF-55.2.2-2532-2-1488-24).

2.2.1.1 Timed Mating

For wildtype mice, timed mating was established by placing two female mice (3-5 months old) with one male in the same cage in the late afternoon and mating overnight; for establishing preeclampsia-like mice (3-9 months old), mating was performed by placing one female mouse with one male mouse in the same cage. The presence of a vaginal plug on the following morning was considered as GD 0.5. To confirm pregnancy, body weight was measured and recorded on GD 0.5, GD 6.5, and GD 10.5. Steady weight gain was considered pregnant.

2.2.1.2 Preeclampsia-like Mouse Model

The preeclampsia-like mouse model used in this study was generously provided by Prof. Dr. Alexandra Gellhaus from the University Hospital Essen, Germany. This model utilizes double-transgenic dams expressing hsFLT1 under the regulation of a reverse rtTA (53,54). To

generate this model, single transgenic Gt(ROSA)26Sor$^{tm1(rtTA*M2)Jae}$ mice, which express rtTA, and single transgenic Col1a1t$^{m2(tetO-Flt1*)Hsc}$ mice, which carry a doxycycline-inducible hsFLT1 transgene, were mated to establish double-transgenic (hsFLT1/rtTA) offspring, in which the hsFLT1 overexpression can be induced upon treatment with doxycycline. These double transgenic hsFLT1/rtTA mice were mated overnight. Starting at GD10.5, a group of dams was provided with drinking water containing 2 mg/mL doxycycline and 30 mg/mL sucrose to induce hsFLT1 overexpression, resulting in preeclampsia-like symptoms. Control dams, which received sucrose-only drinking water, did not express hsFLT1 (53).

2.2.1.3 Intravital Staining

To differentiate between intravascular and tissue-resident leukocytes in preeclampsia-like mice, intravenous (i.v.) injection of an anti-CD45 AF700 antibody (6.25 µg in 200 µL sterile PBS) was performed three minutes prior to euthanasia (as detailed in Section 2.2.1.4).

2.2.1.4 Mouse Euthanasia and Tissue Collection

For wildtype mice, tissue collection was performed on virgin, GD 6.5, GD 10.5, GD 14.5, and GD 18.5. The mice were euthanized with CO_2. Death was confirmed by cervical dislocation. Tissue collection from preeclampsia-like and control mice was performed on GD 14.5. Dams were anesthetized with isoflurane (5% in 1 L/min O_2) prior to sacrifice by cervical dislocation. Afterward, mice were sprayed with 70% ethanol and performed with sterile scissors and forceps for tissue collection.

2.2.2 Isolation of Leucocytes from Mice

The cell isolation process was performed on ice. The following procedures were applied to wildtype adult virgin mice, GD 6.5, GD 10.5, GD 14.5, and GD 18.5 of wildtype pregnant mice, while preeclampsia-like mice and their controls were studied at GD 14.5.

2.2.2.1 Blood

Whole blood was collected by cardiac puncture and transferred into a blood collection microtube containing EDTA-K. Before starting the experiment, the collected blood was transferred to a 50 mL Falcon tube. For every 100 µL of whole blood, 1 mL of 1× RBC lysis buffer was added, followed by incubation on ice for 5 minutes. The reaction was then stopped by adding PBS to a total volume of 50 mL. The sample was centrifuged at 450 × g for 8 minutes, supernatant was discarded. Repeat the washing step, and the cells were resuspended in 1 mL of PBS.

2.2.2.2 Spleen

The spleen was collected into a 15 mL Falcon tube containing ice-cold PBS. A 40 µm cell strainer was placed on top of a 50 mL Falcon tube. Using the piston of a 1 mL syringe, the spleen was smashed over the cell strainer while washing with PBS to allow the tissue to pass through the strainer. After centrifuging at 450 × g for 8 minutes, the supernatant was removed, and 5 mL of RBC lysis buffer was added. The sample was incubated on ice for 5 minutes, then 40 mL of PBS was added to stop the reaction. The solution was filtered again, followed by another centrifugation at 450 × g for 8 minutes. After discarding the supernatant, the cells were resuspended in 2 mL of PBS.

2.2.2.3 Lymph Nodes

Lymph nodes were collected into a 15 mL Falcon tube containing ice-cold PBS. A 40 µm cell strainer was placed on a petri dish. Using the piston of a 1 mL syringe, the lymph node was smashed over the cell strainer while washing with PBS to allow the tissue to pass through the strainer. Transferred the suspension to a 15ml Falcon tube and centrifuged at 450 × g for 8 minutes. After discarding the supernatant, the cells were resuspended in 500 µL of PBS.

2.2.2.4 Uterus

The uterus was processed following a previously published protocol (174). The entire uterus was collected and placed in a petri dish with ice-cold PBS. The fat tissue surrounding the uterus was carefully removed. For the virgin uterus, after clearing the surrounding fat, the tissue was transferred into a 5 mL Eppendorf tube containing ice-cold PBS. For the GD 6.5 uterus, a small incision was made at each implantation site, and the implantations were gently pushed out. The remaining uterine tissue was then transferred into a 5 mL Eppendorf tube with ice-cold PBS. For GD 10.5, GD 14.5, and GD 18.5, each implantation was first separated individually. A small incision was made in the uterine wall near the placenta and mesometrial region. The cut was extended around the placenta edge until it was fully detached from the chorioallantoic membrane. Afterward, the mesometrial triangle was cut from the placental tissue and placed into a 5 mL Eppendorf tube with ice-cold PBS. This procedure was performed for each implantation from GD 10.5 to GD 18.5, including preeclampsia-like mice at GD 14.5.

The uterine tissue was placed in a 5 mL Eppendorf tube containing 1000 µL of ice-cold Accutase for enzymatic digestion. Tissue was carefully dissociated using fine sterile scissors. The homogenized tissue was then transferred to a 15 mL Falcon tube, and 2 mL of ice-cold Accutase was added. All steps were performed on ice to maintain low temperatures. The sample was incubated in a 37°C water bath for 35 minutes with continuous stirring using a magnetic stirrer. To stop the reaction, the sample was immediately placed on ice. The homogenized tissue solution was then filtered through a 40 µm cell strainer while being rinsed with PBS. The filtered suspension was collected into a 50 mL Falcon tube and centrifuged at 1250 × g for 10 minutes at 4°C. After removing the supernatant, 1 mL of RBC lysis buffer was added to virgin uterus samples and incubated on ice for 2 minutes. For GD 6.5 to GD 18.5 pregnant uterus samples, 2 mL of RBC lysis buffer was added and incubated on ice for 4 minutes. The reaction was stopped by filling the tube with PBS. The sample was then centrifuged at 450 × g for 8 minutes. After discarding the supernatant, the cell pellet was resuspended in 1 mL of PBS.

2.2.3 Isolation of Leucocytes from Humans

2.2.3.1 Decidua

Human placentas were collected upon delivery at University Hospital St. Hedwig of the Order of St. John, Department of Gynecology and Obstetrics, University of Regensburg, Germany. The decidua was processed according to an established protocol from the lab of Prof. Dr. Marina Kreutz, University Hospital Regensburg, Germany, with further modifications to optimize the procedure for our specific experimental conditions. 1 cm^3 samples of the placenta and attached decidua basalis were collected from the central region of the placenta from all study participants upon delivery in our clinic and washed in with ice-cold PBS. Using fine sterile scissors, the decidua was carefully separated and placed into a petri dish with 945 µL RPMI medium, 100 µL human collagenase IV, and 42 µL Monensin. The decidual tissue was then minced by sterile scissors, followed by 2-hour incubation at 37°C with 5% CO_2. The homogenized solution was filtered through a 70 µm cell strainer into a new 50 mL Falcon tube. Centrifugation was performed at 1300 rpm for 7 minutes at 4°C, and the supernatant was discarded. 2 ml ammonium-chloride-potassium lysis buffer was added and incubated for 3 minutes at room temperature. The cells were washed by adding 10ml PRMI medium, followed by centrifugation at 1300 rpm for 7 minutes. The supernatant was discarded, and the cell pellet was resuspended in 0.5 ml RPMI medium.

2.2.4 Flow Cytometry

2.2.4.1 Compensation

Compensation beads were used to generate single-stained controls for establishing flow cytometry compensation settings. The kit includes capture beads (Component A), which bind to all isotypes of mouse, rat, hamster, and rabbit immunoglobulins, and negative beads (Component B), which lack antibody-binding ability. Beads were vortexed gently for 10 seconds before use, and 1 drop of component A was added to each FACS tube. A pre-titrated amount of each antibody was added to the FACS tube and mixed well. Incubate for 15 minutes at room temperature, protected from light. 3 mL PBS was added and centrifuged at 250 g for

5 minutes to wash. Carefully removed the supernatant and resuspended the beads with 0.5 ml PBS, then added 2 drops of component B to the FACS tube. Since the viability antibody does not bind to beads, its compensation must be performed using cells. To prepare, 1 million cells were collected, with half heated inactivation at 70°C for 10 minutes. After cooling, the inactivated cells were mixed with live cells and stained with the viability antibody. Additionally, a separate control containing only Component B was prepared as a negative control. The flow cytometer can automatically calculate the compensation, allowing the compensation matrix to be directly applied to the experiment. Further adjustments to the post-compensation matrix were made by FlowJo version 10.

2.2.4.2 FACS Staining of Mouse Tissues

First, 10 µL of cell suspension was diluted 1:10 with TrueBlue. A 10 µL aliquot of the diluted suspension was loaded onto a hemacytometer for cell counting, and the volume of 1 million cells was determined. Then 1 million cells were added in 1 mL PBS in a FACS tube, centrifuged at 450 × g for 8 minutes. Remove the supernatant and add 10 µL blocking buffer (1:200 TrueStain, 1:100 normal rat serum), well mixed and incubated on ice for 15 minutes.

For extracellular staining, each sample was incubated on ice in the dark for 30 minutes with a pre-titrated extracellular antibody panel mix and a viability antibody. The cells were then washed by adding 1 mL PBS, followed by centrifugation at 450 × g for 8 minutes, and resuspended the cell pellet with 200 µL PBS. If intracellular staining or analysis on the following day is required, cell fixation is necessary, since fixation can preserve the structural integrity of the cell and immobilize intracellular antigens prior to membrane permeabilization, while also arresting cellular processes and preventing degradation, which helps maintain the stability of light scatter profiles and fluorescent signals. Therefore, 100 µL of IC fixation buffer was added instead of resuspending, and the cells were incubated on ice in the dark for 30 minutes. Then, 1× permeabilization buffer was added, and the sample was centrifuged at 450 × g for 8 minutes. The supernatant was discarded, and the cells were washed in 2 mL of PBS, followed by

another centrifugation at 450 × g for 8 minutes. Finally, the cell pellet was resuspended in 200 µL of PBS.

2.2.4.3 Antibody Panels for Mouse

Adaptive immune panel		
Extracellular markers		
Fluorochrome	**Specificity**	**Dilution**
BUV496	CD4	1:400
BUV395	CD44	1:200
APC	TCRb	1:100
APC-Cy7	CD45.2	1:200
FITC	PD1	1:100
PE	Ly49	1:100
PerCP efluor 710	CD122	1:200
PE-TR	CD127	1:100
BV421	CD62L	1:200
BV650	CD8a	1:100
BV711	CD11b	1:200
BV785	NK1.1	1:400
AF700	CD45 i.v.	12.5ul+200ulPBS
efluor 506	Viability	1:100
Intracellular markers		
PE-Cy7	Foxp3	1:100

Innate immune panel		
Extracellular markers		
Fluorochrome	**Specificity**	**Dilution**
BUV395	CD11c	1:100
FITC	F4/80	1:200
PE-Tx RED (dazzle)	CD206	1:200
PE-Cy7	CD11b	1:400
APC	FceRIalpha	1:100
AF700	iv cd45	12.5ul+200ulPBS

BV421	MHCII	1:400
BV650	Gr-1	1:200
BV785	CD117	1:200
efluor 506	Viability	1:100
Intracellular markers		
PerCP efluor 710	iNOS	1:200
PE	Arg1-PE	1:200
APC-Cy7	CD45	1:400

2.2.4.4 FACS Staining of Human Decidua

1 million cells isolated from the decidua were added to 1 mL PBS in a FACS tube, centrifuged at 450 × g for 8 minutes. Remove the supernatant, and 5 µl of Human TruStain FcX™ was added for 5 minutes. For extracellular staining, each sample was incubated on ice in the dark for 30 minutes with a pre-titrated extracellular antibody panel mix and a viability antibody. The cells were then washed by adding 1 mL PBS, followed by centrifugation at 450 × g for 8 minutes. Cells were fixed with 100 µL IC fixation buffer, and the cells were incubated on ice in the dark for 30 minutes. Next, 1× permeabilization buffer was added, and the sample was centrifuged at 450 × g for 8 minutes. The supernatant was discarded, and the cells were washed in 2 mL PBS, followed by another centrifugation at 450 × g for 8 minutes. Finally, the cell pellet was resuspended in 200 µL of PBS for analysis.

2.2.4.5 Antibody Panels for Human

T cell effector and memory		
Fluorochrome	**Specificity**	**Dilution**
BUV496	CD69	1:200
BV785	CD25	1:16.7
BV711	CD45RA	1:250
BV650	CD3	1:167
BV605	KLRG1	1:100
PE-Cy7	CD39	1:100
PerCP Cy5.5	CD127	1:400

PE-Dazzle 594	CD103	1:200
FITC	CD4	1:200
APC-Cy7	CD27	1:250
AF700	CD8	1:250
efluor 506	Viability	1:250

CD8+ T regulatory subtype		
Fluorochrome	**Specificity**	**Dilution**
BUV395	γδ TCR	1:200
BV785	KIR2DL2/L3	1:200
BV650	CD3	1:167
BV421	KIR3DL1	1:200
AF700	CD8	1:250
APC, AF647	PD1	1:100
efluor 506	Viability	1:250

2.2.5 Mouse Histology

2.2.5.1 Tissue Preparation

After tissue collection, samples were fixed in 4% formalin for 24 hours and then transferred to PBS until paraffin embedding, which was performed by the Pathology Department of University Hospital Regensburg. The embedded tissue was cut into 4 µm-thick sections and mounted onto slides, with two sections per slide. The slides were dried overnight at room temperature.

2.2.5.2 Immunohistochemistry

Paraffin-embedded tissue sections were baked at 60°C for 1 hour, followed by deparaffinization in Roti-Histol (3 × 10 min) and rehydration through a graded ethanol series (100-70%, 5 min each). Slides were then washed in the appropriate buffer (depending on the primary antibody protocol). Antigen retrieval was performed by immersing sections in 1× Citrate buffer and heating in a microwave (800 W) for 5 min until reaching 98°C. After cooling for 10 min and incubation in ice-cold water for 30 min with two additional 5-min buffer washes,

endogenous peroxidase activity was blocked with 3% H_2O_2 for 5 min. Sections were washed three times before proceeding to primary antibody incubation according to the specific staining protocols, as described in the section from 2.2.5.2.1 to 2.2.5.2.4.

2.2.5.2.1 Detection of Leucocytes by CD45 Immunohistochemistry

Tissue sections were blocked with 5% normal goat serum in TBST for 1 hour at room temperature. Sections were incubated overnight at 4°C with CD45 primary antibody (1:1000, DAKO), while negative controls received DAKO alone. After three washes with TBST, sections were incubated with biotinylated goat anti-rabbit IgG (1:200, DAKO) for 1 hour, washed, and then incubated with streptavidin for 1 hour. DAB chromogen/substrate solution was applied for visualization, and development was monitored microscopically. The reaction was stopped by rinsing in distilled water. Sections were counterstained with hematoxylin (1:2 in distilled water) for 30 seconds, rinsed under running water for 15 minutes, dehydrated through graded ethanol (70-100%), cleared in Roti-Histol (3 × 5 min), and mounted with xylol-based medium.

2.2.5.2.2 Detection of Macrophages by F4/80

The procedure was similar to CD45, with the following modifications: TBS was used as the washing buffer, and the blocking solution consisted of 1% BSA and 20% normal goat serum, diluted in DAKO. The primary antibody was F4/80 (1:800, diluted in DAKO), the secondary antibody was goat anti-rat Biotin (1:1000, diluted in DAKO).

2.2.5.2.3 Detection of $CD8^+$ T cells by CD8

Except for the primary antibody, which was CD8 (1:50, diluted in DAKO), all other steps and reagents were the same for CD45 staining.

2.2.5.2.4 Detection of CEACAM1 Expression

Except for the primary antibody, which was CEACAM1 (1:8000, diluted in DAKO), all other steps and reagents were the same for CD45 staining.

2.2.5.2.5 Antibodies for Mouse Immunohistochemistry

Reagent	Dilution	Clone
Anti-CD45 antibody	1:1000	Polyclonal
Anti-Mouse F4/80 antibody	1:800	Cl:A3-1
CD8α (D4W2Z) XP® Rabbit mAb	1:50	D4W2Z
CEACAM1	1:8000	Provided by UKE
Goat Anti-Rat IgG H&L (Biotin)	1:1000	Polyclonal
Goat Anti-rabbit IgG H&L (Biotin)	1:200	Polyclonal

2.2.6 Human Histology

2.2.6.1 Tissue Preparation

Human placentas were obtained at delivery from the Clinic St. Hedwig of the Order of St. John, Department of Gynecology and Obstetrics, University Hospital Regensburg, Germany. A placental tissue sample (~2 cm × 2 cm) was collected from the central region of the placenta and fixed in 4% formalin for 24 hours and then transferred to PBS until paraffin embedding, which was performed by the Pathology Department of University Hospital Regensburg. The embedded tissue was cut into 4 µm-thick sections and mounted onto slides; the number of sections on a slide depends on the size of the tissue. The slides were dried overnight at room temperature.

2.2.6.2 Immunohistochemistry

The deparaffinization process and antigen retrieval were performed as previously described in section 2.2.5.2. Subsequently, the following procedures were performed as described in the section from 2.2.6.2.1 to 2.2.6.2.4.

2.2.6.2.1 Detection of $CD8^+$ T cells

Staining was performed as described in Section 2.2.5.2.1, using PBS as washing buffer, 1% BSA, and 20% normal goat serum in DAKO as the blocking solution. The primary antibody was CD8 (1:400, DAKO), and the secondary antibody was goat anti-rabbit IgG (1:200, DAKO).

2.2.6.2.2 Detection of Macrophage by CD68

Except that the blocking solution was 5% Normal Goat Serum in TBST, the primary antibody was CD68 (1:400, diluted in DAKO), and the washing buffer was TBST, all other steps and reagents were the same with human CD8 staining.

2.2.6.2.3 Detection of Endothelial Cells by CD31

Except that the primary antibody was CD31+ (1:1000, diluted in DAKO) and the secondary antibody was Goat anti-mouse IgG (H+L), Biotin(1:1000 in DAKO), all other steps and reagents were the same as human CD8 staining.

2.2.6.2.4 Detection of CXCL10

Except that the blocking solution was 1% BSA + 20% normal Donkey serum in DAKO, the primary antibody was CXCL10 (1:50, diluted in DAKO), and the secondary antibody was Donkey anti-Goat IgG (H+L), Biotin(1:2000 in DAKO); all other steps and reagents were the same as human CD8 staining.

2.2.6.2.5 Antibodies for Human Immunohistochemistry

Reagent	Dilution	Clone
CD8 Monoclonal Antibody (SP16)	1:400	SP16
CXCL10 Polyclonal Antibody	1:50	Polyclonal
CD68 (D4B9C) XP® Rabbit mAb	1:400	D4B9C
CD31 Monoclonal Antibody	1:1000	JC/70A
Goat Anti-rabbit IgG H+L (Biotin)	1:200	Polyclonal
Donkey anti-Goat IgG H+L (Biotin)	1:2000	Polyclonal

Goat anti-Mouse IgG H+L (Biotin)	1:1000	Polyclonal

2.2.6.3 Masson-Goldner Trichrome Staining

Paraffin-embedded slides were baked at 60°C for 1 hour, deparaffinized in Roti-Histol (3 × 10 min) and rehydrated through graded ethanol (100-70%). Sections were washed in distilled water and sequentially stained with Mayer's hematoxylin (3 min, rinsed 15 min), Xylidin Ponceau (2 min), phosphotungstic acid/Orange G (1 min), and Light Green Solution (3 min), with brief dips in 1% glacial acetic acid between steps. Slides were dehydrated through ascending ethanol (70-100%), cleared in Roti-Histol (3 × 5 min), and mounted with a xylene-based medium.

2.2.6.4 Immunofluorescence

The deparaffinization process and antigen retrieval were carried out as previously described in section 2.2.5.2. Subsequently, the following procedures were performed as described in the section from 2.2.6.4.1 to 2.2.6.4.2.

2.2.6.4.1 Colocalization of α-Smooth Muscle Actin (αSMA) and VCAM1

Tissue sections were blocked with 1% BSA, 20% normal donkey serum, and 20% normal goat serum in DAKO for 1 hour at room temperature. Sections were incubated overnight at 4°C with a primary antibody mix (αSMA 1:1000, VCAM1 1:1000, DAKO), while negative controls received DAKO alone. All subsequent steps were performed protected from light. After three 5-minute TBST washes, sections were incubated with secondary antibodies (Donkey anti-mouse AF488, 1:200 + Goat anti-rabbit AF647, 1:200 each in DAKO) for 1 hour, washed, and counterstained with Hoechst 33342 (1:1000, 5 min). Slides were washed and mounted with a water-based medium.

2.2.6.4.2 Colocalization of αSMA and CD8

Except that the primary antibody mix was 1:1000 αSMA and 1:400 CD8, diluted in DAKO, all other steps and reagents were the same in Colocalization of αSMA and VCAM1 as mentioned above.

2.2.6.4.3 Antibodies for Human Immunofluorescence

Reagent	Dilution	Clone
Alpha-Smooth Muscle Actin Monoclonal Antibody	1:1000	1A4
VCAM-1 (CD106) Recombinant Rabbit Monoclonal Antibody	1:1000	SA05-04
Goat Anti-Rabbit IgG H&L (Alexa Fluor® 647) preabsorbed	1:200	Polyclonal
Donkey Anti-Mouse IgG H&L (Alexa Fluor® 488)	1:200	Polyclonal

2.2.7 Gene Expression Analysis

2.2.7.1 RNA Extraction

Prepared a 2 ml sterile tube containing beads (6 large beads + 0.6 g small beads) and added 700 µl of QIAzol Lysis Reagent. Placed a ~5 x 5 mm decidua sample into the tube. Using the Precellys 24, program it to run at 6500 rpm for 3 cycles of 30 seconds each, until the tissue is fully homogenized. Liquid nitrogen was supplied to the Precellys system throughout the process to maintain a low-temperature environment. After homogenization, pipetted the lysate into a new sterile 1.5 ml Eppendorf tube. Added 100 µl of gDNA Eliminator solution, shaking for 15 seconds to mix thoroughly, then added 180 µl of chloroform and shook for another 15 seconds. Incubated the tube at room temperature for 5 minutes. Next, centrifuge the mixture at 12,000 × g for 15 minutes at 4℃. The sample was separated into three phases: the upper aqueous phase (~400 µl), which contained RNA, was transferred into a new sterile 1.5 ml Eppendorf tube. Added 400 µl of 70% ethanol and mixed by pipetting up and down. Transferred the mixture to a spin column placed in a 2 ml collection tube and centrifuged at 8000 × g for 30 seconds at room temperature, then discarded the flow-through. Added 700 µl of Buffer RWT to the spin column, centrifuged at 8000 × g for 15 seconds, and discarded the

flow-through. Then, added 500 µl of Buffer RPE to the spin column, centrifuged at 8000 × g for 15 seconds, and discarded the flow-through. Repeated with another 500 µl of Buffer RPE, centrifuged at 8000 × g for 2 minutes, and discarded the flow-through. Placed the spin column in a new 2 ml collection tube and centrifuged at 14,000 × g for 1 minute at room temperature to dry the membrane. Finally, placed the column in a new 1.5 ml Eppendorf tube, added 50 µl of RNase-free water directly to the membrane, and centrifuged at 8000 × g for 1 minute at room temperature to collect RNA.

2.2.7.2 cDNA Synthesis (Reverse Transcription)

First-strand complementary DNA (cDNA) was synthesized from 1 µg of total RNA using the High-Capacity cDNA Reverse Transcription Kit (Applied Biosystems, Thermo Fisher Scientific, Foster City, CA, USA), according to the manufacturer's protocol. The resulting cDNA was diluted to 5 ng/µL with nuclease-free water and stored at -20°C prior to qPCR analysis.

2.2.7.3 Quantitative Polymerase Chain Reaction (qPCR)

Gene expression was quantified by qPCR using specific TaqMan® primers and probes (listed in the material section) and Universal PCR Master Mix (4324018, Thermo Fisher Scientific) on a QuantStudio™ 5 Real-Time PCR System (Thermo Fisher Scientific). Each qPCR reaction was performed in a total volume of 10 µL, containing 1 µL of diluted cDNA, 0.5 µL of each primer, 5 µL of Taqman Universal Master mix, and 3.5 µL of nuclease-free water.

The thermal cycling conditions were as follows: an initial UNG incubation for carryover prevention at 50°C for 2 minutes, followed by polymerase activation and initial denaturation at 95°C for 10 minutes. This was succeeded by 40 cycles of denaturation at 95°C for 15 seconds and a combined annealing/extension step at 60°C for 1 minute, during which fluorescence data were acquired. A melt curve analysis was performed at the end of each run to confirm the specificity of the amplification product. All samples were run in triplicate, and a no-template control was included in one run.

2.2.8 Data analysis

2.2.8.1 Flow Cytometry

Flow cytometry data acquisition was performed using a BD LSRFortessa Cell Analyser, and analysis was conducted using FlowJo version 10. Individual cell populations were identified through manual gating, and data visualization was primarily performed using dot plots and histograms generated in FlowJo. Meanwhile, bar plots were created using GraphPad Prism 10 for further representation of the data.

2.2.8.2 Immunohistochemistry

Tissue slides were scanned by the Pathology Department at University Hospital Regensburg. Image analysis was performed using SlideViewer 2.6. Positive cell numbers and $CD31^+$ vessels were manually counted in three representative areas per slide; the final cell density was calculated as the mean of three counts (counts/area). The CEACAM1 mean gray value was measured using ImageJ 1.53t (175). The Mean Gray Value was measured within 3 manually drawn Regions of Interest (ROIs). The final signal f was recorded as the average of these three measurements.

2.2.8.3 Immunofluorescence

Tissue sections were imaged using the FLUOVIEW FV3000 Confocal Laser Scanning Microscope, and quantitative analysis was performed using ImageJ 1.53t and Qupath (Version 0.5.1) (176). To assess αSMA and VCAM-1 coverage, vessels were manually outlined along their entire circumference (360°) through the smooth muscle cell layer and the endothelium, respectively, as an ROI in Qupath. Gray value was measured at each point (1 pixel) along this line in ImageJ. Points showing signal intensities over the predefined thresholds for αSMA and VCAM1 (each with separate thresholds) were determined as positive. The percentage of positive points relative to the total number of measured points was then calculated. αSMA and VCAM1 were analyzed in three vessels per sample, and the final coverage percentage was

calculated as the mean of the three percentages. The FV3000 confocal microscope was funded by a grant (INST 89/506-1 FUGG, 91b GG) from the German Research Foundation.

2.2.8.4 qPCR

qPCR data were analyzed using QuantStudio Design & Analysis. Gene expression levels were quantified based on the ΔΔCt method, with housekeeping gene (mouse decidua: Rn18s and RPL13A, human decidua: Ubc and Ywhaz (177,178) serving as an internal reference. Data visualization was carried out using bar plots, generated in GraphPad Prism 10, to represent relative expression differences. The expression of target genes was normalized to the expression of the housekeeping gene. The fold change for mouse samples was calculated relative to the control group, while for human samples, it was calculated relative to the normal BMI control women.

2.2.9 Statistics

Statistical analyses were performed using GraphPad Prism version 10 and SPSS version 29.0.0.0 (241). For comparisons between two groups, either a non-parametric Mann-Whitney test or a parametric t-test was applied, depending on the normality of data distribution. One-way ANOVA was applied for comparisons involving more than two groups with a single variable. Two-way ANOVA was used to assess interactions between BMI category (normal vs. high) and pregnancy condition (normal pregnancy vs. preeclampsia). Spearman correlation analysis was performed to evaluate associations between experimental and clinical data. Statistical significance was denoted as follows: *$p < 0.05$; **$p < 0.01$; ***$p < 0.001$; ****$p < 0.0001$.

3. Results

3.1 Human Late-onset Preeclampsia (LOPE)

A total of 64 pregnant women were enrolled in this study. The control group consisted of women with healthy term pregnancies, who were randomly selected from BMI-matched normotensive women. Considering that elevated pre-pregnancy BMI is an independent risk factor for preeclampsia (170,171), we split the participant data according to pre-pregnancy BMI. Women with a BMI between 18.5 and 25 kg/m² were considered to have a normal weight, while those with a BMI ≥ 25 kg/m², including individuals with obesity (BMI ≥ 30 kg/m²), were generally defined as overweight (69). The detailed clinical characteristics of these four patient groups are summarized in Table 5. These data were collected by Ms. Luisa Maisch. There were no significant differences in basic maternal characteristics, including maternal age, height, and pre-pregnancy weight (normal BMI control vs. normal BMI preeclampsia, and high BMI control vs. high BMI preeclampsia). Similarly, laboratory data of systemic inflammation, such as peripheral leukocyte counts and C-reactive protein (CRP) levels, were not significantly different between the groups. As expected, patients with preeclampsia exhibited significantly higher systolic and diastolic blood pressures compared to their respective normotensive controls. Furthermore, preeclampsia was associated with a significantly lower gestational age at delivery and reduced fetal birth weight in both the normal and high BMI preeclampsia.

Table 5. Clinical maternal patient basic information. Values presented as medians (IQR) or rates (n). *p < 0.05; **p < 0.01; ***p < 0.001.

	Control (BMI < 25) (n = 17)	**Preeclampsia (BMI < 25) (n = 16)**	**Control (BMI≥ 25) (n = 15)**	**Preeclampsia (BMI ≥ 25) (n = 16)**
Age (years)	34 (29-37)	31,5 (29-36)	32 (28-36)	33,5 (29-37)
SBP (mmHg)	115 (111-138)	140 * (128-156)	123 (119-136)	140 ** (130-150)
DBP (mmHg)	74 (70-80)	92 (80-104) **	73 (58-80)	91 (86-100) ***
Weight before pregnancy (kg)	60 (55-66)	60,5 (54-64.5)	92 (78-104)	84,25 (78.3-105.8)

Height (cm)	167 (162-170)	168 (163.5-170)	165 (160-173)	164 (160-172)
BMI (kg/m2)	22.32 (20.2-23.6)	21.71 (20.5-22.9)	32.18 (28.1-36.3)	32.13 (26.7-39.3)
Leukocytes (/nl)	8.5 (8-12.8)	8.7 (7.2-10.4)	11.3 (9.4-13.8)	9.85 (9-10.5)
sFlt-1/PlGF	48.79 (15.9-93.9) [n=4]	135.75* (87.5-188.1)	21.12 [n=2]	125.02 (84.4-221.4)
CRP (mg/l)	2 (1-5)	7 (1.5-17.5)	9 (5-15)	5 (3-11)
Protein in spot urine (g/l)	/	0.6 (0.11-2.15)	/	0.1 (0.1-1.2)
Gestational age (weeks+days)	39w1d (38w3d – 40w5d)	37w1d *** (36w – 38w4d)	39w2d (38w5d – 41w)	37w4d * (36w5d – 40w)
Birth weight (g)	3410 (3177-4037)	2790 ** (2332-3375)	3490 (3293-3749)	2975 ** (2060-3351)
10% below 10th percentile birthweight	5.9% (1)	6.3% (1)	0% (0)	18.8% (3)
AC percentile	48 (34-77)	44 (21-68)	59 (24-73)	22 ** (0.07-31)
HC /AC percentile	41.5 (16.5-58.5)	48 (20-76)	38 (22-73)	75 * (63-99.5)
Umbilical artery PI	0.87 (0.73-0.97)	0.97 * (0.88-1.05)	0.81 (0.7-0.98)	0.82 (0.73-1.11)

AC: abdominal circumference. HC: head circumference. PI: pulsatility index.

3.1.1 Human Late-onset Preeclampsia Decidua

In this study, we chose to focus our investigation on the decidua rather than the placental chorionic villi to elucidate the role of maternal $CD8^+$ T cells in the pathogenesis of preeclampsia. The decidua constitutes the critical maternal-fetal interface, the primary site where maternal immune cells are in direct contact with semi-allogeneic fetal-derived extravillous trophoblasts (179). It is at this immunological center that the foundational processes of maternal immune tolerance are established (14). Dysregulation in this tolerance, which is hypothesized to be one of the mechanisms in preeclampsia, might be observed within the decidual immune cell populations.

Furthermore, here we focus on late-onset preeclampsia; the understanding of the pathogenesis of late-onset preeclampsia remains more elusive, and hence the focus of the current research. Evidence pinpoints that rather than impaired placentation, a limited maternal blood supply of the uteroplacental system results in placental hypoxemia (180) and, consequently, in late onset of preeclampsia. The decidua represents the crucial microenvironment where this maternal systemic maladaptation directly confronts the fetoplacental unit. Analyzing the decidual immune milieu thus provides a direct window into the local immunological consequences of the maternal side.

Critically, the villous stroma contains fetal immune cells, such as Hofbauer cells (placental macrophages) (181) and fetal T cells (182). The presence of these fetal-derived immune cells would inevitably confound the analysis of the purely maternal immune response. The decidua, being maternal tissue, allows for a more direct and unambiguous assessment of the maternal local immune cell populations central to our investigation. Thus, to specifically assess the maternal immune response involved in the pathological events of preeclampsia, the decidua represents the most relevant and informative tissue for our analysis.

3.1.1.1 Decidual $CD8^+$ T Cell Decrease in Preeclampsia

We first aimed to assess the decidual $CD8^+$ T cell compartment in the context of preeclampsia. We quantified the $CD8^+$ T cell density in decidual tissues obtained at delivery from preeclampsia patients and BMI-matched normotensive patients, who served as controls. Immunohistochemical analysis revealed scattered infiltration of $CD8^+$ T cells in the decidual stroma of both preeclamptic and control patients (Figure 7, A). Notably, $CD8^+$ T cell density was significantly reduced in the decidua of preeclampsia patients with normal BMI compared to their normotensive counterparts (Figure 7, B).

Considering that elevated pre-pregnancy BMI is an independent risk factor for preeclampsia (170,171), and the high prevalence of overweight or obesity among individuals with preeclampsia (183,184), we also evaluated $CD8^+$ T cell density in a cohort of individuals with

BMI ≥ 25. Interestingly, a similar reduction in decidual CD8⁺ T cell density was also detected in the high-BMI preeclampsia patients (Figure 7, B), suggesting that decreased decidual CD8⁺ T cell density is a general feature of preeclampsia, independent of the maternal BMI. And CD8⁺ T cell density correlated inversely with sFLT1/PlGF ratio (Figure 7, C) within the complete preeclampsia cohort evaluated independently of the BMI. However, a similar analysis of the corresponding placental villi revealed no such difference (Appendix 1, Figure 1).

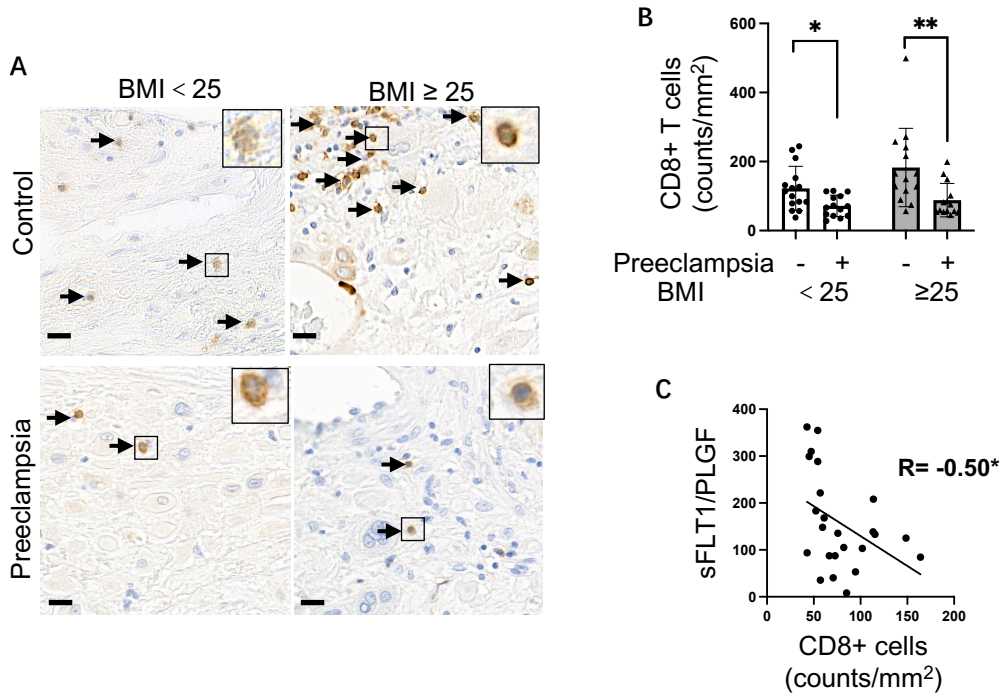

Figure 7. Decidual CD8⁺ T Cell Density is significantly reduced in late-onset preeclampsia, independent of the patient's BMI. A: CD8⁺ T cells of control and preeclampsia patient decidua were assessed by immunohistochemistry, Scale bar=20μm. B: Comparison of the density of CD8⁺ T cells in each group. C: Correlation between decidual CD8⁺ T cell density and maternal serum sFLT1/PlGF in preeclampsia patients (B: Data are presented as mean ± SEM. * $p < 0.05$, ** $p < 0.01$, statistical comparisons performed by two-way ANOVA with Tukey's post-hoc test. C: R values, as analyzed by Spearman correlation analysis. *$p<0.05$, ** $p < 0.01$).

3.1.1.2 Phenotyping of Human Decidual CD8⁺ T Cells in Preeclampsia

The patient information in this part was collected by Ms. Paula Billmayer. There were no significant differences in basic maternal characteristics, including maternal age, height, and pre-pregnancy BMI. Similarly, laboratory data of systemic inflammation, such as peripheral leukocyte counts and CRP levels, were not significantly different between the groups. As

expected, patients with preeclampsia exhibited significantly higher sFLT1/PlGF, systolic and diastolic blood pressures compared to their respective normotensive controls (Appendix 2).

To present some insights on the decidual $CD8^+$ T cell subpopulations in healthy and preeclampsia patients, we included, as follows, a preliminary analysis of our ongoing characterization of CD8+ T cell subsets by flow cytometry. Briefly, leukocytes were isolated from decidual tissue harvested from placentas immediately following delivery, stained with appropriate antibodies, and analyzed by flow cytometry. The gating strategy (Figure 8, A) was designed to identify naive $CD8^+$ T cells, Trm, Tcm, Tpm, Tem, as well as terminally differentiated effector memory cells re-expressing CD45RA (Temra), and effector T cell subsets, including early effector cells (EEC), short-lived effector cells (SLEC), and memory precursor cells (MPEC). However, the flow cytometric analysis did not reveal any significant changes in the differentiation status of the decidual $CD8^+$ T cells (Figure 8, B).

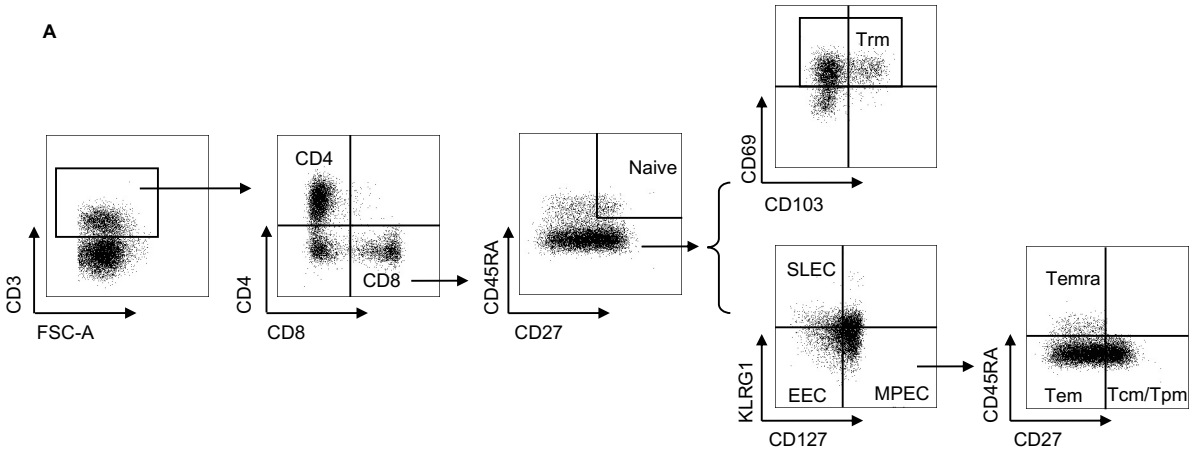

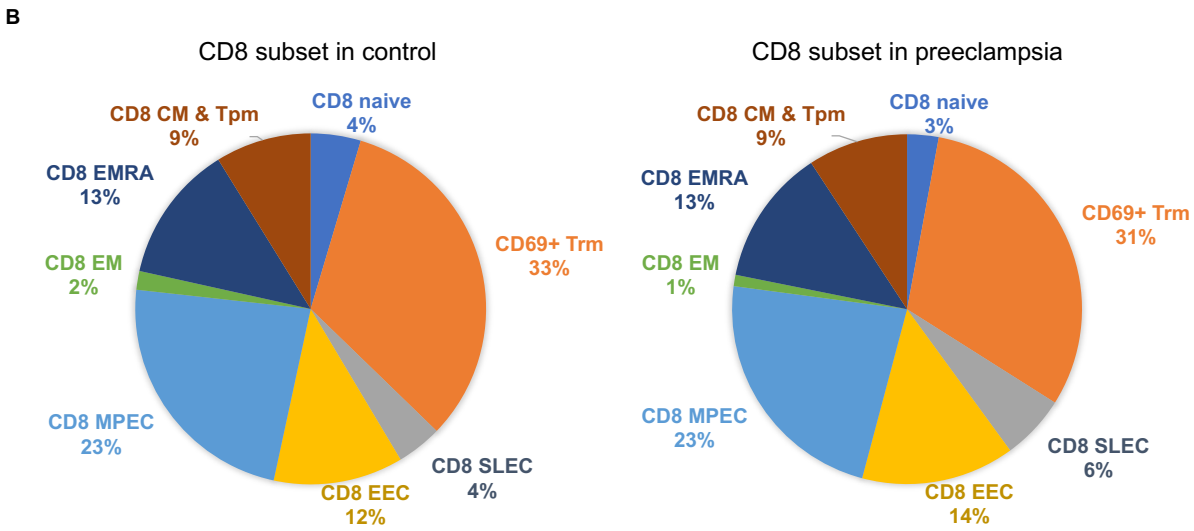

Figure 8. Phenotypic Analysis of Decidual CD8⁺ T Cell Subpopulations in Patients with Preeclampsia. A: Gating strategy for identifying CD8⁺ T cell subpopulations after prior gating on living cells. Dot plots are representative of staining in the decidua. B: Pie charts show the proportion of CD8⁺ T cell subsets in decidua. Control n=21, preeclampsia n=6.

Subsequently, we proceeded to analyze the functional status of decidual CD8⁺ T cells. Previous literature has demonstrated that CD8⁺CD122⁺ regulatory T cell subsets in mice play a role in promoting placental angiogenesis during pregnancy (149). This prompted our investigation into CD8⁺ T cell populations with known regulatory functions in human pregnancy.

One key group of markers for regulatory T cells includes inhibitory receptors. In mice, the Ly49 family of C-type lectin-like receptors serves as a specific surface marker for a regulatory CD8⁺ T cell subset (185). The functional human counterparts to the mouse Ly49 family are the killer-cell immunoglobulin-like receptors (KIRs) (186). Therefore, we focused on CD8⁺ T cells expressing KIRs, particularly the major subtypes KIR3DL1 and KIR2DL3 (145). Additionally, we analyzed the expression of PD-1, as CD8⁺PD1⁺ T cells have also been identified as a subset with immunomodulatory capabilities (187).

Our flow cytometric analysis revealed no significant differences in the median fluorescence intensity (MFI) for KIR2DL2/L3 and KIR3DL1 on CD8⁺ T cells between the study groups (The data are not shown). However, we did observe a trend towards an increased frequency in the

$CD8^+KIR3DL1^+$ T cell subset in preeclampsia. Furthermore, the frequency of $CD8^+PD\text{-}1^+$ T cells exhibited a decreasing trend in the preeclamptic group (Figure 9, A-C).

Based on reports identifying $CD8^+\gamma\delta TCR^+$ T cells (7) and $CD8^+CD39^+$ T cells (188,189) as additional regulatory subsets, we extended our analysis to these populations. However, no significant differences were observed in either their frequency between the two groups (Figure 9, D and E). The regulatory subset gating strategy was based on fluorescence minus one (FMO) control (Appendix 6).

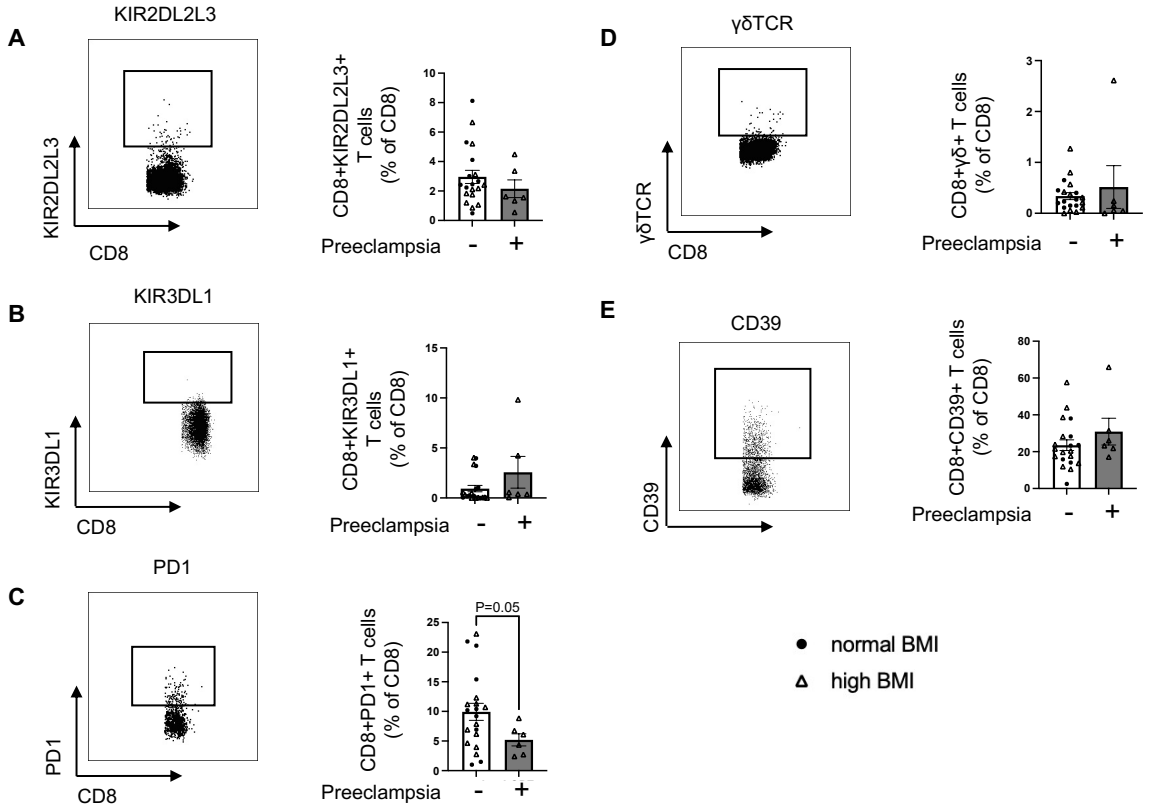

Figure 9. Phenotypic Analysis of Decidual $CD8^+$ T Cell Regulatory Subpopulations in Patients with Preeclampsia. All gating strategy for identifying $CD8^+$ T cell regulatory subpopulations after prior gating on living cells, followed by $CD3^+$ and $CD8^+$ T cells. Dotplots are representative of staining in the decidua. Percentage of each $CD8^+$ T cell population in decidua (A: $KIR2DL2L3^+$, B: $KIR3DL1^+$, C: $PD1^+$, D: γδTCR, E: $CD39^+$). Statistical analyses were performed with the Mann-Whitney U test (all control vs. all preeclampsia). Control n=20, preeclampsia n=6.

3.1.1.3 Gene Expression Analysis of Factors Affecting CD8$^+$ T Cells in the Decidua

To investigate potential mechanisms for the observed reduction in decidual CD8$^+$ T cells, we next performed qPCR to analyze the local gene expression of key factors involved in T cell survival, proliferation, and migration.

3.1.1.3.1 Dysregulation of Decidual IL-7/CD8$^+$ T Cell Homeostasis in Preeclampsia

We first hypothesized that the reduction in CD8$^+$ T cells could be due to an impaired pro-survival or pro-proliferative environment in the preeclamptic decidua. However, we found no significant differences in the mRNA levels of *TNF* or *IFNG* between preeclamptic and healthy patients (Figure 10, A and B), even though chronic inflammation is a hallmark of the disease (190–192), and these cytokines can promote CD8$^+$ T cell proliferation (135,136). Interestingly, we found that *TNF* was significantly higher in the placental villous tissue of the normal BMI preeclampsia patients compared to controls, suggesting that the inflammatory response in preeclampsia with normal BMI may be predominantly localized to the placental villi rather than the decidua (Appendix 1, Figure 2).

Similarly, no changes in the decidual expression of *IL7* or *IL15*, two cytokines critical for T cell homeostasis and survival (133,134), were found between preeclamptic and healthy pregnancy (Figure 10, C and D). In fact, IL-7 expression correlated significantly with CD8$^+$ T cell density in normotensive pregnancy in general (Figure 10, E), but most strongly in those with BMI < 25 (Table 6). In contrast, in preeclampsia, the density of CD8$^+$ T cells did not correlate with *IL7* levels, indicating a dysregulation of local CD8$^+$ T cell responses to this homeostatic cytokine in the decidua in the frame of preeclampsia.

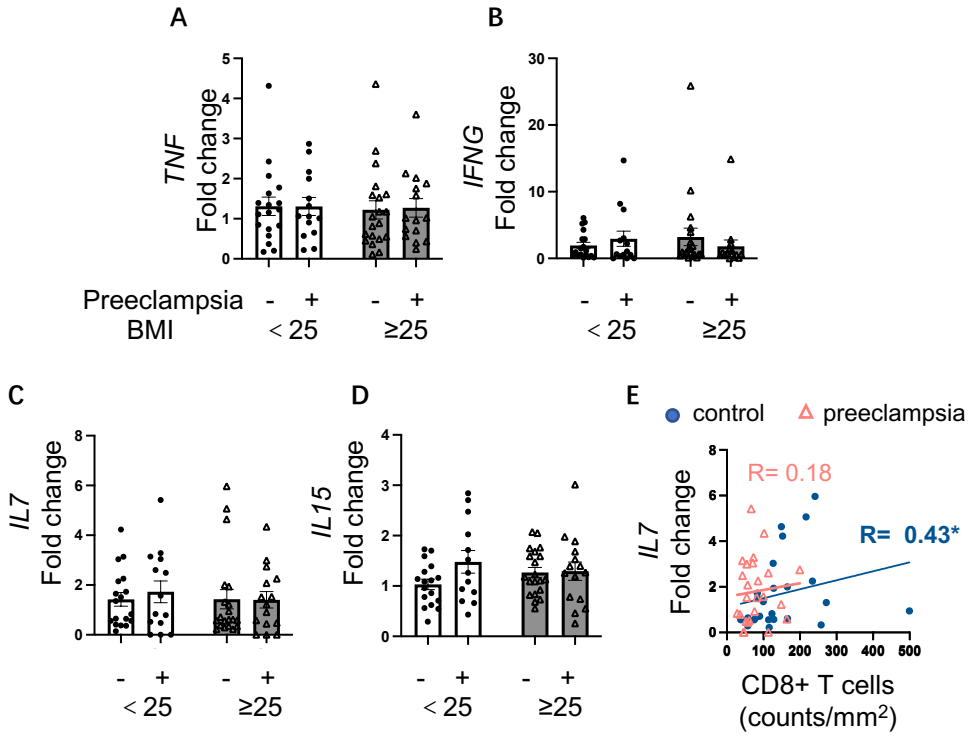

Figure 10. Decidual proliferation and survival-related cytokines stay unchanged in Late-onset Preeclampsia. A-D: qPCR mRNA analysis of *TNF, IFNG, IL7,* and *IL15* in normal BMI (<25) and high BMI (≥25) of control and preeclamptic patient decidua at term. H: Correlation analysis between decidual CD8+ T cell density and *IL7* mRNA level of control and preeclamptic patients. (A-D: Data are presented as mean ± SEM. * p < 0.05, **p < 0.01, statistical comparisons performed by two-way ANOVA with Tukey's post-hoc test. I: R values, as analyzed by Spearman correlation analysis. *p＜0.05. Each dot represents an individual patient sample.

Table 6. Correlation of *IL7* and CD8⁺ T cell density and selected cytokines. Spearman correlation analysis was performed. Correlation coefficients (R) are indicated. * P < 0.05, ** P < 0.

	IL7			
	Control (BMI<25)	**Preeclampsia (BMI<25)**	**Control (BMI≥25)**	**Preeclampsia (BMI≥25)**
$CD8^+$ T cell density	**0.664***	0.119	0.451	0.346
IL15	**0.686****	-0.272	-0.045	0.254
TNF	**0.564***	0.065	**0.678****	**0.731****
IFNG	**0.589***	0.404	0.420	0.301

Values presented as Correlation coefficients (R)

3.1.1.3.2 Exacerbated CXCL10 Expression in Preeclampsia Decidua is Insufficient to Counteract the CD8$^+$ T cell Deficiency

Disrupted CD8$^+$ T cell migration may contribute to the low cell density observed in preeclampsia. To explore this, we examined endothelial cell adhesion molecules and chemokines involved in vascular interaction and recruitment of T cells. mRNA expression of *ICAM1* and *VCAM1* remained unaltered in the decidua of preeclampsia patients (Figure 11, A-B). In contrast, decidual *ICAM1* expression tended to increase in high BMI compared to normal BMI normotensive pregnancies (Figure 11, A). Immunofluorescence detection of VCAM-1 protein revealed its expression in the decidual stroma and along the endothelial lining of the decidual vessels (Figure 11, C). In fact, VCAM-1 coverage along the endothelial lining was significantly increased in preeclampsia patients with normal BMI, but not with high BMI and preeclampsia (Figure 11, D).

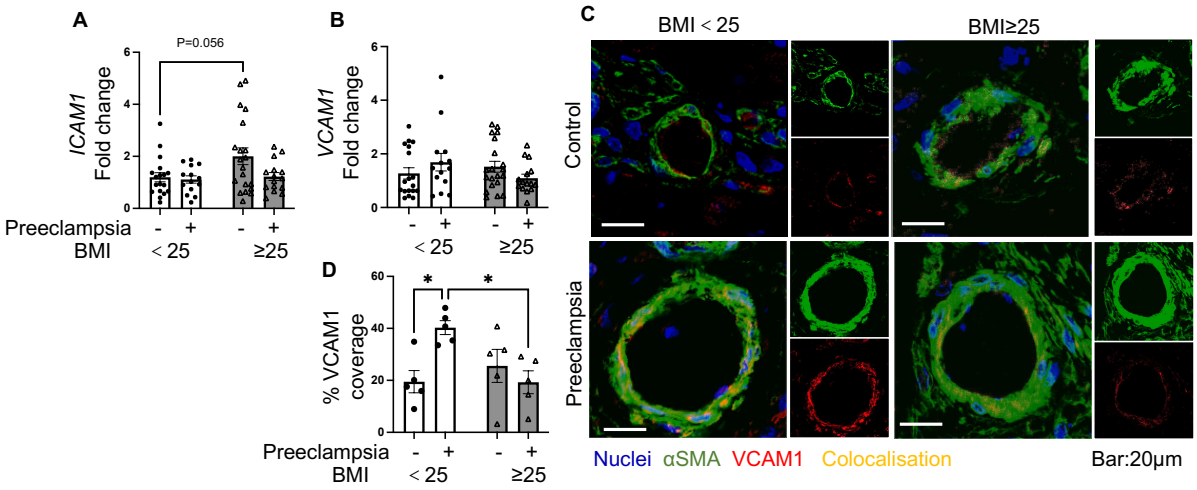

Figure 11. Impaired CD8$^+$ T cell Recruitment Is Associated with Vascular Remodeling in the Decidua of Human Preeclampsia. A: mRNA levels of *ICAM1* assessed by qPCR. B: mRNA levels of *VCAM1* assessed by qPCR. C: Representative immunofluorescence staining of αSMA and VCAM1 expression in decidua, bar=20µm. D: Analysis of VCAM-1 coverage percentage around vessels in each group. (A, B, and D: Data are presented as mean ± SEM. * $p < 0.05$, statistical comparisons performed by two-way ANOVA with Tukey's post-hoc test.

Among chemokines involved in T cell traffic to the decidua, *CCL5* expression did not differ among the groups. In contrast, the expression of *CXCL10* and *CXCL9* was significantly upregulated in the decidua of preeclampsia pregnancies with normal BMI and in high BMI

normotensive pregnancies compared to normotensive normal BMI pregnancies (Figure 12, A-C). Immunohistochemistry served to localize CXCL10 in the decidua, primarily in stromal cells. Higher CXCL10 positivity was observed in normal BMI preeclampsia, as well as in both high BMI control and preeclampsia patients (Figure 12, D), supporting enhanced local expression across these conditions. Meanwhile, our immunohistochemical analysis revealed that a subpopulation of decidual macrophages also expresses CXCL10, as detailed in Appendix 3. Strikingly, *CXCL10* and *ICAM1* mRNA levels correlated with $CD8^+$ T cell density in the decidua of normotensive lean pregnancies. In contrast, in overweight and preeclampsia pregnancies (Figure 12, E and Table 7), $CD8^+$ T cells were not associated with *CXCL10* and *ICAM1*; thus, they remained refractory to these exacerbated migration signals from the tissue.

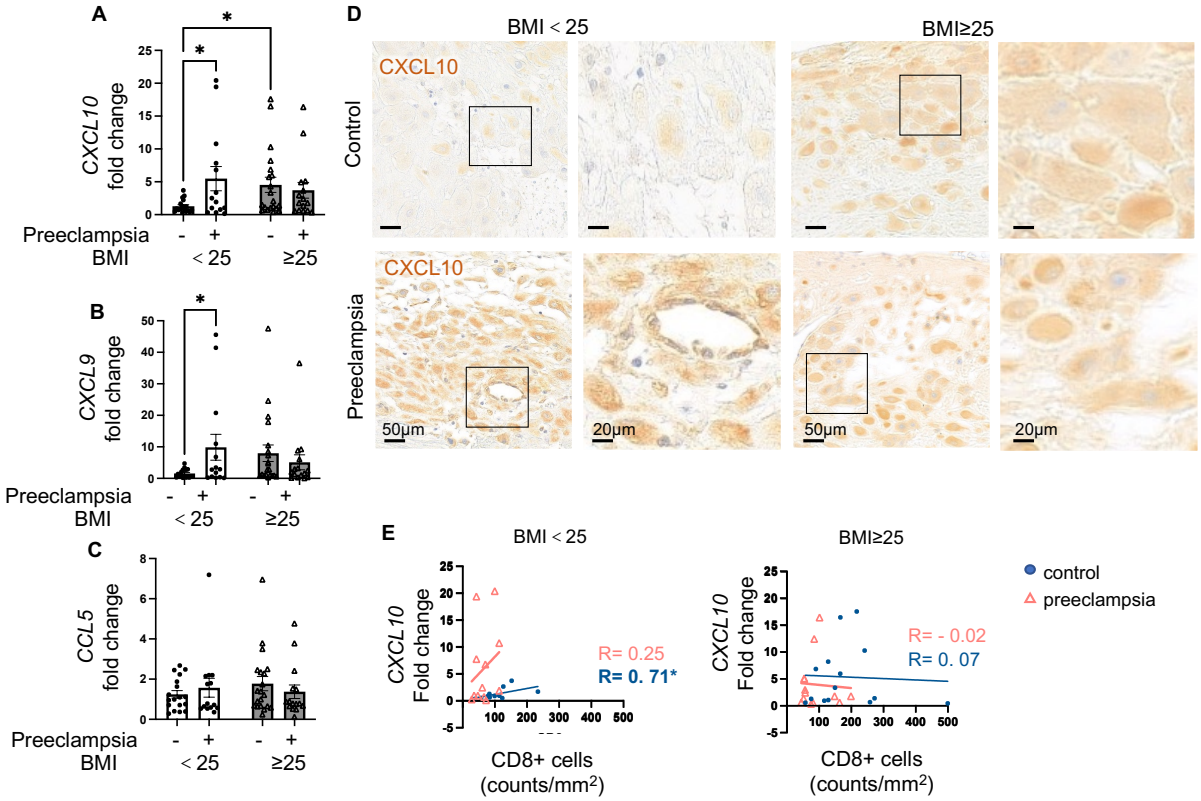

Figure 12. Impaired $CD8^+$ T cell Recruitment Is Associated with *CXCL10* in the Decidua of Human Preeclampsia. A-C: qPCR analysis of *CXCL10, CXCL9, and CCL5* in the decidua of each group. D: Representative immunohistochemistry image showing CXCL10 expression in decidua, bar=20µm. E: Correlation analysis between $CD8^+$ T cell density and *CXCL10.* (A-C: Data are presented as mean ± SEM. * $p < 0.05$, statistical comparisons performed by two-way ANOVA with Tukey's post-hoc test. E: Correlation coefficients (R) upon Spearman correlation analysis between CXCL10 mRNA levels and decidual $CD8^+$T cell density, * $p < 0.05$).

Table 7. The correlation between $CD8^+$ T cell density and mRNA levels of selected chemokines and adhesion molecules in human decidua samples. Spearman correlation analysis was performed. Correlation coefficients (R) are indicated. * P < 0.05

	$CD8^+$ T cell (counts/mm^2)			
	Control (BMI<25)	**Preeclampsia (BMI<25)**	**Control (BMI≥25)**	**Preeclampsia (BMI≥25)**
Chemokines				
CXCL9	0.582	0.154	0.182	0.137
CCL5	0.500	0.042	0.046	0.451
Adhesion molecules				
ICAM1	**0.673***	0.140	0.033	0.341
VCAM1	0.536	-0.175	0.055	0.302

3.1.1.4 Divergent Angiogenesis and Hypoxia Factors in the Preeclamptic Decidua Across Different BMI

Given the central role of angiogenic imbalance in preeclampsia, we evaluated the endothelial marker CD31 (Platelet and Endothelial Cell Adhesion Molecule 1, PECAM1). Although the *PECAM1* remained unchanged at mRNA levels, immunohistochemical analysis revealed that the density of $CD31^+$ vessels was significantly higher in the decidua of preeclampsia patients compared to their respective BMI-matched controls. This increase in vascularization was observed in both normal BMI and high BMI preeclampsia (Figure 13, A to C). Furthermore, we assessed the gene expression of selected angiogenic factors in the decidua and found that only VEGF was reduced in high BMI preeclampsia (Appendix 4). The expression patterns of these angiogenic factors were similar to those observed in placental tissues (Appendix 1, Figure 3).

We next tested the mRNA level of hypoxia-inducible factor 1 alpha (HIF1A), a transcriptional activator inducible by hypoxia and heme oxygenase 1 (HMOX1), responsive to stress, i.e., from hypoxia (193,194). Intriguingly, analysis of *HIF1A* revealed a different pattern between the two preeclampsia subtypes. In normal BMI women, preeclampsia was associated with a marked elevation of *HIF1A*, consistent with a state of tissue hypoxia. In contrast, *HIF1A* levels in high BMI preeclampsia patients were not elevated but were even lower than those in the

normal BMI preeclampsia group (Figure 13, D). In comparison, *HMOX1* tended to increase compared to healthy normal BMI controls. However, no differences were observed among the high BMI cohort (Figure 13, D and E).

Together, these results reveal two distinct pathophysiological conditions: preeclampsia in normal BMI women is characterized by a paradoxical state of increased vascularization coexisting with signs of hypoxia, suggesting the enhanced vasculature might be unable to oxygenate the tissue properly, whereas a similar finding was not observed in high BMI women.

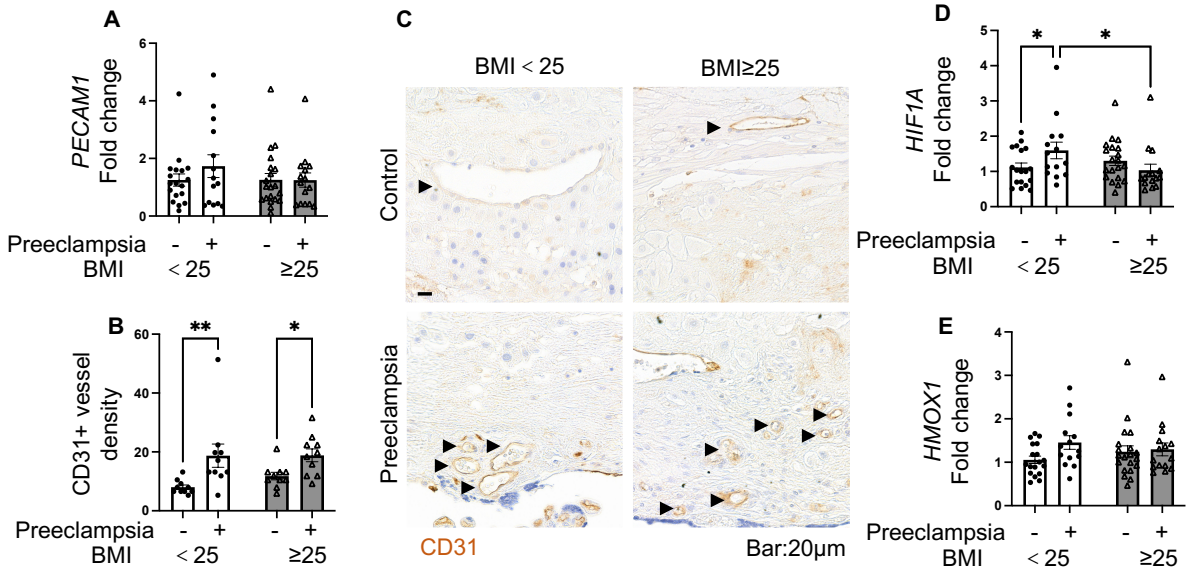

Figure 13. Preeclampsia- and BMI- Associated Changes in Decidua Vascular and Hypoxia-Related mRNA Expression. A: mRNA levels of *PECAM1* assessed by qPCR. B: CD31+ vessel density as quantified in each group. C: Representative immunohistochemistry images of CD31 in the decidua, bar=20μm. D and E: mRNA levels of the *HIF1A* and *HMOX1* by qPCR. Data are presented as mean ± SEM. * $p < 0.05$, **$p < 0.01$, statistical comparisons performed by two-way ANOVA with Tukey's post-hoc test.

3.1.1.5 Preeclampsia and High BMI Affect Decidual Vascular Remodeling

Vascular stiffness is a component of the pathophysiology of preeclampsia (195). Here, we semi-quantified the coverage of the αSMA-positive muscle layer surrounding decidual vessels (Figure 14, A), as indicators for vascular stiffness (78,196).

Consistent with the classical pathophysiology of preeclampsia, decidual vessels from preeclamptic women in the normal BMI group exhibited significantly higher αSMA coverage compared to their healthy, normal BMI counterparts, suggesting a state of vascular remodeling dysregulation (Figure 14, A and B). Intriguingly, we found that a high maternal BMI was also independently associated with increased αSMA coverage. Decidual vessels from high BMI women showed higher αSMA coverage than those from normal BMI women, regardless of a preeclampsia diagnosis (Figure 14, A and B).

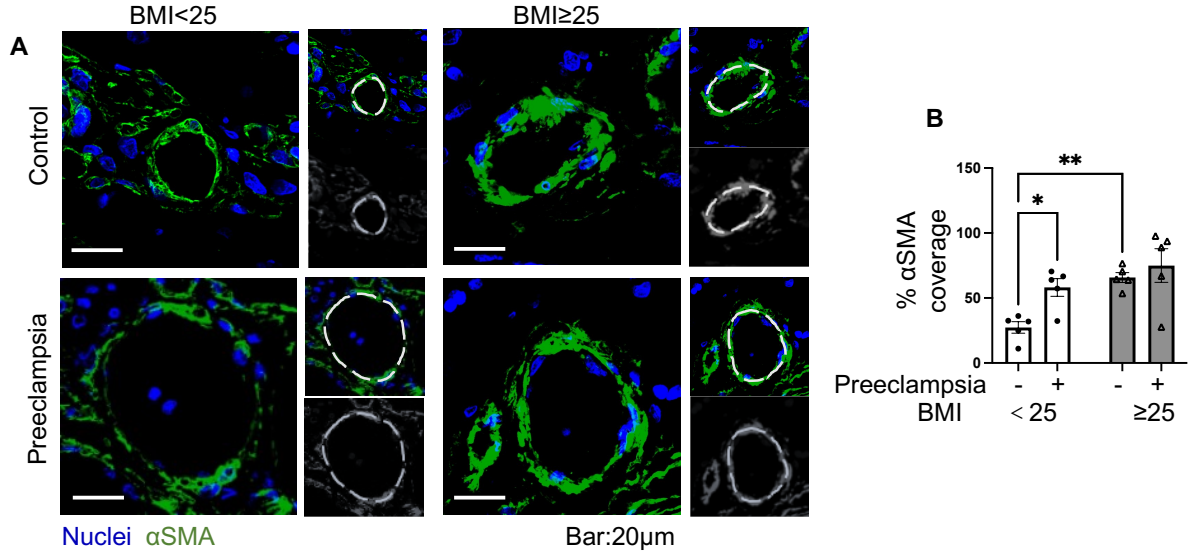

Figure 14. Preeclampsia and BMI- Associated Changes of αSMA coverage in the decidua perivascular area. A: Representative immunofluorescence staining of αSMA in decidual vessels, bar=20μm. The dashed lines indicate the route used to quantify α-smooth muscle actin αSMA coverage. B: Analysis of αSMA coverage percentage around the uterine spiral artery in each group. Data are presented as mean ± SEM. * $p < 0.05$, ** $p < 0.01$, statistical comparisons performed by two-way ANOVA with Tukey's post-hoc test.

3.1.1.6 Increased Decidual Perivascular Collagen Deposition is Associated with Preeclampsia and High BMI

The migration of $CD8^+$ T cells is influenced by the architecture of the tissue's extracellular matrix (ECM), including its network of collagen and fibronectin fibers (197). To assess the ECM condition of the perivascular region in the decidua, we performed Masson-Goldner trichrome staining, which visualizes collagen fibers in blue. In the decidua of the normal BMI control women, collagen deposition around the blood vessels was barely observable, but a more obvious perivascular collagen deposition was found in the decidua of normal BMI preeclampsia

patients, high BMI control women, and high BMI preeclampsia patients (Figure 15). This finding indicates that both preeclampsia and a high BMI are independently associated with an increase in decidual perivascular collagen deposition.

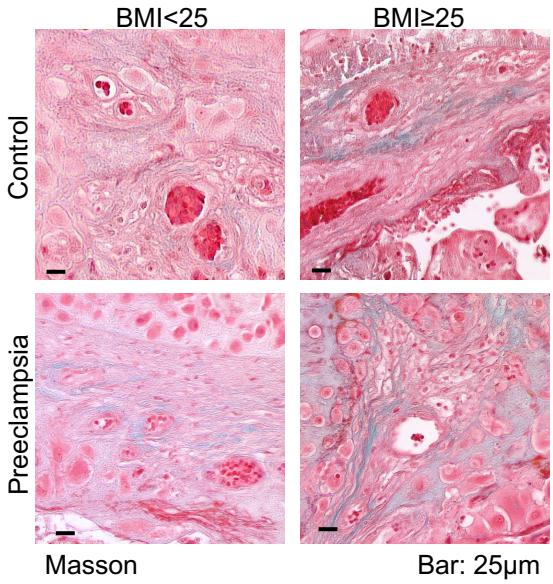

Figure 15. High BMI and Preeclampsia Independently Drive Perivascular Collagen Deposition. Collagen fibers around decidual vasculature were detected by Masson-Goldner trichrome staining in human decidua (Blue staining).

3.1.1.7 Altered Perivascular Localization of Decidual CD8⁺ T Cells in Preeclampsia

In non-preeclamptic women, and particularly in those with a high BMI, $CD8^+$ T cells accumulated around the blood vessels, suggesting recent migration from the circulation (Figure 16). In women with preeclampsia, $CD8^+$ T cells appear more rarely in the vicinity of the dense muscle layer of the vascular smooth muscle (Figure 16). Taken together with our observations of increased decidual perivascular collagen deposition and αSMA coverage, our data suggest that vascular stiffness, characterized by denser muscle layer and more ECM deposition, may interfere with the extravasation of $CD8^+$ T cells, which typically require loose ECM for migration, Intriguingly, while the high BMI control women exhibited similar vascular alterations, their decidual $CD8^+$ T cell density remained unaffected.

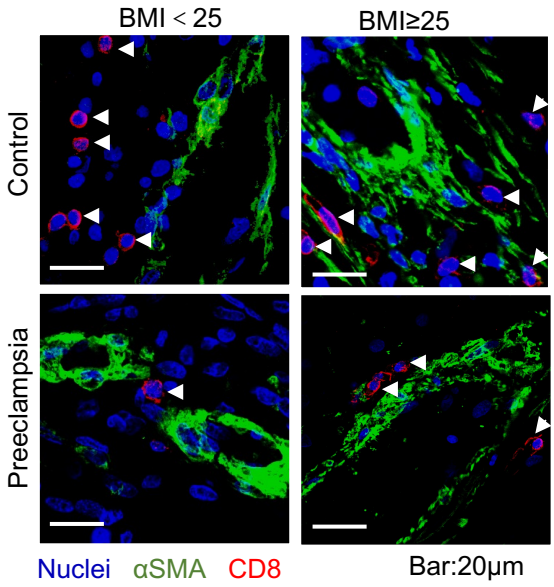

Figure 16. Altered Spatial Distribution of Decidual CD8⁺ T Cells in Preeclampsia. Representative immunofluorescence images of decidual tissue sections from normal BMI and high BMI, control, and preeclamptic women. Sections were stained for the CD8⁺ T cell (red), αSMA (green), and nuclei with DAPI (blue). Bar = 20μm.

3.1.1.8 Disruption and Remodeling of the Decidual CD8⁺ T Cell Correlation Network in Preeclampsia Across Different BMI

In the decidua of normotensive pregnant women, we identified that CD8⁺ T cell has a highly significant and coordinated network. The density of CD8⁺ T cells was positively correlated with the vascular adhesion molecule VCAM-1 coverage (r = 0.709*), *IL7* (r = 0.431*), *CXCL10* (r = 0.438*) and *CXCL9* (r = 0.452*), and *HIF1A* (r = 0.398*). This suggests that in a physiological state, the presence of decidual CD8⁺ T cells is linked to the expression of factors that are related to their migration, survival, and even response to the local tissue environment (Table 8). Interestingly, the significant correlations observed in the control group were not present in the decidua from preeclamptic patients (Table 8).

This loss of correlations may suggest a shift in CD8⁺ T cell regulation, where their presence is no longer tied to a physiological immune network, or those networks might be damaged in the case of preeclampsia (Table 8).

Table 8. Correlation of CD8⁺ T cell density and other variables. Spearman correlation analysis was performed. Correlation coefficients (R) are indicated. * P < 0.05.

	CD8+ T cell (counts/mm^2)	
	Control	**Preeclampsia**
%VCAM1	**0.709***	0.418
Cytokine mRNA		
TNF	0.001	0.116
IFNG	0.217	0.216
IL7	**0.431***	0.177
IL15	0.098	-0.207
Chemokine mRNA		
CXCL10	**0.438***	0.086
CXCL9	**0.452***	0.072
CCL5	0.338	0.210
Adhesion Molecule mRNA		
ICAM1	0.351	0.188
VCAM1	0.302	-0.010
HIF1A	**0.398***	0.002

To further dissect the interplay between decidual CD8$^+$ T cells and the local microenvironment, we performed a correlation analysis stratified by both disease state and maternal BMI. In the normal BMI control women, which represents the physiological baseline, we noticed a highly coordinated network. The density of CD8$^+$ T cells showed positive correlations with *IL7* (r = 0.664*), *CXCL10* (r = 0.709*), *ICAM1* (r = 0.673*), and *PGF* (r = 0.943**) (Table 9). This suggests that in a normal BMI healthy pregnancy, the presence of decidual CD8$^+$ T cells is linked to a network of factors mediating their survival, recruitment, and the local angiogenic environment (Table 9).

However, we found no significant correlations between CD8$^+$ T cell density and these markers in either the preeclampsia group or the high BMI control group. This critical finding suggests that not only the onset of preeclampsia but also high BMI alone in control women have lost the connection to this physiological regulatory network. (Table 9). However, new positive correlations showed up in high BMI preeclampsia, CD8$^+$ T cell density was positively correlated with the VCAM-1 coverage (r = 0.900*) (Table 9). This suggests that the concurrent presence

of a high BMI and preeclampsia is associated with a distinct pattern of immune vascular interactions. Specifically, $CD8^+$ T cell density appears to be linked to markers for endothelial activation , indicating a potentially immune endothelial crosstalk to this subgroup.

Table 9. Correlation of CD8+ T cell density and other variables (data grouped by BMI, control, and preeclampsia). Spearman correlation analysis was performed. Correlation coefficients (R) are indicated. * P < 0.05.

	$CD8^+$ T cell (counts/mm^2)			
	Control (BMI<25)	**Preeclampsia (BMI<25)**	**Control (BMI≥25)**	**Preeclampsia (BMI≥25)**
%VCAM1	0.100	0.700	0.700	**0.900***
Cytokine mRNA				
TNF	0.345	-0.112	-0.077	0.412
IFNG	0.164	0.099	0.121	0.390
IL7	**0.664***	0.119	0.451	0.346
IL15	0.164	-0.077	-0.262	-0.236
Chemokine mRNA				
CXCL10	**0.709***	0.252	0.068	-0.022
CXCL9	0.582	0.154	0.182	0.137
CCL5	0.500	0.042	0.046	0.451
Adhesion Molecule mRNA				
ICAM1	**0.673***	0.140	0.033	0.341
VCAM1	0.536	-0.175	0.055	0.302
HIF1A	0.096	-0.098	0.310	0.297

We further analyzed the correlations between $CD8^+$ T cell density and pre-pregnancy BMI. We found that the density of $CD8^+$ T cells showed a positive trend correlation with normal pregnancy controls but not in preeclampsia (Table 10). This finding again indicates that in the context of preeclampsia, the reduction of $CD8^+$ T cells is a pathological feature, independent of maternal BMI.

Table 10 Correlation of $CD8^+$ T cells with BMI (data grouped by control and preeclampsia). Spearman correlation analysis was performed. Correlation coefficients (R) are indicated. * P < 0.05.

	$CD8^+$ T cell (counts/mm^2)

	Control	Preeclampsia
BMI	0.355 (p=0.06)	0.255

3.1.1.9 Disruption of the Decidual CXCL10 Correlation Network in Preeclampsia

Given that *CXCL10* was upregulated in the decidua of preeclampsia and high BMI women, we next performed a detailed correlation analysis to understand its relationship with $CD8^+$ T cells and other features of the local immune microenvironment.

In the combined normotensive control group (normal BMI + high BMI), *CXCL10* expression showed significant positive correlations with a wide array of factors. These included $CD8^+$ T cell density, maternal BMI, *TNF*, *IFNG*, *IL7*, other chemokines (*CXCL9*, *CCL5*), endothelial adhesion molecules (*PECAM1*, *ICAM1*, *VCAM1*), and the hypoxia marker *HIF1A* (Table 11). CXCL10 can be induced by IFNG and TNF (198,199), which explains the correlation between them; the other correlations suggest that in a normotensive pregnancy, CXCL10 links with maternal metabolic state, local immune environment, and immune cell recruitment. In the preeclampsia group, these associations partially disappeared. Especially, the specific correlations between CXCL10 and both $CD8^+$ T cell density and maternal BMI were completely lost.

To confirm this situation, we further separated the analysis into the four subgroups. This confirmed that the significant positive correlation between CXCL10 and $CD8^+$ T cell density was a unique feature of the normal BMI control women and was absent in all other conditions, including control women with high BMI and all preeclampsia patients (Table 11, Figure 12, E and Figure 17). This selective uncoupling suggests that in preeclampsia, while CXCL10 signal persists, it is no longer effective for the recruitment of $CD8^+$ T cells in the decidua.

Table 11. Correlation of CXCL10 and other variables. Spearman correlation analysis was performed. Correlation coefficients (R) are indicated. * P < 0.05, ** P＜0.01.

	CXCL10	
	Control	**Preeclampsia**
$CD8^+$ T cell density	**0.438***	0.086
BMI	**0.434****	0.204

Cytokines		
TNF	**0.467****	**0.689****
IFNG	**0.642****	**0.651****
IL7	**0.517****	0.318
IL15	0.14	**0.375***
AREG	**0.319***	-0.073
Chemokines		
CXCL9	**0.913****	**0.918****
CCL5	**0.810****	**0.712****
Adhesion molecules		
PECAM1	**0.421****	0.161
ICAM1	**0.552****	**0.655****
VCAM1	**0.657****	**0.536****
HIF1a	**0.676****	**0.370***

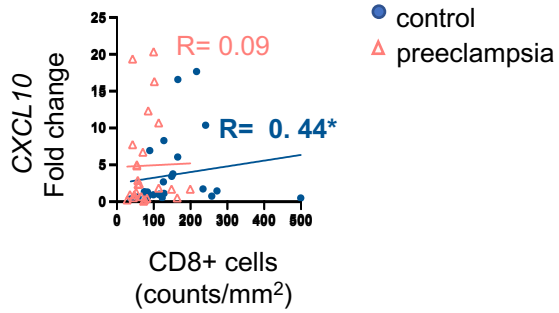

Figure 17. Correlation Analysis between CD8⁺ T Cell Density and *CXCL10*. Data grouped by control and preeclampsia. Spearman correlation analysis was performed. Correlation coefficients (R) are indicated, * $p < 0.05$.

3.1.1.10 Disruption of Decidual IL-7/CD8⁺ T Cell Homeostatic Signaling in Preeclampsia

IL-7 is a key cytokine involved in the regulation of CD8⁺ T cell homeostasis (134). A similar correlation analysis was performed for *IL7*, and a disruption was observed as well. In the combined normotensive control group, *IL7* expression was correlated positively with CD8⁺ T cell density and a broad network of pro-inflammatory cytokines, chemokines, and endothelial adhesion molecules. Mirroring the findings for *CXCL10*, this network was partially absent in

the preeclamptic women. While *IL7* retained its correlations with inflammatory markers *TNF* and *IFNG,* the crucial link between *IL7* and $CD8^+$ T cell density was gone (Table 12). The four-group analysis confirmed this disruption (Figure 18). It revealed that the significant positive correlation between *IL7* and $CD8^+$ T cells was a unique feature of the normal-BMI control group (Table 12, Figure 10, E and Figure 18). This finding suggests that the physiological regulation of the decidual $CD8^+$ T cell is disturbed in preeclampsia, affecting not only their recruitment but also their homeostatic maintenance signals.

Table 12. Correlation of *IL7* and other variables. Spearman correlation analysis was performed. Correlation coefficients (R) are indicated. * P < 0.05, ** P＜0.01

		IL7
	Control	**Preeclampsia**
$CD8^+$ T cell density	**0.431***	0.177
BMI	-0.184	0.052
Cytokines		
TNF	**0.671****	**0.362***
IFNG	**0.484****	**0.390***
IL15	0.288	-0.039
AREG	0.102	-0.172
Chemokines		
CXCL10	**0.517****	0.318
CXCL9	**0.501****	0.277
CCL5	**0.674****	**0.681****
Adhesion molecules		
PECAM1	**0.368***	0.494**
ICAM1	**0.508****	0.342
VCAM1	**0.657****	**0.480****
HIF1a	**0.561****	0.099

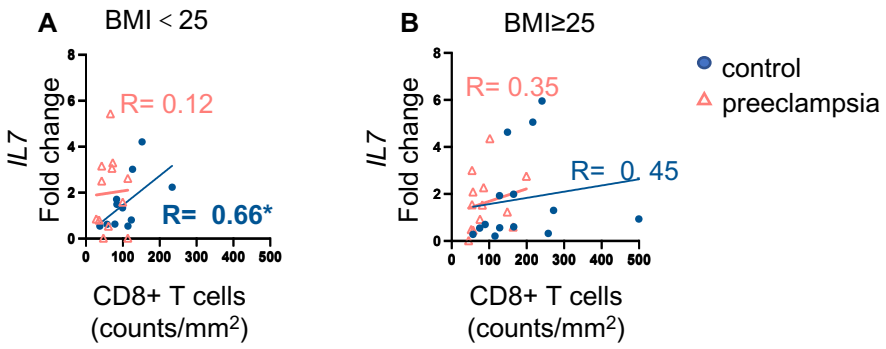

Figure 18. Correlation analysis between CD8⁺ T cell density and *IL7*. A: only contains the BMI<25 data, B: only contains the BMI≥25 data. Spearman correlation analysis was performed. Correlation coefficients (R) are indicated, * p < 0.05.

3.1.1.11 Decidual CD8⁺ T Cell Density Correlates with Fetal Growth Parameters in Preeclampsia

An interesting finding was that significant correlations between decidual CD8⁺ T cell density and fetal growth parameters were observed exclusively in the preeclampsia group; no such associations were found in normotensive controls. Within the preeclampsia patients, the density of CD8⁺ T cells was positively correlated with several fetal growth measurements, including fronto-occipital diameter (FOD) (r = 0.434*), HC (r = 0.397*), AC (r = 0.437*), and birthweight (r = 0.439*). Conversely, the CD8⁺ T cell density was negatively correlated with indicators of potential fetal distress or asymmetric growth. These included the umbilical artery PI (r = –0.445*) and the HC/AC ratio (r = –0.437*) (Table 13). These data may suggest that within the pathological context of preeclampsia, decidual CD8⁺ T cells may affect fetal outcomes.

Table 13. Correlation of CD8⁺ T cell density and parameters of fetal growth. Spearman correlation analysis was performed. Correlation coefficients (R) are indicated. * P < 0.05.

	Decidual CD8⁺ T cells (counts/mm²)	
	Control	**Preeclampsia**
Biparietal Diameter (mm)	0.144	0.123
Fronto-Occipital Diameter (mm)	0.018	**0.434***
Head Circumference (mm)	0.132	**0.397***
Anteroposterior Abdominal Diameter (mm)	-0.146	0.573

Transverse Abdominal Diameter (mm)	-0.080	0.511
Abdominal Circumference (mm)	0.001	**0.437***
Head Circumference / Abdominal Circumference	0.075	**-0.437***
Femur Length (mm)	0.110	0.378
Umbilical Artery Pulsatility Index	-0.258	**-0.445***
Birthweight (g)	0.329	**0.439***

Since the sFLT1/PlGF ratio negatively correlated with $CD8^+$ T cell density in both the control and preeclampsia groups, we next examined the correlation between the sFLT1/PlGF ratio and fetal growth parameters. In the normotensive control group, no significant correlations were observed. In contrast, in the preeclampsia group, the sFLT1/PlGF ratio was significantly correlated with poor fetal growth, including FOD (r = –0.437*, AC (r = –0.484*), and positively correlated with the HC/AC ratio (r = 0.376*) (Table 14). Notably, this pattern is the direct opposite of the correlations observed for $CD8^+$ T cells, which is consistent with the finding that the sFLT1/PlGF ratio is negatively associated with both the density of decidual $CD8^+$ T cells and fetal growth.

Table 14. Correlation of sFLT1/PlGF and parameters of fetal growth. Spearman correlation analysis was performed. Correlation coefficients (R) are indicated. * P < 0.05.

	sFLT1/PLGF	
	Control	**Preeclampsia**
Biparietal Diameter (mm)	0.300	-0.346
Fronto-Occipital Diameter (mm)	0.400	**-0.437***
Head Circumference (mm)	0.400	-0.238
Anteroposterior Abdominal Diameter (mm)	0.500	-0.455
Transverse Abdominal Diameter (mm)	0.100	-0.379
Abdominal Circumference (mm)	0.100	**-.484****
Head Circumference / Abdominal Circumference	-0.300	**0.376***
Femur Length (mm)	0.600	-0.361
Umbilical Artery Pulsatility Index	-0.348	0.030

Birthweight (g)	0.143	-0.286

Although the preeclampsia group was strictly selected according to diagnostic guidelines, the control group consisted of women with normal pregnancies who were randomly selected from BMI-matched normotensive women. We observed that the gestational age in the control group was higher than that in the preeclampsia group, independent of BMI (Table 5). This discrepancy may be attributed to the necessity of earlier delivery in preeclampsia cases. Therefore, we subsequently performed correlation analyses between gestational age and the measured parameters to assess whether gestational age significantly influenced our results (Table 15). Despite its subtle reduction in preeclampsia patients, gestational age at delivery did not correlate with most of the selected biomarkers, justifying the validity of the current comparisons.

Table 15. Correlation of gestational days and measured outcomes. Spearman correlation analysis was performed. Correlation coefficients (R) are indicated. * P < 0.05.

	Gestational Age			
	Control (BMI<25)	**Preeclampsia (BMI<25)**	**Control (BMI≥25)**	**Preeclampsia (BMI≥25)**
$CD8^+$ T cell density	-0.152	0.110	-0.361	0.333
CD31+ density	-0.217	0.254	0.355	0.095
% αSMA	0.500	0.000	-0.600	0.564
%VCAM1	-0.700	-0.200	-0.700	-0.821
IL7	-0.251	-0.322	-0.503	-0.068
PGF	0.073	/	0.018	0.700
ICAM1	0.097	-0.288	-0.038	**0.524***
VCAM1	-0.337	**-0.573***	-0.293	0.274
CXCL10	-0.220	-0.110	-0.318	0.369
CXCL9	-0.042	-0.074	**-0.515***	0.363
HIF1A	-0.077	0.068	-0.433	**0.567***
sFlt-1 pg/ml	0.400	-0.182	-1.000	0.129
PLGF pg/ml	-0.800	0.307	-1.000	0.194
sFLT1/PlGF	0.400	-0.230	1.000	-0.270

CRP mg/l	0.420	-0.313	-0.095	0.120
systolic pressure	0.083	-0.365	0.097	-0.302
diastolic pressure	-0.176	-0.248	-0.165	0.124

3.2 Preeclampsia-like Mouse Model

3.2.1 The Uterine Immune Compartment in a Preeclampsia-like Mouse Model at GD14.5

To better understand how the uterine immune environment is altered in human preeclampsia, it was necessary to establish a physiological baseline of decidual leukocyte dynamics during a normal pregnancy. We established this by analyzing $CD45^+$ and $CD8^+$ T cell expression and spatial distribution in wildtype mice from the virgin state to GD 18.5 via immunohistochemistry (details in Appendix 5).

The observed inverse correlation between sFLT1/ PlGF and decidual $CD8^+$ T cells in human decidua of preeclampsia raised questions on causality. Specifically, whether impaired $CD8^+$ T cell migration is a cause or a consequence of dysregulated angiogenic and vascular features in preeclampsia is questionable. To answer this, we used a mouse model in which preeclampsia symptoms, e.g., hypertension, kidney damage and fetal growth restriction, were elicited by transgenic overexpression of human sFLT1 (53,54) (Figure 19).

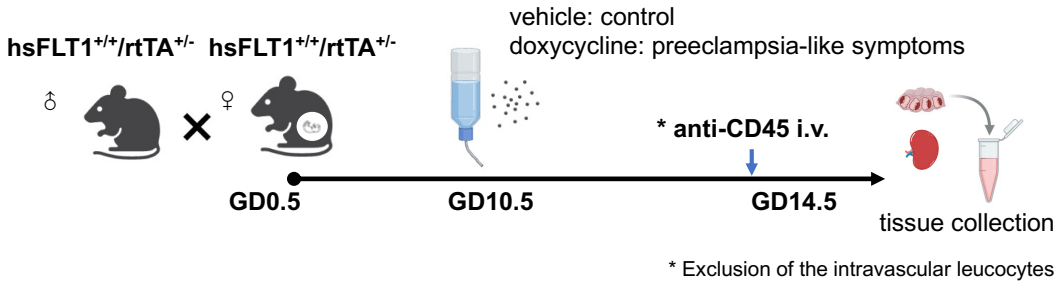

Figure 19. Schematic Representation of The Preeclampsia-Like Mouse Model Building.

3.2.1.1 Characterization of CD45⁺ Cell Expression by Immunohistochemistry in Preeclampsia-Like Mouse Model

We first assessed the leukocyte population by quantifying the density of CD45⁺ cells in the myometrium and decidua of control and preeclampsia-like dams at GD 14.5. In both groups, CD45⁺ leukocytes were abundantly localized throughout the decidua and myometrium, appearing either as scattered individual cells or as clusters in stroma. They were also observed within blood vessels and in the perivascular regions (Figure 20, A). However, quantitative analysis of immunohistochemistry revealed a significant and tissue-specific change. While the density of CD45⁺ cells in the myometrium was unaffected, there was a significant reduction in leukocyte density in the decidua of the preeclampsia-like mice compared to the control group (Figure 20, B and C).

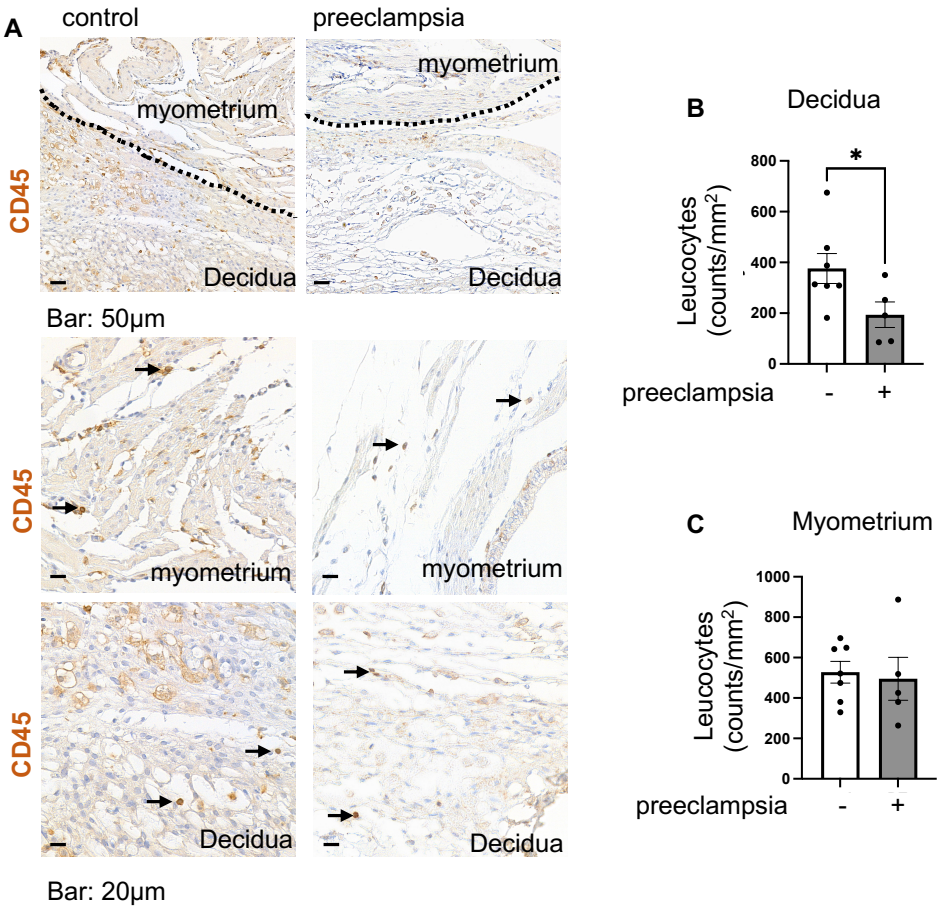

Figure 20. Localization and Expression of CD45+ Leukocyte in The Placenta of The Preeclampsia-Like Mouse Model. A: Representative examples of histological tissue sections stained by immunohistochemistry to detect CD45⁺ leukocytes in mouse pregnant uterus sections. B:

Comparison of the density of CD45+ cells in the decidua. C: Comparison of the density of CD45+ cells in the myometrium. * $p < 0.05$, statistical comparisons performed by Mann-Whitney U test.

3.2.1.2 Characterization of Macrophage by Immunohistochemistry in Preeclampsia-like Mouse Model

Next, we investigated the F4/80$^+$ macrophage population, another key component of the decidual immune environment. Immunohistochemical staining confirmed that macrophages can infiltrate the myometrium and decidua. They were primarily localized within the stroma of the myometrium and decidua, with a smaller number of cells observed in or near blood vessels (Figure 21, A). Quantitative analysis revealed a significant reduction in F4/80$^+$ macrophage density in the preeclampsia-like group compared to controls. Notably, and in contrast to the overall leukocyte population, this decrease was observed in both the myometrium and the decidua (Figure 21, B and C).

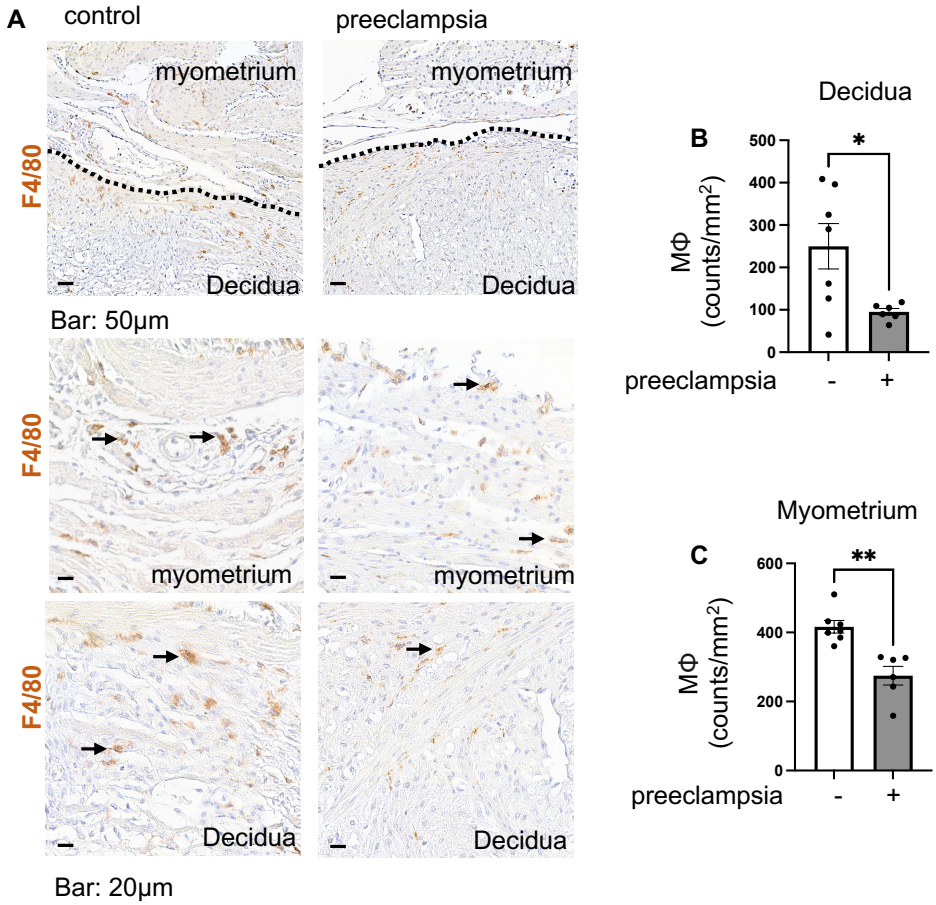

Figure 21. Localization and Expression of F4/80+ Macrophages in The Placenta of The Preeclampsia-Like Mouse Model. A: Representative examples of histological tissue sections stained by immunohistochemistry to detect F4/80+ macrophages of mouse pregnant uterus sections. B: Comparison of the density of F4/80+ macrophages in the decidua. C: Comparison of the density of F4/80+ macrophages in the myometrium. * $p < 0.05$, ** $p < 0.01$, statistical comparisons performed by Mann-Whitney U test.

3.2.1.3 Characterization of $CD8^+$ T Cell Expression by Immunohistochemistry in Preeclampsia-like Mouse Model

Compared to $CD45^+$ leukocytes and macrophages, immunohistochemical staining confirmed that $CD8^+$ T cells were markedly less abundant in both decidua and myometrium. Similar to wildtype mice, $CD8^+$ T cell infiltration could still be found in the myometrium and decidua, most of which in the decidua were in stroma or close to blood vessels (Figure 22, A). Quantitative analysis, however, revealed a significant reduction in $CD8^+$ T cell density in the preeclampsia-like mouse compared to controls, which was restricted to the decidua, with no significant change observed in the myometrium. This decidua-specific reduction of $CD8^+$ T cells, together with the decrease observed in the total $CD45^+$ leukocyte population and $F4/80^+$ macrophage, suggests a local immune alteration at the maternal-fetal interface occurs in this model of preeclampsia (Figure 22, B and C).

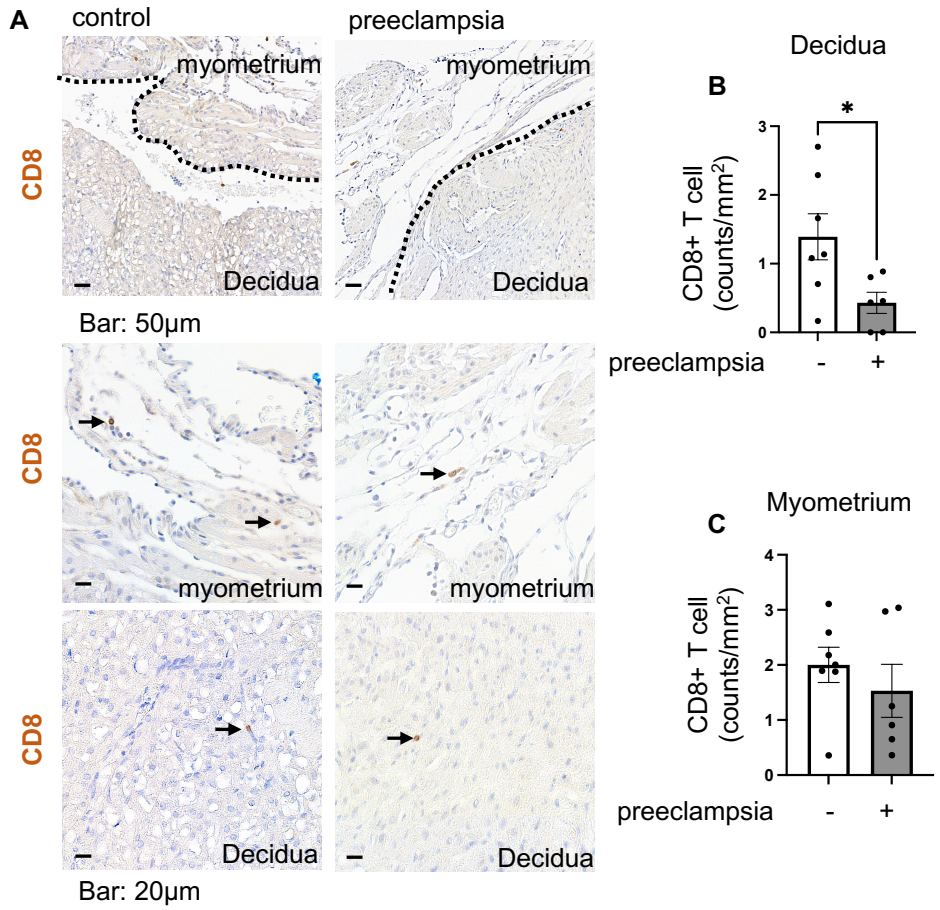

Figure 22. Localization and Expression of CD8⁺ T Cell in The Placenta of The Preeclampsia-Like Mouse Model. A: Representative examples of histological tissue sections stained by immunohistochemistry to detect CD8⁺ T cells in mouse pregnant uterus sections. B: Comparison of the density of CD8⁺ T cells in the decidua. C: Comparison of the density of CD8⁺ T cells in the myometrium. * $p < 0.05$, statistical comparisons performed by Mann-Whitney U test.

3.2.1.4 Identification of Different Immune Cell Populations by Flow Cytometry

To further explore whether additional immune cell populations are affected in preeclampsia, we performed flow cytometry on the preeclampsia mouse model (Figure 23, A). Alongside the decidua, the spleen was taken, a main lymphoid organ that responds swiftly to systemic inflammation.

Flow cytometry results showed no significant changes in the proportions of macrophages ($CD11b^+F4/80^+$), T cells (TCR^+), $CD4^+$ T cells (TCR^+CD4^+), or $CD8^+$ T cells (TCR^+CD8^+) among total leukocytes in the decidua of preeclampsia-like mice, however, $CD8^+CD122^+$ T cell proportion was significantly reduced, which kept in line with human decidual $CD8^+PD1^+$

regulatory T cell reduction and may suggest an impaired immune adaptation to pregnancy which may have consequences for the angiogenesis at the maternal-fetal interface. In the spleen, all mentioned cell populations were unchanged as well, but neutrophils were significantly higher in preeclampsia-like mice (Figure 23, B-G). These increased systemic neutrophils might be associated with the systemic inflammation of preeclampsia.

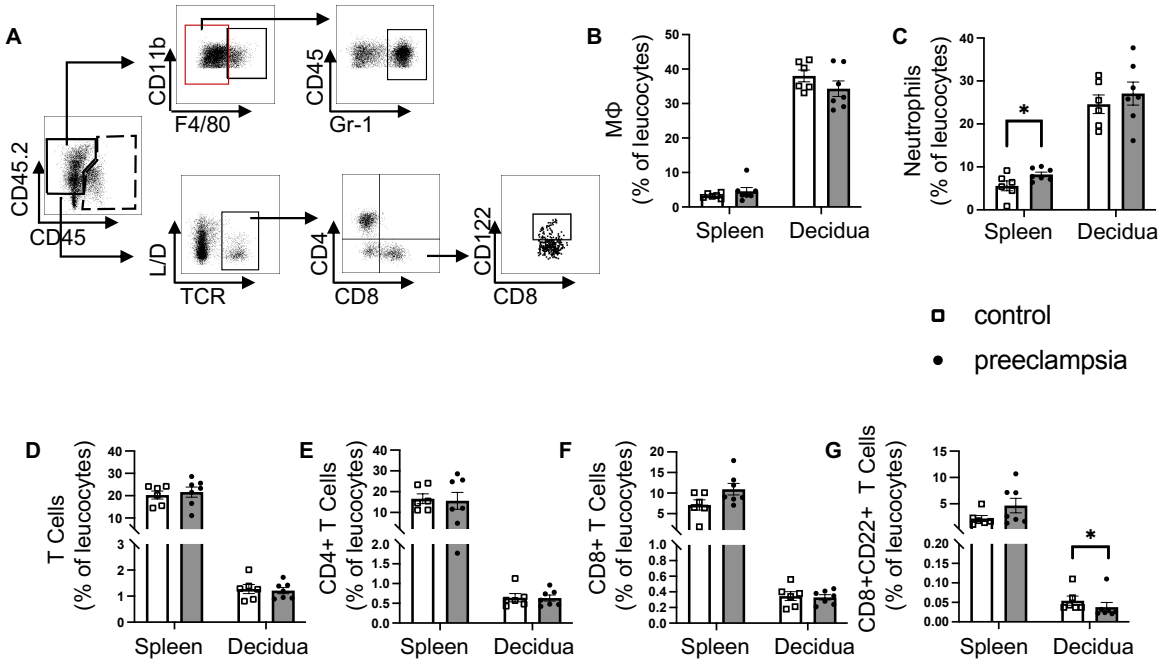

Figure 23. CD8⁺ T Cells Are Reduced in Preeclampsia-Like Mouse Decidua. A: Relevant immune cell populations were characterized by flow cytometry. The dot plots show the gating strategy. B-G: Flow cytometric comparison of macrophage, neutrophil, T cell, CD4⁺ T cell, CD8⁺ T cell and CD8⁺CD122⁺ T cell populations in preeclampsia-like mouse spleen and decidua. * $p < 0.05$, ** $p < 0.01$, statistical comparisons performed by Mann-Whitney U test.

3.2.1.5 Inflammation-Related and T-Cell-Recruitment-Related Gene Expression Profile in Preeclampsia-Like Mouse Decidua

To investigate the mechanism underlying the reduction of decidual CD8⁺ T cells in the preeclampsia-like model, we performed qPCR to analyze the local gene expression of key cytokines, endothelial adhesion molecules, and chemokines.

3.2.1.5.1 T Cell Survival and Proliferation Factors

We first hypothesized that the reduction in $CD8^+$ T cells could be due to a local deficit in factors required for their survival and proliferation. While the expression of *Tnf* was significantly upregulated in the decidua of preeclampsia-like mice, indicating a pro-inflammatory state, the expression of *Ifng* remained unchanged. Furthermore, we found no significant differences in the mRNA levels of *Il15* or *Il7* (Figure 24, A to D). These data suggest that the reduction in $CD8^+$ T cells is unlikely to be caused by an impaired pro-survival cytokine environment and the increasing *Tnf* failed to recruit $CD8^+$ T cells.

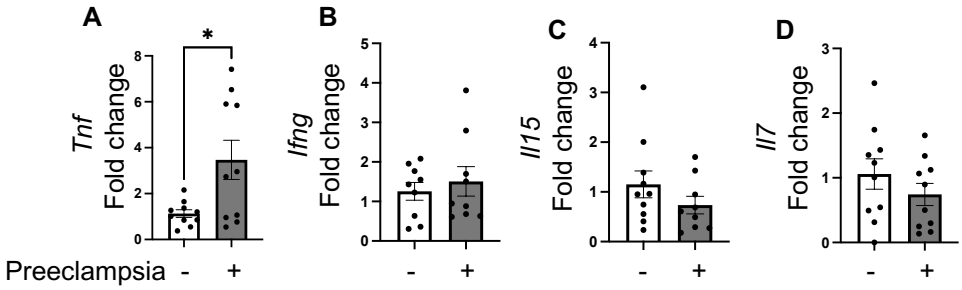

Figure 24. Elevated *Tnf* mRNA Expression in the Decidua of Preeclampsia-Like Mouse. mRNA analysis of *Tnf*, *Ifng*, *Il15*, *Il7* in mouse decidua at GD14.5. * $p < 0.05$, statistical comparisons performed by Mann-Whitney U test.

3.2.1.5.2 T Cell Recruitment Chemokines

We next investigated a second hypothesis: that the reduction in $CD8^+$ T cells was due to impaired migration into the decidual tissue. We therefore measured the expression of key chemokines and endothelial adhesion molecules involved in T cell trafficking. This analysis revealed that the expression of the T cell recruitment-related chemokine.

Cxcl10 was significantly higher in the decidua of preeclampsia-like mice compared to controls, which is in line with human findings, whereas no significant changes were observed in *Icam1, Vcam1*, *Pecam1*, *Ccl5*, and *Cxcl9* (Figure 25, A-F).

In summary, these gene expressions present a paradox. Despite the pro-inflammatory and chemokine signature, particularly elevated levels of *Tnf* and *Cxcl10,* the decidua presented a

reduction in local CD8$^+$ T cell numbers. This suggests that the defect may not lie in signals to recruit T cells, but rather in the ability of CD8$^+$ T cells to respond.

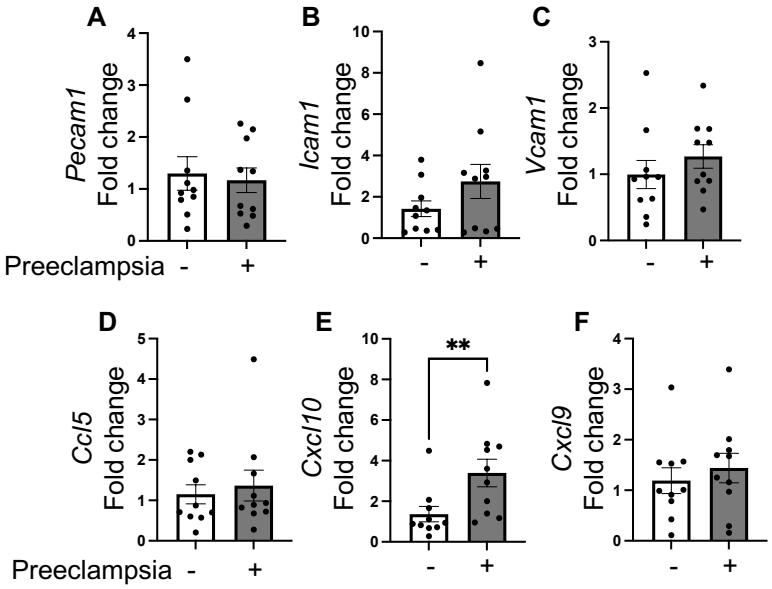

Figure 25. Altered Genes of Endothelial Activation Markers and T Cell Migration-Related Chemokines in Preeclampsia-Like Mouse Decidua. A: mRNA analysis of *Pecam1, Icam1*, *Vcam1*, *Ccl5*, *Cxcl10* and *Cxcl9* in mouse decidua. *p < 0.05, **p < 0.01, statistical comparisons performed by Mann-Whitney U test.

3.3 Carcinoembryonic Antigen-Related Cell Adhesion Molecule 1 (CEACAM1) in Preeclampsia-Like Mouse Model

CEACAM1 is a member of the CEA family expressed on a broad range of cell types, which promotes vascularization, modulates CD8$^+$ T cell activation, proliferation, and survival (200,201). Soluble CEACAM1 levels have been reported to be upregulated in the blood of early-onset preeclampsia patients compared to normal pregnancy (202).

We did qPCR in mouse decidua, but no difference was found within groups (Figure 26, A). Given these relevant functions, we sought to investigate its expression and localization in the preeclampsia-like mouse model. Immunohistochemical staining revealed a highly specific expression pattern, with CEACAM1 predominantly localized to the junctional zone of the mouse placenta. In contrast, staining signals in the labyrinth zone and the maternal decidua were less (Figure 26, B). But quantitative analysis of CEACAM1 expression revealed no

significant difference between the preeclampsia-like mice and their respective controls (Figure 26, C).

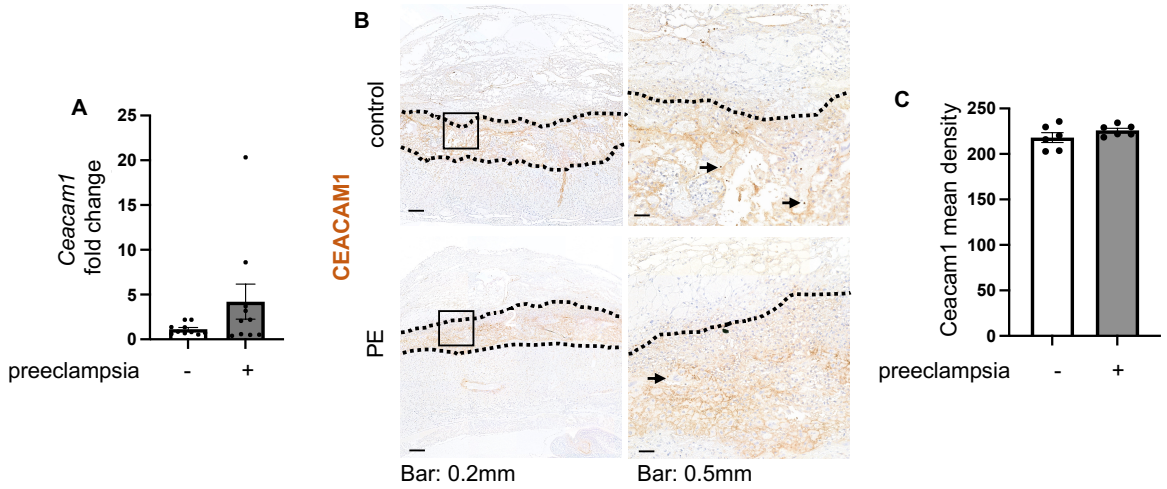

Figure 26. Localization And Expression of CEACAM1 in The Placenta of The Preeclampsia-Like Mouse Model. A: mRNA analysis of *Ceacam1* in preeclampsia-like mouse decidua. B: Representative examples of histological tissue sections stained by immunohistochemistry to detect CEACAM1 expression in mouse placenta sections. C: CEACAM1 mean density in the junctional zone of preeclampsia-like mice and controls, *p < 0.05, statistical comparisons performed by Mann-Whitney U test.

3.4 Human Early-Onset Preeclampsia (EOPE)

We further investigated whether CD8+ T cells deficiency is a general feature in preeclampsia syndrome, also manifesting in the early onset of the disease. In this case, we retrospectively selected biobank samples from patients from our clinic, as categorized into 2 groups: gestational age-matched control (n=12) and early-onset preeclampsia (n=12). Preeclampsia diagnosis was followed by the guideline “Hypertensive Disorders in Pregnancy: Diagnostics and Therapy” (40). The gestational ages of early-onset preeclampsia are defined as after 20 weeks, while before 34 weeks (41). The detailed clinical characteristics of these four patient groups are summarized in Table 16.

Table 16 Clinical Maternal Patient Basic Information of Early-Onset Preeclampsia. Values presented as medians (IQR) or rates (n). *p < 0.05; **p < 0.01; ***p < 0.001; ****p < 0.0001.

	Gestational age-matched control	Early-onset preeclampsia

	(n = 12)	(n = 12)
Age (years)	32.5 (31-36)	32.5 （29-35.5）
SBP (mmHg)	121 (105–130)	147 (140–157) ****
DBP (mmHg)	73 (70–81)	95 (91–105) ****
Weight before pregnancy (kg)	60.2 (55.5–77)	68 (60–80)
Height (cm)	168 (158–169)	163 (158–168)
BMI (kg/m2)	24.3 (20.8–27.3)	26.6 (25.7–30.1)
Leukocytes (/nl)	10.3 (9.3–15.4)	11.1 (8.6–16.0)****
sFlt-1/PlGF	10.84 (2.62–42.69)	285.32 **** (91.32–959.00)
CRP (mg/l)	8 (3–18)	7 (3–12)
Protein in spot urine (g/l)	0.2 (2)	0.60 (0.21–2.17)
Parity	2 (1–2)	1 (1–2)
Gestational age (weeks+days)	31+1 (29+6 – 33+4)	31+1 (26+2 – 33+0)
Birth weight (g)	1695 (1330–2100)	1200 (790–1980) *
10% below 10th percentile birthweight	0% (0)	17% (2)
AC percentile	58 (33–71)	21 (7–44) **
HC/AC percentile	47 (17–80)	54 (46–91)
Umbilical artery PI	1.02 (0.86–1.29)	1.08 (1.03–1.17)

3.4.1 Reduced Decidual CD8$^+$ T Cell Density is Also a Feature of Early-Onset Preeclampsia

To determine if the reduction in decidual CD8$^+$ T cells was specific to the late-onset preeclampsia, we also analyzed it with early-onset preeclampsia. Our analysis was still focused on the decidua. Similar to our findings in late-onset preeclampsia, immunohistochemical analysis revealed scattered CD8$^+$ T cell infiltration within the decidual stroma of both early-onset preeclampsia and preterm control patients (Figure 27, A). The quantitative analysis showed that the density of CD8$^+$ T cells was also significantly lower in the decidua of early-onset preeclampsia patients (Figure 27, B). This result demonstrates that a reduced density of decidual CD8$^+$ T cells is a pathological feature common to both early- and late-onset preeclampsia.

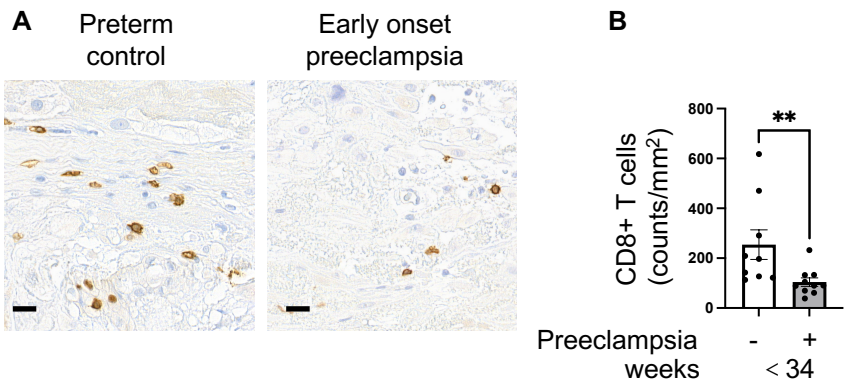

Figure 27. Lower CD8⁺ T Cell Density Was Found in The Decidua of Early-Onset Preeclampsia Patients. A: CD8⁺ T cells of control and preeclampsia patient placenta were assessed by immunohistochemistry, scale bar=20µm. B: Comparison of density of CD8⁺ T cells in each group. * p < 0.05, **p < 0.01, statistical comparisons performed by Mann-Whitney U test.

3.4.2 Downregulation of T Cell-Related Proliferation and Survival Factors in Early-Onset Preeclampsia

Similar to the analyses performed for late-onset preeclampsia, we also explored potential mechanisms underlying the reduction of CD8⁺ T cells in early-onset preeclampsia. In contrast to our findings in late-onset preeclampsia, where these factors were unchanged, the analysis of the early-onset preeclampsia patients revealed a distinct expression pattern. Specifically, the decidual mRNA expression of *IFNG* showed a significant reduction and *IL7* tended to reduce in early-onset preeclampsia patients compared to their gestational age–matched preterm controls (Figure 28), while *TNF* and *IL15* expression showed no significant difference between the groups. This result suggests that the mechanisms driving the reduction of decidual CD8⁺ T cells may be different between the two clinical subtypes of preeclampsia. The reduction of CD8⁺ T cells in early-onset preeclampsia may be linked to a disturbed local environment lacking sufficient pro-proliferative and survival signals.

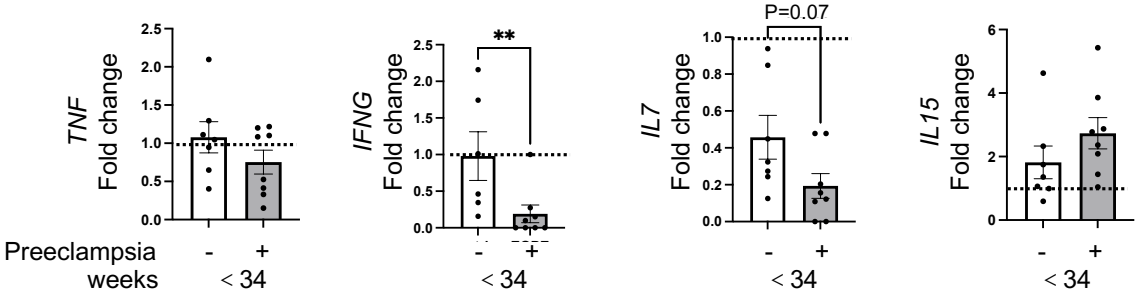

Figure 28. Significant Reduction of Cytokines in Early-Onset Preeclampsia Decidua. mRNA analysis of *TNF*, *IFNG*, *IL7*, and *IL15* in the decidua of preterm control and early-onset preeclamptic patients. The dashed line represents the level of term normal BMI controls. *p < 0.05, **p < 0.01, statistical comparisons performed by Mann-Whitney U test.

3.4.2.1 Decidual Vascular Remodeling in Early-Onset Preeclampsia

To investigate the structural state of the decidual vasculature in early-onset preeclampsia, we assessed the coverage of αSMA by immunofluorescence, as we did in late-onset preeclampsia. This analysis revealed that decidual vessels from women with early-onset preeclampsia exhibited an increasing trend of αSMA coverage compared to those from preterm controls (Figure 29, A and B). This retention of the vascular smooth muscle layer likely contributes to increased vessel stiffness.

Next, we examined the expression of the adhesion molecule VCAM-1. Similar to our observations in the late-onset preeclampsia patients, VCAM-1 protein was localized to both vascular endothelial cells and surrounding decidual stromal cells. But the quantitative analysis demonstrated a significantly lower level of VCAM-1 coverage along decidual vessels in early-onset preeclampsia compared to preterm controls (Figure 29, A and C). The combination of increased αSMA coverage and decreased vascular VCAM-1 expression defines a unique vascular phenotype in early-onset preeclampsia.

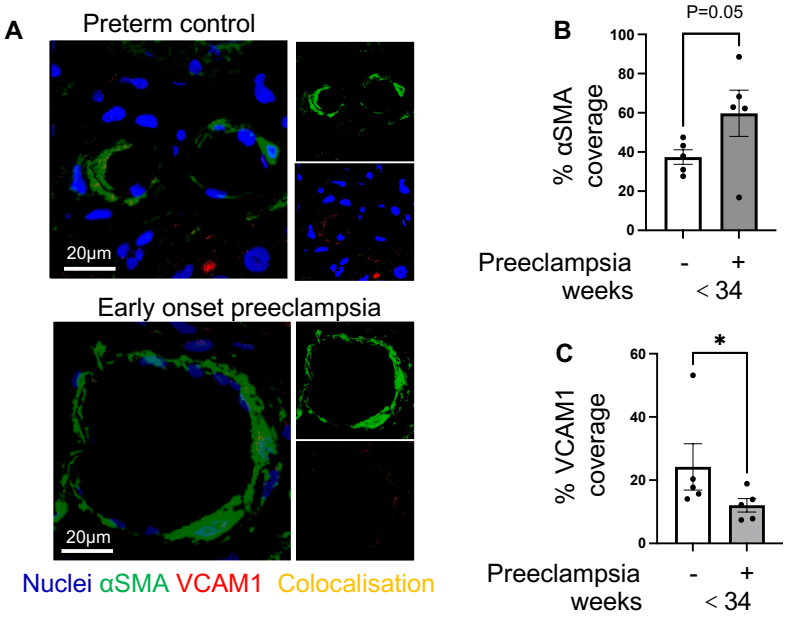

Figure 29. Early-Onset Preeclampsia Associated Co-Localization of VCAM-1 And αSMA in Decidua Perivascular Area. A: Representative immunofluorescence staining of αSMA and VCAM1 expression in decidua, bar=20µm. B: Analysis of αSMA and VCAM-1 coverage percentage around decidual vessels in each group. Data are presented as mean ± SEM. *p < 0.05, statistical comparisons performed by Mann-Whitney U test.

4. Discussion

4.1 Research problem

The pathogenesis of preeclampsia and the contribution of the uterine immune compartment remain incompletely understood. While impaired uteroplacental spiral artery remodeling had long been considered a major cause, recent studies suggest that this defect is predominantly associated with early-onset preeclampsia, and its contribution to late-onset disease is less clear. In contrast, the anti-angiogenic factor sFLT1 has emerged as a contributor to preeclampsia, underscoring dysregulated angiogenesis as a hallmark of the disorder. Furthermore, elevated pre-pregnancy BMI (≥ 25kg/m^2) is an independent risk factor for preeclampsia, yet little is known about how maternal BMI influences the decidual immune compartment and its functional modulation in this context.

Decidual angiogenesis and vascular remodeling during pregnancy are dynamic processes in which immune cells, including subsets of $CD8^+$ T cells, play important roles, including restoring placental angiogenesis and preventing fetal growth restriction (149). However, the mechanisms underlying the presence, phenotype, and regulation of decidual $CD8^+$ T cells in human preeclampsia remain poorly understood and were therefore the subject of the present study.

Our study revealed a significant reduction of decidual $CD8^+$ T cell density in human late-onset preeclampsia, a finding that was independent of the patient's BMI and further associated with a decreasing trend in the $PD1^+$ subset. This reduction was not related to alterations in key homeostatic cytokines for T-cell survival and proliferation, such as IL-7 and IL-15. Rather, a steep upregulation of the T-cell chemoattractant CXCL10 was detected in women with preeclampsia and/ or high BMI. Simultaneously, we observed enhanced levels of circulating CXCL10 in women with preeclampsia, which may at least partly explain the reduced migration of T cells in response to exacerbated decidual CXCL10 levels. Concurrently, we observed evidence of pathological vascular stiffness in the preeclamptic decidua, as evidenced by an

increased perivascular muscle cell layer and collagen deposition. Notably, similar vascular alterations were also observed in the normotensive high BMI control women. However, this $CD8^+$ T cell reduction was specific to the decidua, as no similar change was observed in placental tissue from the same patients. These key aspects of the immunological paradox were recapitulated in our preeclampsia-like mouse model. This model also exhibited a significant reduction in decidual $CD8^+$ T cells, particularly the $CD8^+CD122^+$ regulatory subset, despite a concurrent increase in *Cxcl10* expression.

Intriguingly, we found that this decidual $CD8^+$ T cell reduction is not restrained in late-onset preeclampsia, since a similar change was found in early-onset preeclampsia. However, this reduction was associated with a decrease in decidual *IFNG* and *IL7*. Concurrently, we noted a thickened vascular smooth muscle layer, suggesting that the $CD8^+$ T cell reduction in early-onset preeclampsia may be different from late-onset preeclampsia.

4.2 Late-onset Preeclampsia

4.2.1 Complexity and Contradictions of Decidual $CD8^+$ T Cells in Preeclampsia

In this study, we observed a significant decrease in $CD8^+$ T cell density in the decidua of patients with preeclampsia. This finding was consistent across our patient cohort and was not associated with the patient's BMI, and appeared to be specific to decidua, as no corresponding change was observed in placental tissue from the same patients. In the preeclampsia-like mouse model we used, which involves overexpression of human sFLT1, reliably mimicking key maternal clinical features of preeclampsia (54), we also observed a decreased $CD8^+$ T cell density in the decidua of these preeclampsia-like mouse models. This parallel finding in both human and the animal model strengthens the conclusion that a reduction in decidual $CD8^+$ T cells is a prominent feature of preeclampsia. The use of a robust animal model that closely recapitulates the human preeclampsia provides strong support for the clinical relevance of our findings and underscores the potential role of $CD8^+$ T cells in the pathogenesis of preeclampsia.

Rieger et al. (203) utilized flow cytometry to report significantly lower proportions of cytotoxic $CD8^+$ T lymphocytes in the decidua of preeclampsia patients compared to healthy controls. This study also noted a decrease in αβTCR+ T cells and CD56+/CD16+ NK cells, suggesting a broader dysregulation of decidual immune cell subsets. More recent studies have further elucidated this phenomenon using diverse techniques. Luo et al. (159) employed single-cell RNA sequencing and found a reduced proportion of cytotoxic T cells in the preeclamptic decidua. Similarly, Fu et al. (160) used mass cytometry to confirm the decrease of $CD8^+$ T cells in preeclampsia.

Building on the observation of decreased total $CD8^+$ T cell population, research has also delved into the functional subsets of $CD8^+$ T cells. Kieffer et al. (204) focused on $CD8^+$ memory T cells, observing a significantly lower proportion of activated $CD8^+$ memory cells in late-onset preeclampsia patients compared to healthy pregnancies. They also reported a downward trend in the activation of both $CD8^+$ Tem cells and Trm cells. Interestingly, no significant difference was observed in the activation of $CD8^+$ Tcm cells between the groups, suggesting that the dysregulation may selectively affect specific memory T cell subsets. Hence, this evidence generated diverse methodologies collectively support our finding of impaired maintenance of $CD8^+$ T cell homeostasis at the maternal-fetal interface. However, there are also studies reporting an increase in either $CD8^+$ T cell subsets or the total population. For instance, Wilczyński et al. reported an increased frequency of $CD8^+CD28^+$ T cell subset in the preeclamptic decidua (155), while Milosevic-Stevanovic et al. found a higher total decidual $CD8^+$ T cells in their cohort (150), which is in contrast with ours. This higher decidual $CD8^+$ T cell frequency may reflect cohort-specific characteristics, as their study included a high proportion of intrauterine growth restriction (IUGR), which may influence the local immune environment.

The evaluation of the phenotype of decidual CD8+ T cells in the preeclampsia-like mouse model revealed that the PD1- or Ly49-expressing $CD8^+CD122^+$ T cells were among the most affected populations. Furthermore, in our preliminary analyses of human decidua with and without preeclampsia, we identified a trend towards reduced $CD8^+PD1^+$ T cells in the decidua of preeclampsia women (pooled with normal BMI and high BMI preeclampsia), which is

considered a regulatory subset (205,206). Similarly, the work of Saito and Morita also reported a significant reduction of $CD8^+PD1^+$ T cells in preeclampsia (131,156). Extending beyond the specific subset discussed above, research by Fu et al. (160) identified a reduction in $CD11c^+CD8^+$ T cells in preeclampsia patients, which is known for its functional plasticity, capable of shifting between regulatory and effector roles based on the local inflammatory milieu (207).

Our observation of an increasing trend in human decidual $CD8^+KIR3DL1^+$ T cells requires further experimental validation. Of note, these results so far are consistent with the report by Li et al., who found an elevated frequency of KIR^+CD8^+ T cells in the peripheral blood of preeclamptic patients (146). However, these findings stand in contrast to the reduction seen in other regulatory subsets in mice, such as $CD8^+Ly49^+$ T cells, as mentioned. Mouse CD8+Ly49+ cells are an analogous population to KIR+ CD8+ T cells in humans (145). These disparate findings highlight the need to verify the human flow cytometry results in a bigger cohort and paint a complex picture, suggesting that even within the category of regulatory populations, distinct $CD8^+$ T cell subsets undergo divergent changes during preeclampsia.

Notably, in the present thesis, we could not evaluate the function of decidual $CD8^+$ T cells in the context of preeclampsia. dNK cells, the most abundant leukocyte at the maternal-fetal interface (113), play a crucial role in spiral artery remodeling by secreting angiogenic factors like VEGF and PLGF, while also promoting VSMC migration and apoptosis via IFN-γ (208). The role of dNK is multifaceted, as they also secrete TNF to inhibit excessive trophoblast invasion, ensuring the process remains precisely controlled. Given that the cytokines produced by $CD8^+$ T cells, such as IFN-γ and TNF, overlap with the angiogenic functions attributed to dNK cells, it is plausible that similar pathways may be involved. Actually, previous work of the lab could demonstrate that CD8+ T cells can promote angiogenesis at the placenta (149). Hence, a decrease in $CD8^+$ T cells may suggest a further vascular dysfunction and reinforce preeclampsia symptoms in a feedback loop.

4.2.2 Potential Mechanisms of Impaired CD8$^+$ T Cell Homeostasis in the Preeclamptic Decidua

We observed significantly elevated decidual *Tnf* in the preeclampsia-like mouse model at GD 14.5, whereas levels remained stable in wildtype mice from virgin to GD 14.5 but increased at GD 18.5. Although TNF is known to promote CD8$^+$ T cell proliferation during acute immune responses (135), prolonged TNF signaling can paradoxically deplete the T cell pool via activation-induced cell death (209) through TNFR2 on activated CD8$^+$ T cells (135) This pro-apoptotic mechanism provides a plausible explanation for the reduced decidual CD8$^+$ T cell density we observed in the preeclampsia-like mice despite the high *Tnf* environment.

However, we found no significant changes in the human preeclamptic decidual *TNF,* regardless of BMI. This is intriguing, particularly given that TNF is known to be highly expressed in the adipose tissue of obese individuals (210). This indicates a tissue-specific regulation, suggesting that TNF's role as a systemic inflammatory marker in overweight and obesity does not necessarily reflect in the local decidual microenvironment. Another possible explanation could be the temporal context. In healthy pregnancy, peripheral TNF remains a stable low level in the first and second trimester but increases in the third trimester (211), which is consistent with our own data from wildtype mice, where decidual *Tnf* increased at GD 18.5. But the elevated *Tnf* in preeclampsia-like mice was detected earlier, at mid-gestation (GD 14.5), raising the possibility that TNF signaling is triggered at an earlier stage of the preeclampsia onset but is no longer a prominent feature by late pregnancy.

Notably, despite the unchanged TNF levels in the decidua of women with preeclampsia, our preliminary analysis of placental (villous) tissue revealed elevated *TNF* specifically in preeclamptic women with normal BMI. This discrepancy suggests a distinct, tissue-specific immunological phenotype, also indicating that the local inflammatory response in preeclampsia may be predominantly compartmentalized within the villi rather than the decidua.

Echoing the pattern observed with TNF, our analysis revealed that IFN-γ mRNA levels also remained unchanged in the decidua of both the preeclampsia-like mouse model and human patients with either high or normal BMI. Overweight and obesity are also known to promote IFN-γ production in serum and adipose tissues (212), the stable mRNA level in decidua also indicates a tissue-specific regulation for IFN-γ. Furthermore, the mRNA level does not correlate with $CD8^+$ T cell density in humans, suggesting that the reduction in decidual $CD8^+$ T cells is likely independent of the IFN-γ signaling pathway.

Tissue immunocompetence is sustained by the local production of cytokines that support the survival and persistence of resident immune cells (213). IL-7 and IL-15 are both members of the common gamma-chain (γc) cytokine family (133). IL-7 signaling involves the binding of JAK1 and JAK3 to its receptor chains (IL-7Rα and γc), which activates the STAT3/5 pathway (133). Subsequent STAT5 activation ensures T cell long-term persistence (214). Since our data revealed that the abundance of decidual $CD8^+$ T cells from normal BMI control women positively correlated with local *IL7* gene expression. This finding supports the role of IL-7 for the maintenance of $CD8^+$ T cells in healthy pregnancy (214).

While a significant decline was found in decidual $CD8^+$ T cells in preeclampsia, but without changes in local expression of both *IL7* and *IL15*. This paradox suggests that the defect may not lie in the production of these cytokines, but rather in the ability of the $CD8^+$ T cells themselves to respond to them. This leads to several hypotheses, for example, receptor downregulation. The expression of CD127, the alpha chain of the IL-7 receptor (IL-7Rα), is known to be reduced by chronic immune activation, which is a characteristic immunological finding in preeclampsia (215), thereby rendering $CD8^+$ T cells responsive to the pro-survival signals of IL-7 (216). Another possibility could be impaired downstream signaling. IL-7 promotes lymphocyte survival through the JAK-STAT pathway (217). However, several factors as oxidative stress (218) and obesity (219) can cause dysfunctional JAK/STAT signaling, resulting in impaired T-cell maintenance. Future investigations will be needed and could provide more mechanistic insights into the reduction of $CD8^+$ T cells in preeclampsia.

The maintenance of the memory $CD8^+$ T cell is dependent on IL-15 as well, a deficiency in IL-15 signaling is known to cause a loss of this population (220). This established mechanism is particularly relevant to our findings in the preeclampsia-like mouse model, where we observed a significant reduction in the $CD8^+CD122^+$ T cell subset. As CD122 is a component of the IL-15 receptor (133), a reduction in its expression could directly impair the ability of these cells to receive maintenance signals. As Jarjour et al. have noted, sensitivity and responsiveness can differ between $CD8^+$ memory T subsets (220). Building on this, the concept of context-dependent IL-15 insensitivity, as reported in tumor microenvironments (221), offers a compelling hypothesis for preeclampsia. Additionally, we found no correlation between $CD8^+$ T cell density and *IL15* in human, it is plausible that the pathological environment of the preeclamptic decidua may also impair the responsiveness of $CD8^+$ T cells to IL-15, representing another potential driver for their diminished numbers.

In conclusion, our findings suggest that the human decidual $CD8^+$ T cell deficiency in late-onset preeclampsia could be driven by impaired ability to respond to the homeostatic signal, since $CD8^+$ T cell density correlates with *IL7* in the control cohort, but not in preeclampsia.

4.2.3 Impaired CD8+ T-Cell Trafficking in Preeclampsia

4.2.3.1 Pathological Vascular Remodeling in the Preeclamptic Decidua

Our results indicate more collagen deposition in the decidua of preeclamptic women. This is consistent with the findings of Pijnenborg et al. (222). sFLT1-induced endothelial dysfunction (223) can lead to a reduced NO bioavailability (224), a key molecule that not only regulates vasodilation (225) but also mediates ECM degradation. Research has shown that NO can activate matrix MMPs in the ECM, leading to collagen degradation (226). Therefore, reduced NO bioavailability in preeclampsia (227) is an important factor contributing to ECM accumulation, which directly associates with arterial stiffening (228). But Lyall et al. reported a different perspective, in their study, myometrial vessels in preeclamptic patients showed reduced fibrinoid deposition, as impaired spiral artery remodeling led to less destruction of the myometrial vessel wall, resulting in decreased fibrinoid accumulation (229).

Furthermore, we observed increased perivascular αSMA coverage in human preeclamptic decidua; the preeclampsia-like mouse model also revealed an increase in decidual VSMC (54). We propose that this vascular structural change, coupled with the pronounced collagen deposition, constitutes a physical barrier to $CD8^+$ T cell trafficking. As Salmon et al. suggest, while $CD8^+$ T cells can navigate through matrices of thin collagen fibers, their movement is physically impeded by dense, cross-linked collagen networks (197). This provides a direct mechanistic explanation for our observation of $CD8^+$ T cells accumulating in the perivascular space but failing to infiltrate deeper into the decidual tissue of preeclampsia (230). Therefore, the sFLT1 is a key upstream driver not only driving angiogenesis imbalance but also creating a physical barrier to "trap" $CD8^+$ T cells. It is important to note that our current findings apply to the general $CD31^+$ vasculature within the decidua. A limitation of this approach is that it does not specifically distinguish uterine spiral arteries from other vessels. Future studies employing markers specific to spiral arteries will be necessary to obtain more detailed information about their unique pathological alterations in preeclampsia.

4.2.3.2 Tissue-Specific and BMI-Dependent Regulation of VCAM1 in Preeclampsia

Although our study revealed relatively stable levels of *ICAM1* and *VCAM1* in the human decidua, protein analysis showed a significant upregulation of endothelial VCAM-1, but only in the normal BMI preeclamptic subgroup. This specific upregulation could be explained by the established suppression of VCAM-1 by NO (231); given that reduced NO bioavailability in preeclampsia (227,232), the loss of this inhibitory signal likely drives the VCAM-1 increase we observed, but the similar upregulation was not found in high BMI preeclamptic women. Consistent with reports of a positive correlation between BMI and adhesion molecules in visceral adipose tissue (233)，we also observed a trend towards increased decidual VCAM-1 in our high BMI control women compared to their normal BMI counterparts. However, the VCAM-1 upregulation was not observed in the high BMI preeclamptic cohort.

Our findings on VCAM-1 challenge the report by Haller et al., which proposed that preeclamptic serum can induce ICAM-1 but not VCAM-1 expression on endothelial cells (234). The distinct VCAM-1 patterns observed in normal- and high-BMI preeclamptic decidua suggest that the regulation of VCAM-1 in preeclampsia with different BMI involves a more complex mechanism. A limitation of our current study is the absence of data on ICAM-1 protein expression on the decidual vascular endothelium. Further comprehensive studies with a larger sample size may be required to better understand these intricate dynamics.

4.2.3.3 Impaired CD8+ T cell Recruitment Is Associated with CXCL10 In the Decidua of Preeclampsia

The CCL5/CCR5 pathway is critical for T cell recruitment in the uterus (235), and Zhou et al. found CCL5 was reduced in the peripheral blood of preeclamptic patients (236). Our analysis revealed no such change in the decidua, which suggests the regulation of CCL5 is tissue-dependent in preeclampsia. However, we observed a significant upregulation of *CXCL9* and *CXCL10* in women with normal BMI preeclampsia. *CXCL10* also increased in the high BMI cohort.

CXCL10, a member of the CXC chemokine family, binds to the CXCR3 receptor on target cells (237). The CXCL10-CXCR3 axis is to promote leukocyte trafficking under both homeostatic and inflammatory conditions (237,238).

The cause of increasing human decidual CXCL10 in preeclampsia remains unknown, but our data show that, in both control and preeclamptic women, decidual *CXCL10* levels correlated strongly with its inducers, *TNF* and *IFNG* (198,199). Furthermore, *CXCL10* positively correlated with adhesion molecules such as *ICAM1* and *VCAM1*, and with other related chemokines including *CXCL9* and *CCL5.* These results suggest that the signaling network connecting *CXCL10* with other chemokines, cytokines, and adhesion molecules remains largely preserved in the preeclamptic decidua.

A significant positive correlation between *CXCL10* and $CD8^+$ T cell density was observed in our study, but only in the normal BMI control women. The loss of this relationship in both the preeclamptic cohort and the high BMI control women suggests a defect in the $CD8^+$ T cell trafficking process under the preeclamptic and/or metabolic disorder conditions. This impairment is unlikely to be due to a failure of the decidua CXCL10 production, but rather a defect in the ability of the $CD8^+$ T cells to "answer the call." Several potential mechanisms might account for this trafficking impairment, for example, downregulation or desensitization of the CXCR3 receptor on $CD8^+$ T cells. This hypothesis is supported by Lockwood et al., who showed that high levels of CXCL10 inhibit surface CXCR3 expression on placental NK cells, impairing their migration (239). MD student Ms. Lara Hammer's project revealed elevated CXCL10 in the plasma of preeclamptic patients, which is consistent with Gotsch's research (240). It is plausible to induce a similar CXCR3 desensitization on $CD8^+$ T cells, which would in turn impair their migratory capacity.

CXCL10 can suppress angiogenesis (241) by affecting endothelial cell migration and tube formation (242), resulting in impaired angiogenesis, vascular stiffness, and atherosclerosis (243,244), which further contribute to the worsening of preeclampsia symptoms. Mirroring our findings in the human decidua, the preeclampsia-like mouse model also displayed a significant reduction in $CD8^+$ T cell density, accompanied by an upregulation of *Cxcl10*. Higher decidual *CXCL10* was also observed in the high BMI cohort, which is supported by reported enhanced CXCL10 in overweight and obesity (245,246).

A significant positive correlation between CXCL10 and $CD8^+$ T cell density was observed, but only in the control group. The loss of this relationship in preeclampsia suggests a defect in the CXCL10-mediated T-cell recruitment pathway.

4.2.4 The Role of BMI as a Modulator of Preeclampsia Pathology

4.2.4.1 The Paradox of CD8$^+$ T Cell Recruitment in High-BMI Preeclampsia

Reduction of CD8$^+$ T cells was not found in high BMI control women. Metabolic and inflammatory changes in high BMI individuals (210) have been shown to block endothelial nitric oxide production (247), and, consequently, lead to vascular stiffness (248–250). In addition to the elevated levels of sFLT1 in women with preeclampsia, another outstanding difference surfaced in high BMI women without preeclampsia: CD8$^+$T cells circumvented vessel stiffness to maintain high density in the decidua. These observations contribute to the existing published evidence indicating that BMI influences immune adaptation during pregnancy. For example, increased CD4$^+$ Tregs were observed in the endometrium of women with high BMI (251) as well as in mice subjected to a high-fat diet during pregnancy (184,252). Although more CD8$^+$ T cells have been reported in the circulation and adipose tissue of obese compared to lean individuals (253), little and contrasting evidence exists to date regarding decidual CD8$^+$ T cells. In obese women (BMI>30), lower rather than higher decidual CD8$^+$ T cells were detected(169) by single-cell sequencing. Intriguingly, in mice, a maternal-fetal mismatch-dependent bimodal response to overweight was present in decidual CD8$^+$ T cells (87). In mice mated allogenically, a high-fat diet reduced CD8$^+$ T cell frequencies in abortion-prone and preeclampsia-like (87,254) mating combinations, but increased decidual CD8$^+$ T cells in combinations leading to successful pregnancies. While a high BMI in the absence of preeclampsia appears to support the accumulation of decidual CD8$^+$ T cells, this effect is abrogated when preeclampsia is superimposed. This suggests that the pathophysiology of preeclampsia acts as the dominant driver, overriding the influence of obesity and ultimately causing the impaired CD8$^+$ T cell migration.

4.2.4.2 Differential Hypoxic Responses in Preeclampsia: The Modulating Effect of BMI

In the decidua of normal BMI preeclampsia patients, we observed a state of tended increasing *HMOX1*, elevated *HIF1A*, coexisting with a higher density of CD31$^+$ vessels. However, the

situation in high BMI individuals is different. Overweight and Obesity itself is recognized as a chronic, systemic, low-grade hypoxic state (255). This means that in overweight women, the decidual microenvironment is likely preconditioned by prolonged hypoxia before the onset of preeclampsia. While prolonged hypoxia could lead to negative feedback regulation of HIF1A, this does not necessarily mean the hypoxia is resolved (256,257). Instead, Ginouvès et al. have shown that chronic prolonged hypoxia can activate prolyl hydroxylases domain (PHD), thereby leading to a reduction of HIFα (258). The elevated *HIF1A* in normal BMI preeclampsia patients likely drives a pro-angiogenic program (259), leading to the increased density of $CD31^+$ vessels we observed. However, drawing a parallel to the tumor microenvironment, neovascularization might be insufficient for adequate restoration of oxygen supply (260,261).

4.2.4.3 The self-perpetuating Loop Between Obesity-Induced Vasculopathy and Preeclampsia

Overweight and obesity could induce vascular stiffness, which has been observed across all age groups (248). A key mechanistic link is the dysfunction of perivascular adipose tissue, a specialized adipose depot surrounding blood vessels (249), which exhibits increased production of pro-inflammatory adipokines in obesity, which contributes to the development of vascular stiffness (250).

Vascular stiffness contains both endothelial cell (EC) stiffness and VSMC stiffness (247,262). EC stiffness most often occurs by compromising the NO signaling pathway. Overweight and obesity impair NOS activation and reduce NO production, which enhances endothelial stiffness (247). Meanwhile, lipid droplet accumulation in endothelial cells under obese conditions suppresses eNOS expression and results in EC stiffness as well (263). The NO deficiency directly causes endothelial cell stiffness and contributes to elevated blood pressure, initiating a vicious cycle.

4.3 Causal Evidence from a Preeclampsia-Like Mouse Model

Our preeclampsia-like mouse model served as a critical tool to establish causality. It not only recapitulated the classic clinical symptoms of preeclampsia (54) but also mirrored its key immunological features, including the reduction of decidual $CD8^+$ T cell density (particularly the regulatory subset) and the upregulation of decidual *Cxcl10*, and increased decidual *Hif1α* (54). This specific profile of changes aligns with our findings in the normal BMI preeclamptic cohort. This validation allows us to conclude that the sFLT1-induced angiogenic imbalance is the upstream trigger for the decidual $CD8^+$ T cell deficiency observed in preeclampsia, and not vice versa.

The important alterations in high BMI pregnancies underscore the need for in-depth empirical approaches as overweight mouse models with and without high sFLT1, which should be tested to bridge these gaps in knowledge. Further investigation of the signaling pathways regulating CXCL10 expression, extracellular matrix components, and metabolic factors under preeclampsia conditions could provide valuable insights into the relationship between angiogenic imbalance, immune cell recruitment, metabolic dysregulation, and vascular remodeling, thereby advancing our understanding of the pathogenesis of preeclampsia and identifying potential therapeutic targets.

4.4 A Dysregulated Immuno-Vascular Axis in Early-Onset Preeclampsia Decidua

Our findings in early-onset preeclampsia patients reveal a distinct dysregulated immune environment in the decidua, pointing towards a different pathophysiology compared to late-onset preeclampsia. The significant reduction in decidual $CD8^+$ T cell density in early-onset preeclampsia patients appears to be driven by an impaired decidua T cell supportive cytokine milieu. Unlike in late-onset preeclampsia, we observed downregulation of *TNF, IFNG,* and *IL7.* The decline of these genes, which are critical for T cell proliferation and survival (135,214), provides a direct mechanistic explanation for the diminished $CD8^+$ T cell population observed in early-onset preeclampsia. We also notice the change in the decidual vasculature structure. The increased αSMA coverage on decidual vessels, as observed in late-onset preeclampsia, may lead to vascular stiffness and change the permeability (264,265). Meanwhile, the

significant reduction in vascular VCAM-1 expression could also impede $CD8^+$ T cell migration via impaired adhesion.

This immunopathological profile of early-onset preeclampsia in the decidua has many differences with findings in late-onset preeclampsia, where the reduction in $CD8^+$ T cells occurred despite a stable cytokine milieu and was accompanied by an upregulation of VCAM-1 coverage in lean individuals. This suggests that while a reduction in decidual $CD8^+$ T cell density is a shared Immune feature of both early- and late-onset preeclampsia, the underlying mechanisms driving this deficiency are distinct. In late-onset preeclampsia, our findings point to a defect in migration, rather than the collapse of the decidual pro-survival and pro-proliferation environment that appears to characterize the early-onset form. But our investigation into this subgroup was limited now, and further studies are required to provide a better understanding of the $CD8^+$ T cells in early-onset preeclampsia.

5. Final Remarks

Taken together, based on our results and those reported in the literature and here discussed, we proposed the following hypothetical scenario in the context of preeclampsia (Figure 30). In both early- and late-onset of preeclampsia, and independently of maternal BMI, we observed that decidual $CD8^+$ T cell deficiency appears as a common player, and in late onset of the disease, is associated with elevated sFLT1/PLGF ratio. This is important, as $CD8^+$ T cell density is inversely associated with the severity of preeclampsia manifestations at the fetal-placental unit. Generally, $CD8^+$ T cell recruitment to peripheral tissues starts when they adhere stably to the vascular endothelium through integrins, which is followed by wall-vessel transmigration, guided by the chemokine CXCL10 gradient from the target tissue to induce $CD8^+$ T cell migration. In preeclampsia patients, elevated sFLT1 induces angiogenic imbalance, leading to global impairment of decidual vascular remodeling with structural and functional alterations. These changes alter vascular permeability and impede $CD8^+$ T cell migration. Together, these factors synergistically enhance CXCL10 expression, which contributes to impaired angiogenesis and exacerbates $CD8^+$ T cell recruitment defects. In preeclampsia patients with high BMI, high BMI can independently exacerbate vascular stiffness and further increase CXCL10 levels, increasing the susceptibility of this subset of women to develop preeclampsia. Overall, these results suggest that the mechanism through which CXCL10 recruits $CD8^+$ T cells to the decidua is disrupted in late-onset preeclampsia, independent of patients' BMI, which appears as an interesting target for therapeutic interventions.

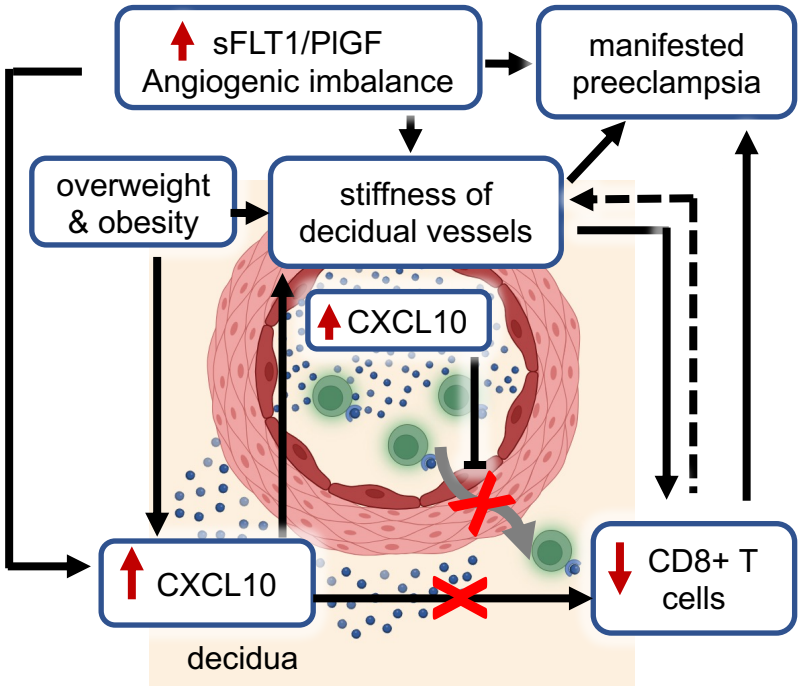

Figure 30. Hypothetical Model: Impaired Vascular Remodeling upon sFLT1 Limits CD8$^+$ T Cell Migration via Altered Vascular Permeability mediated by CXCL10. In healthy pregnancies, CD8+ T cells extravasate to the decidua along a CXCL10 gradient. In preeclampsia patients, elevated sFLT1 induces angiogenic imbalance, leading to global impairment of decidual vascular remodeling with structural and functional alterations. These changes alter vascular permeability and impede the migration of CD8+ T cells. Concomitantly, elevated circulating CXCL10 desensitizes CD8+ T cells' chemotaxis to the decidua, exacerbating recruitment defects and preeclampsia manifestations.

6. Zusammenfassung

Zusammenfassend schlagen wir auf Grundlage unserer Ergebnisse sowie der in der Literatur berichteten und hier diskutierten Daten folgendes hypothetisches Szenario im Kontext der Präeklampsie vor (Abbildung 30): Sowohl bei früh- als auch bei spätbeginnender Präeklampsie – und unabhängig vom mütterlichen BMI – zeigt sich eine verminderte Dichte decidualer $CD8^+$-T-Zellen als gemeinsamer Faktor. Bei der spätbeginnenden Form der Erkrankung ist diese zudem mit einem erhöhten sFLT1/PLGF-Verhältnis assoziiert. Dies ist von Bedeutung, da die Dichte der $CD8^+$-T-Zellen invers mit der Schwere der präeklamptischen Manifestationen an der feto-plazentaren Einheit korreliert.

Unter physiologischen Bedingungen beginnt die Rekrutierung von $CD8^+$-T-Zellen in periphere Gewebe mit ihrer stabilen Adhärenz an das vaskuläre Endothel über Integrine, gefolgt von der Transmigration durch die Gefäßwand, die durch den Chemokin-Gradienten von CXCL10 aus dem Zielgewebe gesteuert wird. Bei Präeklampsie-Patientinnen führt ein erhöhter sFLT1-Spiegel zu einem angiogenen Ungleichgewicht, das zu einer globalen Beeinträchtigung des decidualen Gefäßumbaus mit strukturellen und funktionellen Veränderungen führt. Diese Veränderungen beeinflussen die Gefäßpermeabilität und behindern die Migration von $CD8^+$-T-Zellen.

Zusammen verstärken diese Faktoren synergistisch die Expression von CXCL10, was sowohl zu einer weiteren Hemmung der Angiogenese als auch zu einer Verschärfung der Rekrutierungsdefekte von $CD8^+$-T-Zellen beiträgt. Bei Präeklampsie-Patientinnen mit hohem BMI kann dieser unabhängig die Gefäßsteifigkeit erhöhen und die CXCL10-Spiegel weiter ansteigen lassen, was die Anfälligkeit dieser Patientinnengruppe für die Entwicklung einer Präeklampsie zusätzlich erhöht. Insgesamt deuten unsere Ergebnisse darauf hin, dass der Mechanismus, über den CXCL10 $CD8^+$-T-Zellen in die Dezidua rekrutiert, bei spätbeginnender Präeklampsie unabhängig vom BMI gestört ist und somit ein vielversprechendes Ziel für therapeutische Interventionen darstellen könnte.

7. Appendix

7.1 Appendix 1. Human late-onset preeclampsia placenta

When we first started this study, both decidual and placental tissues were collected for this study, our primary investigation focused on the immunological changes within the decidua as the site of the maternal-fetal interface. Although a dataset was also generated for placental tissues, these analyses were more limited with fewer sample numbers compared to the decidua. Notably, placental villi from subsequently added samples were not subjected to further experiments.

7.1.1 Identification Of CD8$^+$ T Cells in the Placenta

We assessed the CD8$^+$ T cell compartment within the late-onset preeclampsia placenta, only in the high BMI control and high BMI preeclampsia groups. Immunohistochemical analysis revealed an abundant infiltration of CD8$^+$ T cells in the placentas of both groups. These cells exhibited a scattered distribution and were observed within the villi, in the surrounding connective tissue, and in perivascular locations. However, despite their abundance, quantitative analysis showed no statistically significant difference in the density of placental CD8$^+$ T cells between the high BMI control and high BMI preeclampsia groups (Appendix 1, Figure 1).

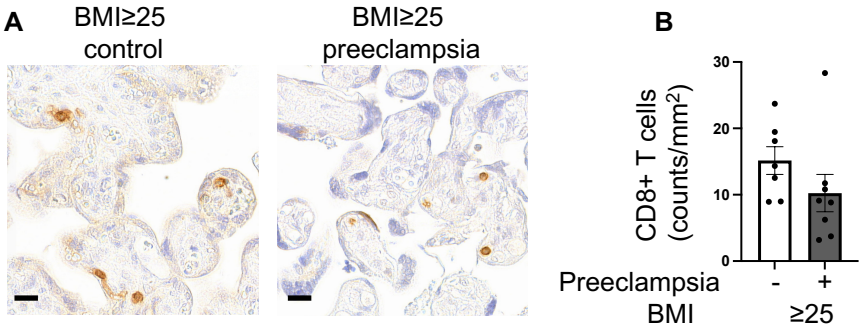

Appendix 1. Figure 1. CD8$^+$ T Cell Density Was Unaffected in The Placenta of Late-Onset Preeclampsia Patients. A: CD8$^+$ T cells of the control and preeclampsia patient placenta were assessed by immunohistochemistry. B: Comparison of the density of CD8$^+$ T cells in each group. * $p < 0.05$, two-way ANOVA, $p < 0.05$. Scale bar=20μm.

7.1.2 Placental mRNA Levels of Cytokines and Angiogenic Factors

We performed similar expression analyses on placental tissues of a few of the patients in this study to generate preliminary data. The number of replicates in this pilot study was low and hence, allows no conclusions on these results.

The mRNA levels of *IFNG, IL7* and *IL15* in placentas from both normal BMI and high BMI group has no significant differences among control and preeclampsia patients, but the *TNF* level was significantly upregulated in normal BMI preeclampsia and tended to increase in high BMI preeclampsia, which is not found in decidua, suggesting the need for further evaluation of these soluble mediators that could affect the decidual immunity (Appendix 1, Figure 2).

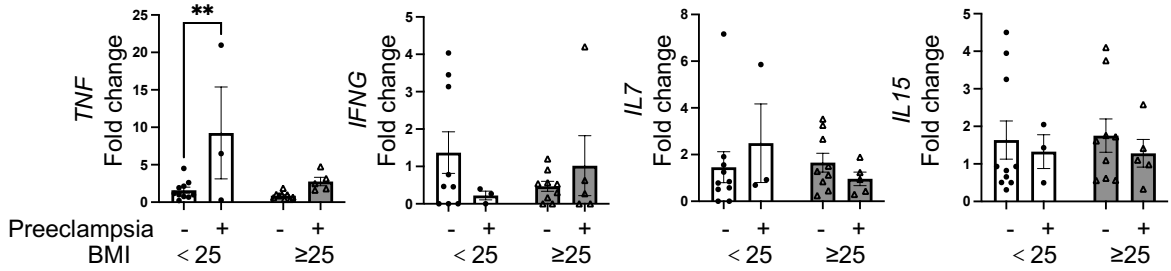

Appendix 1. Figure 2. *TNF* Upregulated in the Placenta of Normal BMI Late-Onset Preeclampsia. mRNA analysis of *TNF*, *IFNG*, *IL7*, and *IL15* in normal BMI and high BMI of control and preeclamptic patient placenta. * $p < 0.05$, ** $p < 0.01$, statistical comparisons performed by two-way ANOVA with Tukey's post-hoc test.

To investigate the influence of BMI on placental angiogenesis, we next examined the mRNA levels of selected angiogenic factors. Overall, this analysis revealed no significant differences in the expression of most factors between the control and preeclampsia women, independent of BMI. However, we identified two notable exceptions. First, the expression of *VEGF* was significantly higher in placentas from preeclamptic women with a normal BMI compared to those with a high BMI. Second, the lymphatic vessel endothelial hyaluronan receptor *LYVE1* was significantly decreased in normotensive high-BMI women compared to their normal-BMI counterparts. This may suggest that not only preeclampsia, but also high BMI alone or in combination with preeclampsia can affect angiogenesis (Appendix 1, Figure 3).

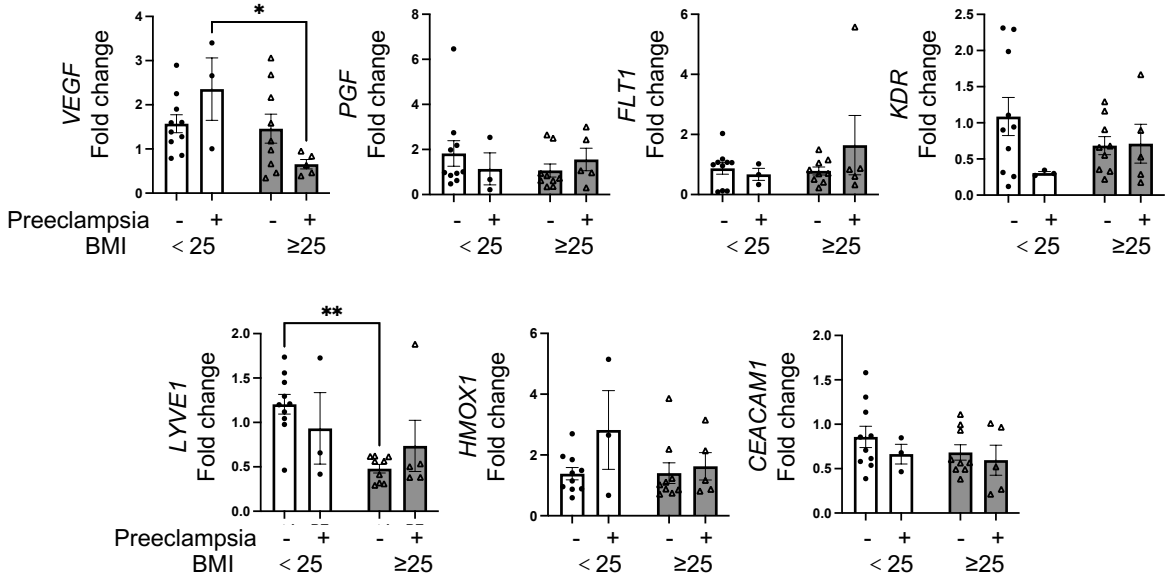

Appendix 1. Figure 3. Relatively Stable mRNA Level of Angiogenic Factor in Human Preeclampsia Placenta. mRNA analysis of angiogenic factors: *VEGF*, *PGF*, Kinase Insert Domain Receptor (*KDR*), Fms-like Tyrosine Kinase 1 (*FLT1*), *HMOX1*, *CEACAM1* in human preeclampsia placenta. * $p < 0.05$, **$p < 0.01$, statistical comparisons performed by two-way ANOVA with Tukey's post-hoc test.

7.2 Appendix 2. Clinical Characteristics of Preeclampsia and Control Women Included in the Flow Cytometry Analysis.

	Control (n = 21)	**Preeclampsia (n = 6)**
Age (years)	36 (33–38)	33 (31–42)
SBP (mmHg)	120 (113–133)	151 (145–160)****
DBP (mmHg)	73 (65–80)	88 (85–110)****
Weight before pregnancy (kg)	68 (60–79)	82 (69–108)*
Height (cm)	165 (160–170)	172 (170–174)*
BMI (kg/m2)	26.56 (20.9–31.22)	28.11 (22.31–36.09)
Leukocytes (/nl)	10.6 (7.8–12.6)	10.6 (9.9–15.5)
sFlt-1/PlGF	4.65 (5)	151.46 (72.27–510.63)**
CRP (mg/l)	2 (3)	5 (3–17)
Protein in spot urine (g/l)	/	0.4 (2)
Gestational age (weeks+days)	38w+3d (38w+1d – 38w+6d)	36w+6d (33w+1d – 38w+5d)

Birth weight (g)	3260 (3060–3580)	3230 (1880–3460)
10% below 10th percentile birthweight	19%	37.5%
AU percentile	50 (30–76)	43 (28–63)
KU/AU percentile	1.02 (0.94–1.04)	1.05 (0.94–1.12)
Umbilical artery PI	0.95 (0.80–1.06)	1.14 (0.85–1.49)

Values presented as medians (IQR) or rates (n). *p < 0.05; **p < 0.01; ***p < 0.001.

7.3 Appendix 3. Expression of CXCL10 in CD68+ cells in Late-Onset Preeclampsia

We performed immunohistochemical staining to identify the source of the upregulated *CXCL10* mRNA in the decidua of late-onset preeclampsia. This analysis revealed that the majority of CXCL10 was expressed by decidual stromal cells. In line with our qPCR data, we observed stronger CXCL10 staining signal in the decidua from normal BMI preeclampsia patients, high BMI controls, and high BMI preeclampsia patients when compared to the normal BMI control group.

Given that macrophages have also been reported to express CXCL10 (266,267), we performed another immunohistochemistry with the macrophage marker CD68 on the same tissue and found a small subset of CD68^{+} macrophages co-expressed CXCL10 (Appendix 3, Figure 1). This indicates that a fraction of decidual macrophages also contributes to the local production of this chemokine.

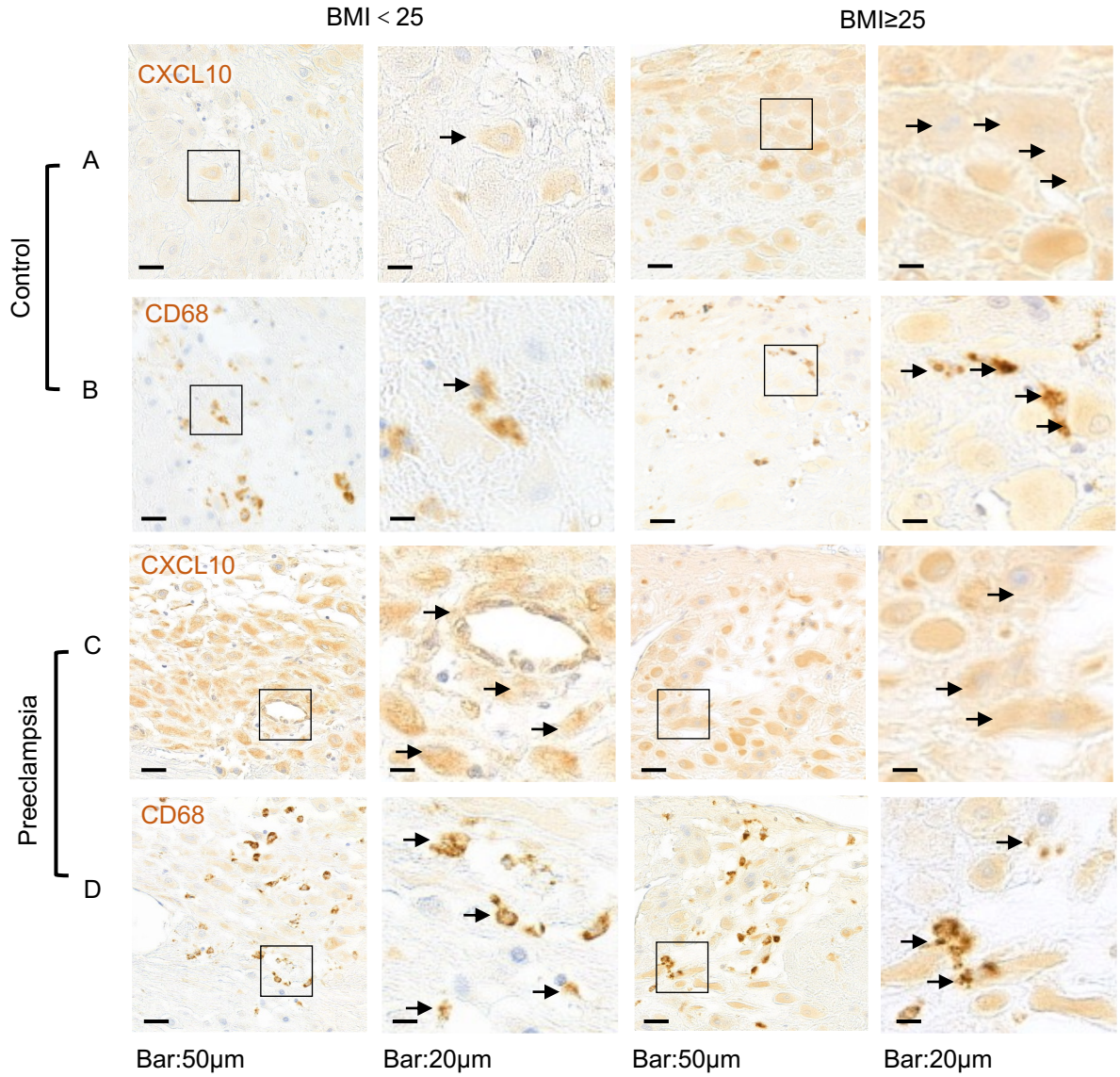

Appendix 3. Figure 1. Decidual Stromal Cells Are the Primary Source of CXCL10 at The Human Maternal-Fetal Interface. Row A and C: Representative images of immunohistochemical staining for CXCL10 in decidual tissues. Row B and D: Representative images of the macrophage marker CD68. A small subset of $CD68^{+}$ macrophages show positive staining for CXCL10 (arrows).

7.4 Appendix 4. Decidual mRNA Levels of Angiogenic Factors in Late-Onset Preeclampsia

We performed a preliminary screening of angiogenic factors in the decidua by qPCR (Appendix 4, Figure 1). This initial analysis was carried out only within the high BMI group, which revealed a significant downregulation of *VEGF* mRNA in the high BMI preeclampsia group. The expression of other selected angiogenic factors showed no changes between groups.

Since this screening revealed no major differences in the expression of most angiogenic factors we tested, we thought that this was unlikely to be the primary driver of the $CD8^+$ T cell changes observed in late-onset preeclampsia patients. Therefore, we did not include these markers in further analyses after expanding the sample size and group and focused more on the chemokine signaling pathways as described in the preceding sections.

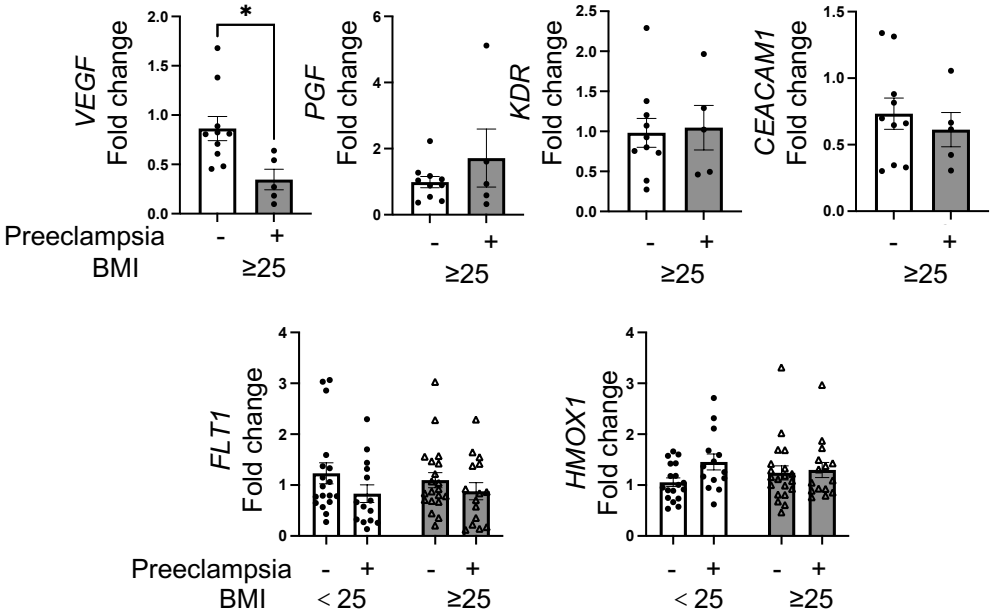

Appendix 4 Figure 1. Decreased mRNA Level of *VEGF* in Human Preeclampsia Decidua. mRNA analysis of angiogenic factors: *VEGF*, *PGF*, *KDR*, *FLT1*, *CEACAM1* in human late-onset preeclampsia decidua. *VEGF, PGF, KDR,* and *CEACMA1*: * $p < 0.05$, statistical comparisons performed by Mann-Whitney U test. *FLT1* and *HMOX1*: * $p < 0.05$, statistical comparisons performed by two-way ANOVA with Tukey's post-hoc test.

7.5 Appendix 5. The Uterine Immune Environment Across Wildtype Mouse Pregnancy

To investigate lymphocyte dynamics during pregnancy, we used a semi-allogeneic mouse pregnancy model by crossing male Balb/c with female C57BL/6 (B6) mice. This specific pairing was chosen for its distinct classical H-2K alleles (H-2Kd and H-2Kb, respectively), which effectively model the semi-allogeneic nature of human pregnancy. Virgin mice were included as non-pregnant controls to assess baseline lymphocyte profiles. Key gestational time points were selected for analysis: GD 6.5, representing the implantation stage; GD 10.5, placental formation; GD 14.5, the onset of late pregnancy when the placenta is fully developed; and GD

18.5, which is late pregnancy (Appendix 5, figure 1). For virgin mice and those at GD 6.5, the myometrium and endometrium were selected for analysis. From GD 10.5 to GD 18.5, the myometrium and decidua were examined to investigate local immune responses at the feto-maternal interface. For this study, each group consisted of 5-9 mice.

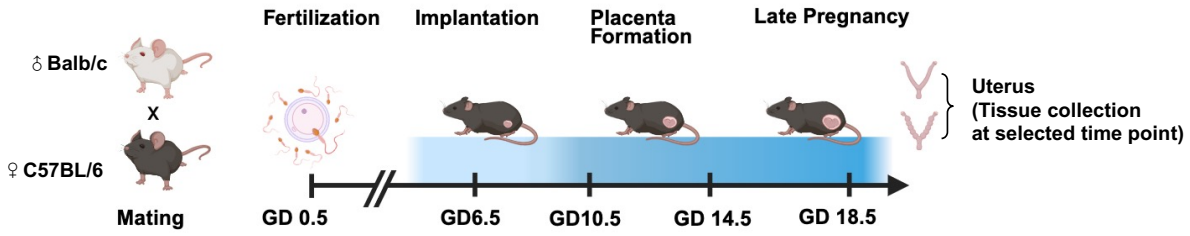

Appendix 5 Figure 1. A Schematic Overview of The Experimental Design. Uterus were collected from C57Bl/6 females mated with Balb/c males on GD 6.5, 10.5, and 14.5, as well as from virgin controls (n = 5-9). Tissue samples were analyzed and characterized using immunohistochemistry.

7.5.1 Uterine CD45+ Leucocyte and CD8⁺ T Cell Across Mouse Pregnancy

First, we assessed the density of total leukocytes using the marker CD45. With immunohistochemistry, abundant CD45⁺ cells were observed in both the myometrium and decidua throughout pregnancy. In the myometrium, the density of CD45⁺ cells significantly increased from the virgin state to GD 6.5 and remained at a high level until GD 14.5, before declining at GD 18.5. In contrast, the decidua exhibited a progressive decline in CD45⁺ cell density as gestation developed. In both compartments, the lowest density of leukocytes was observed at GD 18.5, just before parturition (Appendix 5, Figure 2, A, C, and D).

Next, we focused on the CD8⁺ T cell. Immunohistochemical staining revealed that CD8⁺ T cells infiltrated both the myometrium and decidua. Within the decidua, CD8⁺ T cells were primarily located in the stroma, some were found close to vessels. CD8+ T cells were observed as scattered, individual cells rather than organized clusters. Quantification of these cells revealed a dynamic and tissue-specific pattern. In the myometrium, CD8⁺ T cell density increased from the virgin, peaking around GD 10.5, and followed by a gradual decreasing trend towards GD 18.5. A different trend was observed in the decidua, where the density began to decline earlier,

after GD 6.5. Similar to the total leukocyte population, the density of $CD8^+$ T cells declined and reached its lowest point at GD 18.5 (Appendix 5, Figure 2, B, E, and F).

Cytokine expression in the mouse decidua also underwent dynamic changes during gestation. The mRNA levels of *Il15* were significantly higher in virgin mice compared to those at GD 18.5 (overall ANOVA, $p < 0.05$). Both *Il15* and *Il7* peaked at GD10.5. Although no significant intergroup differences were detected for *Ifng* and *Tnf*, the overall ANOVA for both was significant ($p < 0.05$). *Ifng* also peaked at GD10.5, whereas *Tnf* levels were markedly elevated before parturition (Appendix 5 figure 2. G-J).

Together, these results demonstrate that both the CD45+ leukocyte and the $CD8^+$ T cell populations undergo a significant, tissue-specific change throughout gestation, with a decline in both populations near parturition.

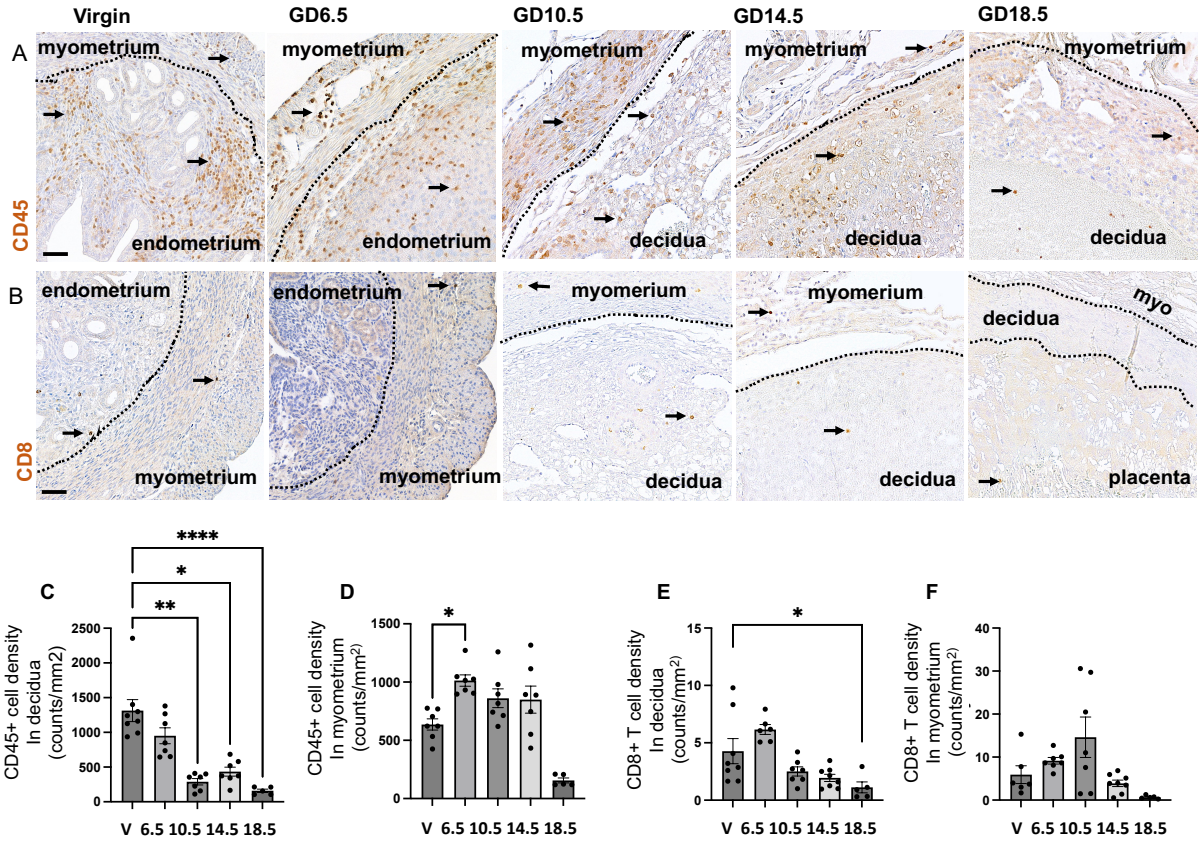

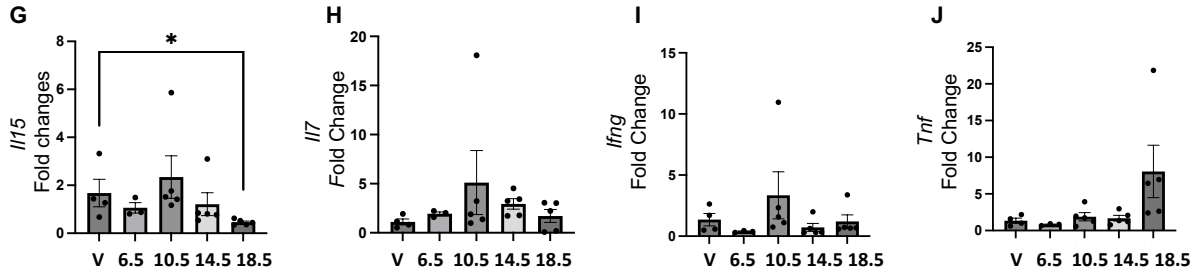

Appendix 5 Figure 2. Dynamic Changes of the Decidual Leukocyte Composition and the CD8⁺ T Cell Compartment. A: CD45+ cells of different time point tissue sections from normal mouse placenta, Bar = 50μm. B: CD8⁺ T cells of different time point tissue sections from normal mouse placenta, Bar = 50μm. C: Analysis of CD45+ cell density in decidua of different time points, D: Analysis of CD45+ cell density in myometrium of different time points. E: Analysis of CD8⁺ T cell density in decidua of different time points, F: Analysis of CD8⁺ T cell density in myometrium of different time points. Data are presented as mean ± SEM. G-J: mRNA analysis of *Il15, Il7, Ifng, and Tnf* in decidua of different time points. * $p < 0.05$, statistical comparisons performed by one-way ANOVA with Dunn's post-hoc test.

7.6 Appendix 6. Validation of Human CD8⁺ Regulatory T cell Subset Gating Strategy Using FMO Controls

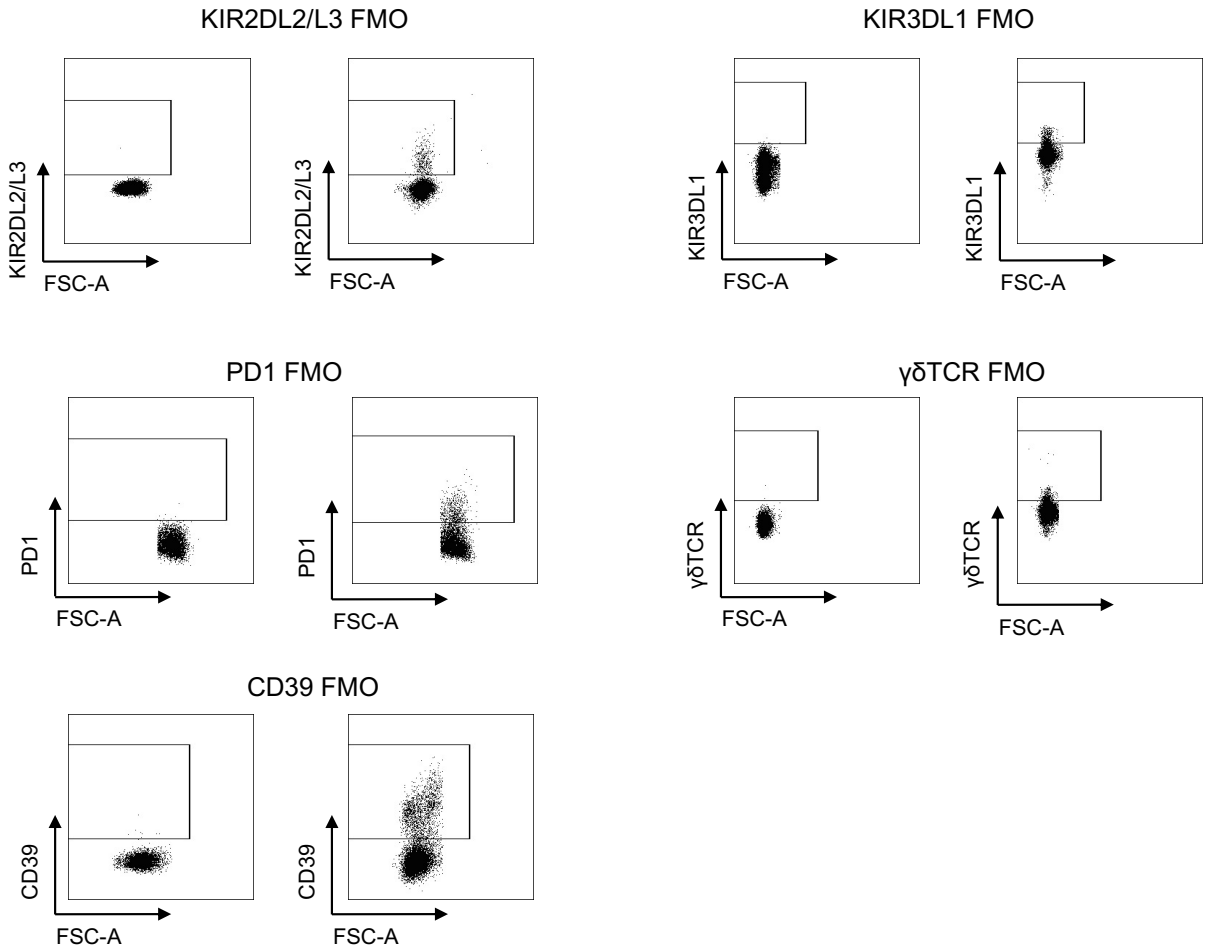

Appendix 6 Figure 1. FMO controls for human flow cytometry gating. Representative FMO controls for KIR2DL2/L3, KIR3DL1, PD1, γδTCR, and CD39 used to define $CD8^+$ regulatory T cell subsets. The FMO plots were used to determine gating thresholds for positive and negative populations.

7.7 Appendix 7. Abbreviations

AC	abdominal circumference
ACOG	American college of obstetricians and gynecologists
APS	antiphospholipid syndrome
AREG	amphiregulin
BMI	body mass index
CEACAM1	carcinoembryonic antigen-related cell adhesion molecule 1
CRP	c-reactive protein
CTB	cytotrophoblast
CTL	cytotoxic t lymphocyte
CXCL10	C-X-C motif chemokine ligand 10
CXCL9	C-X-C motif chemokine ligand 9
CXCR3	C-X-C motif chemokine receptor 3
dNK	decidual natural killer cell
EC	endothelial cells
ECM	extracellular matrix
EEC	early effector cell
eNOS	endothelial nitric oxide synthase
EOPE	early-onset preeclampsia
ESC	endometrium stroma cell
EVT	extravillous trophoblast
FGR	fetal growth restriction
FLT1	fms-like tyrosine kinase 1
FMO	fluorescence minus one
FMO	fluorescence minus one
FOD	fronto-occipital diameter
GD	gestational day
GlyT	glycogen trophoblast cell

HC	head circumference
HIF1A	hypoxia-inducible factor alpha
HLA	human leukocyte antigen
HMOX1	heme oxygenase 1
hsFLT1	human soluble fms-like tyrosine kinase 1
i.v.	intravenous
ICAM-1	intercellular adhesion molecule 1
ICM	inner cell mass
IFN-γ	interferon-γ
IL-15	interlukin-15
IL-7	interlukin-7
ISSHP	international society for the study of hypertension in pregnancy
IUGR	intrauterine growth restriction
KDR	kinase insert domain receptor
KIR	killer cell immunoglobulin-like receptor
LFA-1	lymphocyte function-associated antigen 1
LOPE	late-onset preeclampsia
MFI	median fluorescence intensity
MHC	major histocompatibility complex
MLAp	mesometrial lymphoid aggregate of pregnancy
MMP	matrix metalloproteinase
MPEC	memory precursor effector cell
NCR1	natural cytotoxicity receptor 1
NO	nitric oxide
oxLDL	oxidized low-density lipoprotein
PAI-1	plasminogen activator inhibitor 1
PD-1	programmed cell death protein 1
PECAM1	platelet and endothelial cell adhesion molecule 1

PHD	prolyl hydroxylases domain
PlGF	placental growth factor
P-TGC	parietal trophoblast giant cell
PVAT	perivascular adipose tissue
qPCR	quantitative polymerase chain reaction
ROI	regions of interest
ROS	reactive oxygen species
rtTA	reverse tetracycline-controlled trans-activator
sFLT1	soluble fms-like tyrosine kinase 1
SLE	systemic lupus erythematosus
SLEC	short-lived effector cell
SpT	spongiotrophoblast cell
STB	syncytiotrophoblast
Tcm	central memory t cell
TCR	t cell receptor
TE	trophectoderm
Tem	effector memory t cell
Temra	effector memory t cells that have re-expressed cd45ra
TNF	tumor necrosis factor
Tpm	peripheral memory t cell
Treg	regulatory t cell
Trm	tissue-resident memory t cell
Tscm	stem cell memory t cell
UA-PI	umbilical artery pulsatility index
uNK	uterine natural killer cell
VCAM-1	vascular cell adhesion molecule 1
VEGF	vascular endothelial growth factor
VLA-4	very late antigen 4
VSMC	vascular smooth muscle cell

WHO	world health organization
αSMA	α-smooth muscle actin

8. Bibliography

1. Cha J, Sun X, Dey SK. Mechanisms of implantation: strategies for successful pregnancy. Nat Med. 2012 Dec;18(12):1754–67.
2. Wang H, Dey SK. Roadmap to embryo implantation: clues from mouse models. Nat Rev Genet. 2006 Mar;7(3):185–99.
3. Vento-Tormo R, Efremova M, Botting RA, Turco MY, Vento-Tormo M, Meyer KB, et al. Single-cell reconstruction of the early maternal–fetal interface in humans. Nature. 2018 Nov;563(7731):347–53.
4. Xu L, Li Y, Sang Y, Li DJ, Du M. Crosstalk Between Trophoblasts and Decidual Immune Cells: The Cornerstone of Maternal-Fetal Immunotolerance. Front Immunol. 2021 Feb 25;12:642392.
5. Hsu P, Nanan RKH. Innate and Adaptive Immune Interactions at the Fetal–Maternal Interface in Healthy Human Pregnancy and Pre-Eclampsia. Front Immunol [Internet]. 2014 Mar 28 [cited 2025 Oct 18];5. Available from: https://www.frontiersin.org/journals/immunology/articles/10.3389/fimmu.2014.00125/full
6. Robertson SA, Care AS, Moldenhauer LM. Regulatory T cells in embryo implantation and the immune response to pregnancy. J Clin Invest. 2018 Oct 1;128(10):4224–35.
7. Hu X, Wu H, Yong X, Wang Y, Yang S, Fan D, et al. Cyclical endometrial repair and regeneration: Molecular mechanisms, diseases, and therapeutic interventions. MedComm (2020). 2023 Dec 1;4(6):e425.
8. Ameer MA, Peterson DC. Anatomy, Abdomen and Pelvis: Uterus. In: StatPearls [Internet]. Treasure Island (FL): StatPearls Publishing; 2025 [cited 2025 Aug 2]. Available from: http://www.ncbi.nlm.nih.gov/books/NBK470297/
9. Gee SE, Frey HA. Contractions: Traditional concepts and their role in modern obstetrics. Seminars in Perinatology. 2020 Mar 1;44(2):151218.
10. Ono M, Maruyama T, Masuda H, Kajitani T, Nagashima T, Arase T, et al. Side population in human uterine myometrium displays phenotypic and functional characteristics of myometrial stem cells. Proc Natl Acad Sci U S A. 2007 Nov 20;104(47):18700–5.
11. Farquharson RG, Stephenson MD, editors. Early Pregnancy [Internet]. 2nd ed. Cambridge: Cambridge University Press; 2017 [cited 2025 Oct 19]. Available from: https://www.cambridge.org/core/books/early-pregnancy/5AAB0223BF9603D29AA11DCE9E1F2F9A
12. Ochoa-Bernal MA, Fazleabas AT. Physiologic Events of Embryo Implantation and Decidualization in Human and Non-Human Primates. International Journal of Molecular Sciences. 2020 Jan;21(6):1973.
13. Okada H, Tsuzuki T, Murata H. Decidualization of the human endometrium. Reprod Med Biol. 2018 Feb 1;17(3):220–7.
14. Yang F, Zheng Q, Jin L. Dynamic Function and Composition Changes of Immune Cells During Normal and Pathological Pregnancy at the Maternal-Fetal Interface. Front Immunol [Internet]. 2019 Oct 18 [cited 2025 Oct 18];10. Available from: https://www.frontiersin.org/journals/immunology/articles/10.3389/fimmu.2019.02317/full

15. Vornic I, Buciu V, Furau CG, Zara F, Novacescu D, Barb AC, et al. The Interplay of Molecular Factors and Morphology in Human Placental Development and Implantation. Biomedicines. 2024 Dec;12(12):2908.
16. Kramer AC, Jansson T, Bale TL, Powell TL. Maternal-fetal cross-talk via the placenta: influence on offspring development and metabolism. Development. 2023 Oct 13;150(20):dev202088.
17. Herrick EJ, Bordoni B. Embryology, Placenta. In: StatPearls [Internet]. Treasure Island (FL): StatPearls Publishing; 2025 [cited 2025 Oct 18]. Available from: http://www.ncbi.nlm.nih.gov/books/NBK551634/
18. Jin J, Menon R. Placental exosomes: A proxy to understand pregnancy complications. Am J Reprod Immunol. 2018 May;79(5):e12788.
19. Hoo R, Nakimuli A, Vento-Tormo R. Innate Immune Mechanisms to Protect Against Infection at the Human Decidual-Placental Interface. Front Immunol. 2020 Sep 10;11:2070.
20. Zhang S, Lin H, Kong S, Wang S, Wang H, Wang H, et al. Physiological and molecular determinants of embryo implantation. Mol Aspects Med. 2013 Oct;34(5):939–80.
21. Norwitz ER, Schust DJ, Fisher SJ. Implantation and the Survival of Early Pregnancy. New England Journal of Medicine. 2001 Nov 8;345(19):1400–8.
22. Benirschke K. The human placenta. J. D. Boyd and W. J. Hamilton. Heffer, Cambridge, 365 pp. 1970. Teratology. 1973;8(1):77–8.
23. Niakan KK, Eggan K. Analysis of human embryos from zygote to blastocyst reveals distinct gene expression patterns relative to the mouse. Developmental Biology. 2013 Mar 1;375(1):54–64.
24. Schlafke S, Enders AC. Cellular Basis of Interaction Between Trophoblast and Uterus at Implantation. Biol Reprod. 1975 Feb 1;12(1):41–65.
25. Hertig AT, Rock J, Adams EC. A description of 34 human ova within the first 17 days of development. American Journal of Anatomy. 1956;98(3):435–93.
26. Chesley's Hypertensive Disorders in Pregnancy [Internet]. 2021 [cited 2025 Oct 18]. Available from: https://shop.elsevier.com/books/chesleys-hypertensive-disorders-in-pregnancy/taylor/978-0-12-818417-2
27. Turco MY, Moffett A. Development of the human placenta. Development. 2019 Nov 27;146(22):dev163428.
28. Aplin JD, Whittaker H, Jana Lim YT, Swietlik S, Charnock J, Jones CJP. Hemangioblastic foci in human first trimester placenta: Distribution and gestational profile. Placenta. 2015 Oct 1;36(10):1069–77.
29. Burton GJ, Woods AW, Jauniaux E, Kingdom JCP. Rheological and Physiological Consequences of Conversion of the Maternal Spiral Arteries for Uteroplacental Blood Flow during Human Pregnancy. Placenta. 2009 Jun;30(6):473–82.
30. Espinoza J, Romero R, Kim YM, Kusanovic JP, Hassan S, Erez O, et al. NORMAL AND ABNORMAL TRANSFORMATION OF THE SPIRAL ARTERIES DURING PREGNANCY. J Perinat Med. 2006;34(6):447–58.
31. Brosens I, Pijnenborg R, Vercruysse L, Romero R. THE "GREAT OBSTETRICAL SYNDROMES" ARE ASSOCIATED WITH DISORDERS OF DEEP PLACENTATION. Am J Obstet Gynecol. 2011 Mar;204(3):193–201.

32. Whitley GStJ, Cartwright JE. Cellular and Molecular Regulation of Spiral Artery Remodelling: Lessons from the Cardiovascular Field. Placenta. 2010 Jun;31(6):465–74.
33. Pijnenborg R, Vercruysse L, Hanssens M. The Uterine Spiral Arteries In Human Pregnancy: Facts and Controversies. Placenta. 2006 Sep 1;27(9):939–58.
34. Staff AC, Fjeldstad HE, Fosheim IK, Moe K, Turowski G, Johnsen GM, et al. Failure of physiological transformation and spiral artery atherosis: their roles in preeclampsia. American Journal of Obstetrics and Gynecology. 2022 Feb 1;226(2, Supplement):S895–906.
35. Gauster M, Moser G, Wernitznig S, Kupper N, Huppertz B. Early human trophoblast development: from morphology to function. Cell Mol Life Sci. 2022 Jun 5;79(6):345.
36. Opichka MA, Rappelt MW, Gutterman DD, Grobe JL, McIntosh JJ. Vascular Dysfunction in Preeclampsia. Cells. 2021 Nov;10(11):3055.
37. Eriksson JG, Forsén T, Tuomilehto J, Osmond C, Barker DJ. Early growth and coronary heart disease in later life: longitudinal study. BMJ. 2001 Apr 21;322(7292):949–53.
38. Rana S, Lemoine E, Granger JP, Karumanchi SA. Preeclampsia. Circulation Research. 2019 Mar 29;124(7):1094–112.
39. Dimitriadis E, Rolnik DL, Zhou W, Estrada-Gutierrez G, Koga K, Francisco RPV, et al. Pre-eclampsia. Nat Rev Dis Primers. 2023 Feb 16;9(1):1–22.
40. AWMF Leitlinienregister [Internet]. [cited 2025 Sep 19]. Available from: https://register.awmf.org/de/leitlinien/detail/015-018
41. Aneman I, Pienaar D, Suvakov S, Simic TP, Garovic VD, McClements L. Mechanisms of Key Innate Immune Cells in Early- and Late-Onset Preeclampsia. Front Immunol. 2020;11:1864.
42. Huppertz B. The Critical Role of Abnormal Trophoblast Development in the Etiology of Preeclampsia. Curr Pharm Biotechnol. 2018 Aug;19(10):771–80.
43. Brosens I, Robertson WB, Dixon HG. The physiological response of the vessels of the placental bed to normal pregnancy. J Pathol Bacteriol. 1967 Apr;93(2):569–79.
44. Redman CWG. Pre-eclampsia and the placenta. Placenta. 1991 Jul 1;12(4):301–8.
45. Staff AC. The two-stage placental model of preeclampsia: An update. Journal of Reproductive Immunology. 2019 Sep 1;134–135:1–10.
46. Fosheim IK, Alnaes-Katjavivi P, Redman C, Roald B, Staff AC, Størvold GL. Acute atherosis of decidua basalis; characterization of spiral arteries, endothelial status and activation. Placenta. 2019 Jul 1;82:10–6.
47. Redman CWG, Staff AC, Roberts JM. Syncytiotrophoblast stress in preeclampsia: the convergence point for multiple pathways. American Journal of Obstetrics & Gynecology. 2022 Feb 1;226(2):S907–27.
48. Pankiewicz K, Fijałkowska A, Issat T, Maciejewski TM. Insight into the Key Points of Preeclampsia Pathophysiology: Uterine Artery Remodeling and the Role of MicroRNAs. International Journal of Molecular Sciences. 2021 Jan;22(6):3132.
49. Cox LS, Redman C. The role of cellular senescence in ageing of the placenta. Placenta. 2017 Apr 1;52:139–45.
50. Rana S, Burke SD, Karumanchi SA. Imbalances in circulating angiogenic factors in the pathophysiology of preeclampsia and related disorders. Am J Obstet Gynecol. 2022 Feb;226(2 Suppl):S1019–34.

51. Geindreau M, Ghiringhelli F, Bruchard M. Vascular Endothelial Growth Factor, a Key Modulator of the Anti-Tumor Immune Response. International Journal of Molecular Sciences. 2021 Jan;22(9):4871.
52. Lee C, Kim MJ, Kumar A, Lee HW, Yang Y, Kim Y. Vascular endothelial growth factor signaling in health and disease: from molecular mechanisms to therapeutic perspectives. Sig Transduct Target Ther. 2025 May 19;10(1):170.
53. Vogtmann R, Kühnel E, Dicke N, Verkaik-Schakel RN, Plösch T, Schorle H, et al. Human sFLT1 Leads to Severe Changes in Placental Differentiation and Vascularization in a Transgenic hsFLT1/rtTA FGR Mouse Model. Front Endocrinol (Lausanne). 2019;10:165.
54. Vogtmann R, Heupel J, Herse F, Matin M, Hagmann H, Bendix I, et al. Circulating Maternal sFLT1 (Soluble fms-Like Tyrosine Kinase-1) Is Sufficient to Impair Spiral Arterial Remodeling in a Preeclampsia Mouse Model. Hypertension. 2021 Oct;78(4):1067–79.
55. Fukumura D, Gohongi T, Kadambi A, Izumi Y, Ang J, Yun CO, et al. Predominant role of endothelial nitric oxide synthase in vascular endothelial growth factor-induced angiogenesis and vascular permeability. Proceedings of the National Academy of Sciences. 2001 Feb 27;98(5):2604–9.
56. Hood JD, Meininger CJ, Ziche M, Granger HJ. VEGF upregulates ecNOS message, protein, and NO production in human endothelial cells. American Journal of Physiology-Heart and Circulatory Physiology. 1998 Mar;274(3):H1054–8.
57. Zeisler H, Llurba E, Chantraine F, Vatish M, Staff AC, Sennström M, et al. Predictive Value of the sFlt-1:PlGF Ratio in Women with Suspected Preeclampsia. New England Journal of Medicine. 2016 Jan 7;374(1):13–22.
58. Zeisler H, Llurba E, Chantraine FJ, Vatish M, Staff AC, Sennström M, et al. Soluble fms-like tyrosine kinase-1 to placental growth factor ratio: ruling out pre-eclampsia for up to 4 weeks and value of retesting. Ultrasound in Obstetrics & Gynecology. 2019;53(3):367–75.
59. Karpova NS, Dmitrenko OP, Budykina TS. Literature Review: The sFlt1/PlGF Ratio and Pregestational Maternal Comorbidities: New Risk Factors to Predict Pre-Eclampsia. International Journal of Molecular Sciences. 2023 Jan;24(7):6744.
60. Costa ML, Cavalli R de C, Korkes HA, Cunha Filho EV da, Peraçoli JC. Diagnosis and Management of Preeclampsia: Suggested Guidance on the Use of Biomarkers. Rev Bras Ginecol Obstet. 2022 Apr 25;44(9):878–83.
61. Melamed N, Kingdom JC, Fu L, Yip PM, Arruda-Caycho I, Hui D, et al. Predictive and Diagnostic Value of the Angiogenic Proteins in Patients With Chronic Kidney Disease. Hypertension. 2024 Nov;81(11):2251–62.
62. Hernández-Pacheco JA, Rosales-Zamudio CI, Borboa-Olivares H, Espejel-Núñez A, Parra-Hernández S, Estrada-Gutiérrez G, et al. The sFlt-1/PlGF ratio as a triage tool to identify superimposed preeclampsia in women with chronic hypertension in emergency rooms. Pregnancy Hypertension. 2020 Jul 1;21:38–42.
63. Stepan H, Herraiz I, Schlembach D, Verlohren S, Brennecke S, Chantraine F, et al. Implementation of the sFlt-1/PlGF ratio for prediction and diagnosis of pre-eclampsia in

singleton pregnancy: implications for clinical practice. Ultrasound Obstet Gynecol. 2015 Mar;45(3):241–6.
64. Kumar N, Das V, Agarwal A, Agrawal S. Correlation of sFlt/PlGF ratio with severity of preeclampsia in an Indian population. AJOG Glob Rep. 2023 May;3(2):100177.
65. Tanner MS, Malhotra A, Davey MA, Wallace EM, Mol BW, Palmer KR. Maternal and neonatal complications in women with medical comorbidities and preeclampsia. Pregnancy Hypertens. 2022 Mar;27:62–8.
66. Wiles K, Chappell LC, Lightstone L, Bramham K. Updates in Diagnosis and Management of Preeclampsia in Women with CKD. Clin J Am Soc Nephrol. 2020 Sep 7;15(9):1371–80.
67. Magee LA, Brown MA, Hall DR, Gupte S, Hennessy A, Karumanchi SA, et al. The 2021 International Society for the Study of Hypertension in Pregnancy classification, diagnosis & management recommendations for international practice. Pregnancy Hypertension. 2022 Mar;27:148–69.
68. Gestational Hypertension and Preeclampsia: ACOG Practice Bulletin, Number 222. Obstetrics & Gynecology. 2020 Jun;135(6):e237.
69. Obesity and overweight [Internet]. [cited 2025 Sep 19]. Available from: https://www.who.int/news-room/fact-sheets/detail/obesity-and-overweight
70. Xiong Y, Wang J, Huang S, Liu C, Liu Y, Qi Y, et al. Association between maternal prepregnancy body mass index and pregnancy outcomes following assisted reproductive technology: A systematic review and dose-response meta-analysis. Obes Rev. 2021 Jun;22(6):e13219.
71. Bartsch E, Medcalf KE, Park AL, Ray JG. Clinical risk factors for pre-eclampsia determined in early pregnancy: systematic review and meta-analysis of large cohort studies. 2016 Apr 19 [cited 2025 Oct 18]; Available from: https://www.bmj.com/content/353/bmj.i1753
72. Najafi F, Hasani J, Izadi N, Hashemi-Nazari SS, Namvar Z, Mohammadi S, et al. The effect of prepregnancy body mass index on the risk of gestational diabetes mellitus: A systematic review and dose-response meta-analysis. Obes Rev. 2019 Mar;20(3):472–86.
73. Vats H, Saxena R, Sachdeva MP, Walia GK, Gupta V. Impact of maternal pre-pregnancy body mass index on maternal, fetal and neonatal adverse outcomes in the worldwide populations: A systematic review and meta-analysis. Obes Res Clin Pract. 2021;15(6):536–45.
74. Van Gaal LF, Mertens IL, De Block CE. Mechanisms linking obesity with cardiovascular disease. Nature. 2006 Dec 14;444(7121):875–80.
75. Xia N, Horke S, Habermeier A, Closs EI, Reifenberg G, Gericke A, et al. Uncoupling of Endothelial Nitric Oxide Synthase in Perivascular Adipose Tissue of Diet-Induced Obese Mice. Arterioscler Thromb Vasc Biol. 2016 Jan;36(1):78–85.
76. Kim F, Tysseling KA, Rice J, Pham M, Haji L, Gallis BM, et al. Free fatty acid impairment of nitric oxide production in endothelial cells is mediated by IKKbeta. Arterioscler Thromb Vasc Biol. 2005 May;25(5):989–94.
77. Haslam DW, James WPT. Obesity. Lancet. 2005 Oct 1;366(9492):1197–209.

78. Herzog MJ, Müller P, Lechner K, Stiebler M, Arndt P, Kunz M, et al. Arterial stiffness and vascular aging: mechanisms, prevention, and therapy. Sig Transduct Target Ther. 2025 Sep 1;10(1):282.
79. Poirier P, Giles TD, Bray GA, Hong Y, Stern JS, Pi-Sunyer FX, et al. Obesity and cardiovascular disease: pathophysiology, evaluation, and effect of weight loss. Arterioscler Thromb Vasc Biol. 2006 May;26(5):968–76.
80. Huang CJ, McAllister MJ, Slusher AL, Webb HE, Mock JT, Acevedo EO. Obesity-Related Oxidative Stress: the Impact of Physical Activity and Diet Manipulation. Sports Med Open. 2015;1(1):32.
81. Samad F, Ruf W. Inflammation, obesity, and thrombosis. Blood. 2013 Nov 14;122(20):3415–22.
82. Kim B, Arany Z. Endothelial Lipid Metabolism. Cold Spring Harb Perspect Med. 2022 Jul 21;12(6):a041162.
83. Catalano PM, Shankar K. Obesity and pregnancy: mechanisms of short term and long term adverse consequences for mother and child. BMJ. 2017 Feb 8;356:j1.
84. Almutairi FS, Alsaykhan AM, Almatrood AA. Obesity Prevalence and Its Impact on Maternal and Neonatal Outcomes in Pregnant Women: A Systematic Review. Cureus. 16(12):e75262.
85. Albrecht M, Worthmann A, Heeren J, Diemert A, Arck PC. Maternal lipids in overweight and obesity: implications for pregnancy outcomes and offspring's body composition. Semin Immunopathol. 2025;47(1):10.
86. Young CF, Isaacs D. A call for a multidisciplinary intervention to address severe insulin resistance during pregnancy. Nat Rev Endocrinol. 2025 Oct;21(10):586–7.
87. Li Y, Chen J, Lin Y, Xu L, Sang Y, Li D, et al. Obesity Challenge Drives Distinct Maternal Immune Response Changes in Normal Pregnant and Abortion-Prone Mouse Models. Front Immunol [Internet]. 2021 Jun 9 [cited 2025 Jul 23];12. Available from: https://www.frontiersin.org/journals/immunology/articles/10.3389/fimmu.2021.694077/full
88. Bernhardt GV, Shivappa P, Bernhardt K, Bhat S, Pinto JRT, Jhancy M, et al. Markers of inflammation in obese pregnant women: Adenosine deaminase and high sensitive C – reactive protein. Eur J Obstet Gynecol Reprod Biol X. 2022 Oct 14;16:100167.
89. Zhang CXW, Candia AA, Sferruzzi-Perri AN. Placental inflammation, oxidative stress, and fetal outcomes in maternal obesity. Trends in Endocrinology & Metabolism. 2024 Jul 1;35(7):638–47.
90. Joó JG, Sulyok E, Bódis J, Kornya L. Disrupted Balance of the Oxidant-Antioxidant System in the Pathophysiology of Female Reproduction: Oxidative Stress and Adverse Pregnancy Outcomes. Curr Issues Mol Biol. 2023 Oct 4;45(10):8091–111.
91. Teefey CP, Durnwald CP, Srinivas SK, Levine LD. Adverse Maternal Outcomes Differ between Obese and Nonobese Women with Severe Preeclampsia. Am J Perinatol. 2019 Jan;36(1):74–8.
92. Brunner K, Linder T, Klaritsch P, Tura A, Windsperger K, Göbl C. The Impact of Overweight and Obesity on Pregnancy: A Narrative Review of Physiological Consequences, Risks and Challenges in Prenatal Care, and Early Intervention Strategies. Curr Diab Rep. 2025 Apr 21;25(1):30.

93. Kagami K, Ono M, Iizuka T, Matsumoto T, Hosono T, Sekizuka-Kagami N, et al. A novel third mesh-like myometrial layer connects the longitudinal and circular muscle fibers -A potential stratum to coordinate uterine contractions-. Sci Rep. 2020 May 19;10(1):8274.
94. Velicky P, Knöfler M, Pollheimer J. Function and control of human invasive trophoblast subtypes: Intrinsic vs. maternal control. Cell Adh Migr. 2016 Mar 3;10(1–2):154–62.
95. Helige C, Ahammer H, Moser G, Hammer A, Dohr G, Huppertz B, et al. Distribution of decidual natural killer cells and macrophages in the neighbourhood of the trophoblast invasion front: a quantitative evaluation. Hum Reprod. 2014 Jan;29(1):8–17.
96. ScienceDirect [Internet]. [cited 2025 Oct 18]. The Guide to Investigation of Mouse Pregnancy. Available from: https://www.sciencedirect.com/book/9780123944450/the-guide-to-investigation-of-mouse-pregnancy
97. Elia A, Georgiades P. Investigation of the pregnancy-induced muscle bundle dispersal of the inner myometrium of adult mouse uterus and its relationship to the metrial gland/MLAp. Biochem Biophys Res Commun. 2021 Dec 20;584:66–72.
98. Das A, Mantena SR, Kannan A, Evans DB, Bagchi MK, Bagchi IC. De novo synthesis of estrogen in pregnant uterus is critical for stromal decidualization and angiogenesis. Proc Natl Acad Sci U S A. 2009 Jul 28;106(30):12542–7.
99. Hirota Y, Acar N, Tranguch S, Burnum KE, Xie H, Kodama A, et al. Uterine FK506-binding protein 52 (FKBP52)-peroxiredoxin-6 (PRDX6) signaling protects pregnancy from overt oxidative stress. Proc Natl Acad Sci U S A. 2010 Aug 31;107(35):15577–82.
100. Elmore SA, Cochran RZ, Bolon B, Lubeck B, Mahler B, Sabio D, et al. Histology Atlas of the Developing Mouse Placenta. Toxicol Pathol. 2022 Jan 1;50(1):60–117.
101. Cross JC, Werb Z, Fisher SJ. Implantation and the placenta: key pieces of the development puzzle. Science. 1994 Dec 2;266(5190):1508–18.
102. Malassiné A, Frendo JL, Evain-Brion D. A comparison of placental development and endocrine functions between the human and mouse model. Hum Reprod Update. 2003;9(6):531–9.
103. Georgiades P, Ferguson-Smith AC, Burton GJ. Comparative developmental anatomy of the murine and human definitive placentae. Placenta. 2002 Jan;23(1):3–19.
104. Hu D, Cross JC. Development and function of trophoblast giant cells in the rodent placenta. Int J Dev Biol. 2010;54(2–3):341–54.
105. Oh-McGinnis R, Bogutz AB, Lefebvre L. Partial loss of Ascl2 function affects all three layers of the mature placenta and causes intrauterine growth restriction. Dev Biol. 2011 Mar 15;351(2):277–86.
106. Varberg KM, Soares MJ. Paradigms for investigating invasive trophoblast cell development and contributions to uterine spiral artery remodeling. Placenta. 2021 Sep 15;113:48–56.
107. Ain R, Canham LN, Soares MJ. Gestation stage-dependent intrauterine trophoblast cell invasion in the rat and mouse: novel endocrine phenotype and regulation. Dev Biol. 2003 Aug 1;260(1):176–90.
108. Dilworth MR, Sibley CP. Review: Transport across the placenta of mice and women. Placenta. 2013 Mar;34 Suppl:S34-39.
109. Hardardottir L. CD8+ T cells in pregnancy: Characterization and function of uterine CD8+ T cells [Internet] [doctoralThesis]. Staats- und Universitätsbibliothek Hamburg

Carl von Ossietzky; 2023 [cited 2025 Sep 30]. Available from: https://ediss.sub.uni-hamburg.de/handle/ediss/10196
110. Solano ME. Decidual immune cells: Guardians of human pregnancies. Best Practice & Research Clinical Obstetrics & Gynaecology. 2019 Oct 1;60:3–16.
111. Petroff MG, Nguyen SL, Ahn SH. Fetal-placental antigens and the maternal immune system: Reproductive immunology comes of age. Immunological Reviews. 2022;308(1):25–39.
112. Faas MM, De Vos P. Innate immune cells in the placental bed in healthy pregnancy and preeclampsia. Placenta. 2018 Sep 1;69:125–33.
113. Jiang X, Du MR, Li M, Wang H. Three macrophage subsets are identified in the uterus during early human pregnancy. Cell Mol Immunol. 2018 Dec;15(12):1027–37.
114. Moffett A, Colucci F. Uterine NK cells: active regulators at the maternal-fetal interface. J Clin Invest. 2014 May;124(5):1872–9.
115. Xiong S, Sharkey AM, Kennedy PR, Gardner L, Farrell LE, Chazara O, et al. Maternal uterine NK cell-activating receptor KIR2DS1 enhances placentation. J Clin Invest. 2013 Oct;123(10):4264–72.
116. Thielens A, Vivier E, Romagné F. NK cell MHC class I specific receptors (KIR): from biology to clinical intervention. Curr Opin Immunol. 2012 Apr;24(2):239–45.
117. Erlebacher A. Immunology of the maternal-fetal interface. Annu Rev Immunol. 2013;31:387–411.
118. Gustafsson C, Mjösberg J, Matussek A, Geffers R, Matthiesen L, Berg G, et al. Gene expression profiling of human decidual macrophages: evidence for immunosuppressive phenotype. PLoS One. 2008 Apr 30;3(4):e2078.
119. Jena MK, Nayak N, Chen K, Nayak NR. Role of Macrophages in Pregnancy and Related Complications. Arch Immunol Ther Exp (Warsz). 2019 Oct;67(5):295–309.
120. Lash GE, Pitman H, Morgan HL, Innes BA, Agwu CN, Bulmer JN. Decidual macrophages: key regulators of vascular remodeling in human pregnancy. J Leukoc Biol. 2016 Aug;100(2):315–25.
121. Heyward CY, Sones JL, Lob HE, Yuen LC, Abbott KE, Huang W, et al. The decidua of preeclamptic-like BPH/5 mice exhibits an exaggerated inflammatory response during early pregnancy. J Reprod Immunol. 2017 Apr;120:27–33.
122. Bartmann C, Segerer SE, Rieger L, Kapp M, Sütterlin M, Kämmerer U. Quantification of the predominant immune cell populations in decidua throughout human pregnancy. Am J Reprod Immunol. 2014 Feb;71(2):109–19.
123. van der Zwan A, Bi K, Norwitz ER, Crespo ÂC, Claas FHJ, Strominger JL, et al. Mixed signature of activation and dysfunction allows human decidual CD8+ T cells to provide both tolerance and immunity. Proc Natl Acad Sci U S A. 2018 Jan 9;115(2):385–90.
124. Yu Y, Ma X, Gong R, Zhu J, Wei L, Yao J. Recent advances in CD8+ regulatory T cell research. Oncol Lett. 2018 Jun;15(6):8187–94.
125. Qin Z, Long Y. Immunological dysregulation in preeclampsia: Pathogenesis and clinical implications. Int Immunopharmacol. 2025 Oct 10;163:115314.
126. Yue S, Meng J. Role of Decidual Natural Killer Cells in the Pathogenesis of Preeclampsia. Am J Reprod Immunol. 2025 Jan;93(1):e70033.

127. Du M, Wang W, Huang L, Guan X, Lin W, Yao J, et al. Natural killer cells in the pathogenesis of preeclampsia: a double-edged sword. J Matern Fetal Neonatal Med. 2022 Mar;35(6):1028–35.
128. Fraser R, Whitley GSJ, Thilaganathan B, Cartwright JE. Decidual natural killer cells regulate vessel stability: implications for impaired spiral artery remodelling. J Reprod Immunol. 2015 Aug;110:54–60.
129. Zhou J, Yan P, Ma W, Li J. Cytokine modulation and immunoregulation of uterine NK cells in pregnancy disorders. Cytokine Growth Factor Rev. 2025 Feb;81:40–53.
130. Faas MM, Spaans F, De Vos P. Monocytes and macrophages in pregnancy and pre-eclampsia. Front Immunol. 2014;5:298.
131. Saito S, Tsuda S, Nakashima A. T cell immunity and the etiology and pathogenesis of preeclampsia. Journal of Reproductive Immunology. 2023 Sep 1;159:104125.
132. Hardardottir L, Bazzano MV, Glau L, Gattinoni L, Köninger A, Tolosa E, et al. The New Old CD8+ T Cells in the Immune Paradox of Pregnancy. Front Immunol. 2021;12:765730.
133. Schluns KS, Lefrançois L. Cytokine control of memory T-cell development and survival. Nat Rev Immunol. 2003 Apr;3(4):269–79.
134. Jarjour NN, Dalzell TS, Maurice NJ, Wanhainen KM, Peng C, O'Flanagan SD, et al. Collaboration between interleukin-7 and -15 enables adaptation of tissue-resident and circulating memory CD8+ T cells to cytokine deficiency. Immunity. 2025 Mar 11;58(3):616-631.e5.
135. Ye LL, Wei XS, Zhang M, Niu YR, Zhou Q. The Significance of Tumor Necrosis Factor Receptor Type II in CD8+ Regulatory T Cells and CD8+ Effector T Cells. Frontiers in Immunology [Internet]. 2018 [cited 2023 Dec 26];9. Available from: https://www.frontiersin.org/articles/10.3389/fimmu.2018.00583
136. Iwai Y, Hemmi H, Mizenina O, Kuroda S, Suda K, Steinman RM. An IFN-γ-IL-18 Signaling Loop Accelerates Memory CD8+ T Cell Proliferation. PLOS ONE. 2008 Jun 11;3(6):e2404.
137. Koh CH, Lee S, Kwak M, Kim BS, Chung Y. CD8 T-cell subsets: heterogeneity, functions, and therapeutic potential. Exp Mol Med. 2023 Nov;55(11):2287–99.
138. Nolz JC. Molecular mechanisms of CD8(+) T cell trafficking and localization. Cell Mol Life Sci. 2015 Jul;72(13):2461–73.
139. Khew-Goodall Y, Butcher CM, Litwin MS, Newlands S, Korpelainen EI, Noack LM, et al. Chronic Expression of P-Selectin on Endothelial Cells Stimulated by the T-Cell Cytokine, Interleukin-3. Blood. 1996 Feb 15;87(4):1432–8.
140. Zhang J, Huang S, Zhu Z, Gatt A, Liu J. E-selectin in vascular pathophysiology. Front Immunol. 2024;15:1401399.
141. Kinashi T, Katagiri K. Regulation of immune cell adhesion and migration by regulator of adhesion and cell polarization enriched in lymphoid tissues. Immunology. 2005 Oct;116(2):164–71.
142. Nancy P, Tagliani E, Tay CS, Asp P, Levy DE, Erlebacher A. Chemokine gene silencing in decidual stromal cells limits T cell access to the maternal-fetal interface. Science. 2012 Jun 8;336(6086):1317–21.

143. Chaturvedi V, Ertelt JM, Jiang TT, Kinder JM, Xin L, Owens KJ, et al. CXCR3 blockade protects against Listeria monocytogenes infection-induced fetal wastage. J Clin Invest. 2015 Apr;125(4):1713–25.
144. Tilburgs T, Schonkeren D, Eikmans M, Nagtzaam NM, Datema G, Swings GM, et al. Human decidual tissue contains differentiated CD8+ effector-memory T cells with unique properties. J Immunol. 2010 Oct 1;185(7):4470–7.
145. Li J, Zaslavsky M, Su Y, Guo J, Sikora MJ, van Unen V, et al. KIR+CD8+ T cells suppress pathogenic T cells and are active in autoimmune diseases and COVID-19. Science. 376(6590):eabi9591.
146. Li J, Wang X, Lackner AI, Narasimhan P, Li L, Mallajosyula V, et al. Regulatory KIR+CD8+ T cells are elevated during human pregnancy. Science Translational Medicine. 2025 Aug 6;17(810):eadm7697.
147. Wang S, Sun F, Li M, Qian J, Chen C, Wang M, et al. The appropriate frequency and function of decidual Tim-3+CTLA-4+CD8+ T cells are important in maintaining normal pregnancy. Cell Death Dis. 2019 May 28;10(6):407.
148. XU YY, WANG SC, LIN YK, LI DJ, DU MR. Tim-3 and PD-1 regulate CD8+ T cell function to maintain early pregnancy in mice. J Reprod Dev. 2017 Jun;63(3):289–94.
149. Solano ME, Kowal MK, O'Rourke GE, Horst AK, Modest K, Plösch T, et al. Progesterone and HMOX-1 promote fetal growth by CD8+ T cell modulation. J Clin Invest. 2015 Apr;125(4):1726–38.
150. Milosevic-Stevanovic J, Krstic M, Stefanovic M, Zivadinovic R, Vukomanovic P, Trajkovic-Dinic SP, et al. T lymphocytes in the third trimester decidua in preeclampsia. Hypertension in Pregnancy. 2019 Jan 2;38(1):52–7.
151. Williams PJ, Bulmer JN, Searle RF, Innes BA, Robson SC. Altered decidual leucocyte populations in the placental bed in pre-eclampsia and foetal growth restriction: a comparison with late normal pregnancy. 2009 Jul 1 [cited 2024 Dec 13]; Available from: https://rep.bioscientifica.com/view/journals/rep/138/1/177.xml
152. Nakabayashi Y, Nakashima A, Yoshino O, Shima T, Shiozaki A, Adachi T, et al. Impairment of the accumulation of decidual T cells, NK cells, and monocytes, and the poor vascular remodeling of spiral arteries, were observed in oocyte donation cases, regardless of the presence or absence of preeclampsia. Journal of Reproductive Immunology. 2016 Apr 1;114:65–74.
153. Quinn KH, Lacoursiere DY, Cui L, Bui J, Parast MM. The unique pathophysiology of early-onset severe preeclampsia: role of decidual T regulatory cells. Journal of Reproductive Immunology. 2011 Sep 1;91(1):76–82.
154. Johnsen GM, Størvold GL, Alnaes-Katjavivi PH, Roald B, Golic M, Dechend R, et al. Lymphocyte characterization of decidua basalis spiral arteries with acute atherosis in preeclamptic and normotensive pregnancies. Journal of Reproductive Immunology. 2019 Apr 1;132:42–8.
155. Wilczyński JR, Tchórzewski H, Banasik M, Głowacka E, Wieczorek A, Lewkowicz P, et al. Lymphocyte subset distribution and cytokine secretion in third trimester decidua in normal pregnancy and preeclampsia. European Journal of Obstetrics and Gynecology and Reproductive Biology. 2003 Jul 1;109(1):8–15.

156. Morita K, Tsuda S, Kobayashi E, Hamana H, Tsuda K, Shima T, et al. Analysis of TCR Repertoire and PD-1 Expression in Decidual and Peripheral CD8+ T Cells Reveals Distinct Immune Mechanisms in Miscarriage and Preeclampsia. Frontiers in Immunology [Internet]. 2020 [cited 2022 Nov 2];11. Available from: https://www.frontiersin.org/articles/10.3389/fimmu.2020.01082
157. Kieffer TEC, Laskewitz A, Scherjon SA, Faas MM, Prins JR. Memory T Cells in Pregnancy. Frontiers in Immunology [Internet]. 2019 [cited 2023 May 23];10. Available from: https://www.frontiersin.org/articles/10.3389/fimmu.2019.00625
158. Soljic V, Barbaric M, Vukoja M, Curlin M, Vlaho MO, Obrdalj EC, et al. Decreased Expression of Cytotoxic Proteins in Decidual CD8+ T Cells in Preeclampsia. Biology. 2021 Oct 13;10(10):1037.
159. Luo F, Liu F, Guo Y, Xu W, Li Y, Yi J, et al. Single-cell profiling reveals immune disturbances landscape and HLA-F-mediated immune tolerance at the maternal-fetal interface in preeclampsia. Front Immunol. 2023 Oct 3;14:1234577.
160. Fu M, Zhang X, Liu C, Lyu J, Liu X, Zhong S, et al. Phenotypic and functional alteration of CD45+ immune cells in the decidua of preeclampsia patients analyzed by mass cytometry (CyTOF). Front Immunol. 2023 Jan 6;13:1047986.
161. Ferrara N, Gerber HP, LeCouter J. The biology of VEGF and its receptors. Nat Med. 2003 Jun;9(6):669–76.
162. Facciabene A, Peng X, Hagemann IS, Balint K, Barchetti A, Wang LP, et al. Tumour hypoxia promotes tolerance and angiogenesis via CCL28 and Treg cells. Nature. 2011 Jul;475(7355):226–30.
163. Woidacki K, Meyer N, Schumacher A, Goldschmidt A, Maurer M, Zenclussen AC. Transfer of regulatory T cells into abortion-prone mice promotes the expansion of uterine mast cells and normalizes early pregnancy angiogenesis. Sci Rep. 2015 Sep 10;5(1):13938.
164. Deliyanti D, Figgett WA, Gebhardt T, Trapani JA, Mackay F, Wilkinson-Berka JL. CD8+ T Cells Promote Pathological Angiogenesis in Ocular Neovascular Disease. Arteriosclerosis, Thrombosis, and Vascular Biology. 2023 Apr;43(4):522–36.
165. St-Germain LE, Castellana B, Baltayeva J, Beristain AG. Maternal Obesity and the Uterine Immune Cell Landscape: The Shaping Role of Inflammation. Int J Mol Sci. 2020 May 27;21(11):3776.
166. Perdu S, Castellana B, Kim Y, Chan K, DeLuca L, Beristain AG. Maternal obesity drives functional alterations in uterine NK cells. JCI Insight. 2016 Jul 21;1(11):e85560.
167. Baltayeva J, Konwar C, Castellana B, Mara DL, Christians JK, Beristain AG. Obesogenic diet exposure alters uterine natural killer cell biology and impairs vasculature remodeling in mice†. Biol Reprod. 2020 Feb 12;102(1):63–75.
168. Challier JC, Basu S, Bintein T, Minium J, Hotmire K, Catalano PM, et al. Obesity in pregnancy stimulates macrophage accumulation and inflammation in the placenta. Placenta. 2008 Mar;29(3):274–81.
169. Sureshchandra S, Doratt BM, True H, Mendoza N, Rincon M, Marshall NE, et al. Multimodal profiling of term human decidua demonstrates immune adaptations with pregravid obesity. Cell Reports [Internet]. 2023 Jul 25 [cited 2025 Sep 29];42(7). Available from: https://www.cell.com/cell-reports/abstract/S2211-1247(23)00780-5

170. Sudjai D. Association of pre-pregnancy body mass index with early- and late-onset severe preeclampsia. Eur J Obstet Gynecol Reprod Biol X. 2023 Aug 2;19:100223.
171. Mao J, Sun H, Shen Q, Zou C, Yang Y, Du Q. Impact of pre-pregnancy body mass index on preeclampsia. Front Med (Lausanne). 2025;12:1529966.
172. Harris PA, Taylor R, Thielke R, Payne J, Gonzalez N, Conde JG. Research electronic data capture (REDCap)—A metadata-driven methodology and workflow process for providing translational research informatics support. Journal of Biomedical Informatics. 2009 Apr 1;42(2):377–81.
173. Harris PA, Taylor R, Minor BL, Elliott V, Fernandez M, O'Neal L, et al. The REDCap consortium: Building an international community of software platform partners. Journal of Biomedical Informatics. 2019 Jul 1;95:103208.
174. Arenas-Hernandez M, Sanchez-Rodriguez EN, Mial TN, Robertson SA, Gomez-Lopez N. Isolation of Leukocytes from the Murine Tissues at the Maternal-Fetal Interface. J Vis Exp. 2015 May 21;(99):e52866.
175. Schneider CA, Rasband WS, Eliceiri KW. NIH Image to ImageJ: 25 years of Image Analysis. Nat Methods. 2012 Jul;9(7):671–5.
176. Bankhead P, Loughrey MB, Fernández JA, Dombrowski Y, McArt DG, Dunne PD, et al. QuPath: Open source software for digital pathology image analysis. Sci Rep. 2017 Dec 4;7(1):16878.
177. Berruien NNA, Murray JF, Smith CL. Pregnancy influences the selection of appropriate reference genes in mouse tissue: Determination of appropriate reference genes for quantitative reverse transcription PCR studies in tissues from the female mouse reproductive axis. Gene. 2021 Oct 30;801:145855.
178. Cleal JK, Day P, Hanson MA, Lewis RM. Measurement of Housekeeping Genes in Human Placenta. Placenta. 2009 Nov 1;30(11):1002–3.
179. Kaipe H, Raffetseder J, Ernerudh J, Solders M, Tiblad E. MAIT Cells at the Fetal-Maternal Interface During Pregnancy. Front Immunol [Internet]. 2020 Aug 19 [cited 2025 Oct 18];11. Available from: https://www.frontiersin.org/journals/immunology/articles/10.3389/fimmu.2020.01788/full
180. Köninger A, Enekwe A, Mach P, Andrikos D, Schmidt B, Frank M, et al. Afamin: an early predictor of preeclampsia. Arch Gynecol Obstet. 2018;298(5):1009–16.
181. Reyes L, Golos TG. Hofbauer Cells: Their Role in Healthy and Complicated Pregnancy. Front Immunol. 2018;9:2628.
182. Toothaker JM, Olaloye O, McCourt BT, McCourt CC, Silva TN, Case RM, et al. Immune landscape of human placental villi using single-cell analysis. Development. 2022 Apr 15;149(8):dev200013.
183. Poorolajal J, Jenabi E. The association between body mass index and preeclampsia: a meta-analysis. J Matern Fetal Neonatal Med. 2016 Nov;29(22):3670–6.
184. Vieira MC, Poston L, Fyfe E, Gillett A, Kenny LC, Roberts CT, et al. Clinical and biochemical factors associated with preeclampsia in women with obesity. Obesity. 2017;25(2):460–7.
185. Kim HJ, Wang X, Radfar S, Sproule TJ, Roopenian DC, Cantor H. CD8+ T regulatory cells express the Ly49 Class I MHC receptor and are defective in autoimmune prone B6-Yaa mice. Proc Natl Acad Sci U S A. 2011 Feb 1;108(5):2010–5.

186. Rahim MM, Tu M, Mahmoud A, Wight A, Abou-Samra E, Lima P, et al. Ly49 Receptors: Innate and Adaptive Immune Paradigms. Frontiers in Immunology [Internet]. 2014 [cited 2022 Dec 2];5. Available from: https://www.frontiersin.org/articles/10.3389/fimmu.2014.00145
187. Yokosuka T, Takamatsu M, Kobayashi-Imanishi W, Hashimoto-Tane A, Azuma M, Saito T. Programmed cell death 1 forms negative costimulatory microclusters that directly inhibit T cell receptor signaling by recruiting phosphatase SHP2. J Exp Med. 2012 May 28;209(6):1201–17.
188. Vieyra-Lobato MR, Vela-Ojeda J, Montiel-Cervantes L, López-Santiago R, Moreno-Lafont MC. Description of CD8+ Regulatory T Lymphocytes and Their Specific Intervention in Graft-versus-Host and Infectious Diseases, Autoimmunity, and Cancer. J Immunol Res. 2018;2018:3758713.
189. Noble A, Mehta H, Lovell A, Papaioannou E, Fairbanks L. IL-12 and IL-4 activate a CD39-dependent intrinsic peripheral tolerance mechanism in CD8(+) T cells. Eur J Immunol. 2016 Jun;46(6):1438–48.
190. Prasad J, Van Steenwinckel J, Gunn AJ, Bennet L, Korzeniewski SJ, Gressens P, et al. Chronic Inflammation Offers Hints About Viable Therapeutic Targets for Preeclampsia and Potentially Related Offspring Sequelae. International Journal of Molecular Sciences. 2024 Jan;25(23):12999.
191. Michalczyk M, Celewicz A, Celewicz M, Woźniakowska-Gondek P, Rzepka R. The Role of Inflammation in the Pathogenesis of Preeclampsia. Mediators Inflamm. 2020 Oct 5;2020:3864941.
192. Harmon AC, Cornelius DC, Amaral LM, Faulkner JL, Cunningham MW, Wallace K, et al. The role of inflammation in the pathology of preeclampsia. Clin Sci (Lond). 2016 Mar;130(6):409–19.
193. Semenza GL. HIF-1 and mechanisms of hypoxia sensing. Current Opinion in Cell Biology. 2001 Apr 1;13(2):167–71.
194. Dunn LL, Kong SMY, Tumanov S, Chen W, Cantley J, Ayer A, et al. Hmox1 (Heme Oxygenase-1) Protects Against Ischemia-Mediated Injury via Stabilization of HIF-1α (Hypoxia-Inducible Factor-1α). Arterioscler Thromb Vasc Biol. 2021 Jan;41(1):317–30.
195. Hausvater A, Giannone T, Sandoval YHG, Doonan RJ, Antonopoulos CN, Matsoukis IL, et al. The association between preeclampsia and arterial stiffness. Journal of Hypertension. 2012 Jan;30(1):17.
196. Castleman JS, Shantsila A, Brown RA, Shantsila E, Lip GYH. Altered cardiac and vascular stiffness in pregnancy after a hypertensive pregnancy. J Hum Hypertens. 2023 Mar;37(3):189–96.
197. Salmon H, Franciszkiewicz K, Damotte D, Dieu-Nosjean MC, Validire P, Trautmann A, et al. Matrix architecture defines the preferential localization and migration of T cells into the stroma of human lung tumors. J Clin Invest. 2012 Mar 1;122(3):899–910.
198. Gangur V, Estelle F, Simons R, Hayglass KT. Human IP-10 selectively promotes dominance of polyclonally activated and environmental antigen-driven IFN-γ over IL-4 responses. The FASEB Journal. 1998;12(9):705–13.

199. Dufour JH, Dziejman M, Liu MT, Leung JH, Lane TE, Luster AD. IFN-gamma-inducible protein 10 (IP-10; CXCL10)-deficient mice reveal a role for IP-10 in effector T cell generation and trafficking. J Immunol. 2002 Apr 1;168(7):3195–204.
200. Gray-Owen SD, Blumberg RS. CEACAM1: contact-dependent control of immunity. Nat Rev Immunol. 2006 Jun;6(6):433–46.
201. Yu S, Ren X, Meng F, Guo X, Tao J, Zhang W, et al. TIM3/CEACAM1 pathway involves in myeloid-derived suppressor cells induced CD8+ T cells exhaustion and bone marrow inflammatory microenvironment in myelodysplastic syndrome. Immunology. 2023;168(2):273–89.
202. Mach P, Andrikos D, Schmidt B, Gellhaus A, Rusch P, Birdir C, et al. Evaluation of carcinoembryonic antigen-related cell adhesion molecule 1 blood serum levels in women at high risk for preeclampsia. American Journal of Reproductive Immunology. 2021;85(5):e13375.
203. Rieger L, Segerer S, Bernar T, Kapp M, Majic M, Morr AK, et al. Specific subsets of immune cells in human decidua differ between normal pregnancy and preeclampsia - a prospective observational study. Reproductive Biology and Endocrinology. 2009 Nov 23;7(1):132.
204. Kieffer TEC, Laskewitz A, Vledder A, Scherjon SA, Faas MM, Prins JR. Decidual memory T-cell subsets and memory T-cell stimulatory cytokines in early- and late-onset preeclampsia. Am J Reprod Immunol. 2020 Oct;84(4):e13293.
205. Wang SC, Li YH, Piao HL, Hong XW, Zhang D, Xu YY, et al. PD-1 and Tim-3 pathways are associated with regulatory CD8+ T-cell function in decidua and maintenance of normal pregnancy. Cell Death Dis. 2015 May;6(5):e1738.
206. Meggyes M, Miko E, Lajko A, Csiszar B, Sandor B, Matrai P, et al. Involvement of the PD-1/PD-L1 Co-Inhibitory Pathway in the Pathogenesis of the Inflammatory Stage of Early-Onset Preeclampsia. Int J Mol Sci. 2019 Jan 29;20(3):583.
207. Vinay DS, Kwon BS. CD11c+CD8+ T cells: two-faced adaptive immune regulators. Cell Immunol. 2010;264(1):18–22.
208. Chang RQ, Zhou WJ, Li DJ, Li MQ. Innate Lymphoid Cells at the Maternal-Fetal Interface in Human Pregnancy. Int J Biol Sci. 2020;16(6):957–69.
209. Zhang M, Wang J, Jia L, Huang J, He C, Hu F, et al. Transmembrane TNF-α promotes activation-induced cell death by forward and reverse signaling. Oncotarget. 2017 Sep 8;8(38):63799–812.
210. Hotamisligil GS. Inflammation and metabolic disorders. Nature. 2006 Dec;444(7121):860–7.
211. Azizieh FY, Raghupathy RG. Tumor Necrosis Factor-α and Pregnancy Complications: A Prospective Study. Med Princ Pract. 2015 Feb;24(2):165–70.
212. Huang LY, Chiu CJ, Hsing CH, Hsu YH. Interferon Family Cytokines in Obesity and Insulin Sensitivity. Cells. 2022 Dec 14;11(24):4041.
213. Mueller SN, Mackay LK. Tissue-resident memory T cells: local specialists in immune defence. Nat Rev Immunol. 2016 Feb;16(2):79–89.
214. Surh CD, Sprent J. Homeostasis of naive and memory T cells. Immunity. 2008 Dec 19;29(6):848–62.

215. Saito S, Shiozaki A, Nakashima A, Sakai M, Sasaki Y. The role of the immune system in preeclampsia. Mol Aspects Med. 2007 Apr;28(2):192–209.
216. Kiazyk SAK, Fowke KR. Loss of CD127 expression links immune activation and CD4(+) T cell loss in HIV infection. Trends Microbiol. 2008 Dec;16(12):567–73.
217. Zhao Y, Wei K, Chi H, Xia Z, Li X. IL-7: A promising adjuvant ensuring effective T cell responses and memory in combination with cancer vaccines? Front Immunol. 2022;13:1022808.
218. Kaur N, Lu B, Monroe RK, Ward SM, Halvorsen SW. Inducers of oxidative stress block ciliary neurotrophic factor activation of Jak/STAT signaling in neurons. J Neurochem. 2005 Mar;92(6):1521–30.
219. Wen X, Zhang B, Wu B, Xiao H, Li Z, Li R, et al. Signaling pathways in obesity: mechanisms and therapeutic interventions. Sig Transduct Target Ther. 2022 Aug 28;7(1):298.
220. Jarjour NN, Wanhainen KM, Peng C, Gavil NV, Maurice NJ, Borges da Silva H, et al. Responsiveness to interleukin-15 therapy is shared between tissue-resident and circulating memory CD8+ T cell subsets. Proc Natl Acad Sci U S A. 2022 Oct 25;119(43):e2209021119.
221. Doedens AL, Rubinstein MP, Gross ET, Best JA, Craig DH, Baker MK, et al. Molecular Programming of Tumor-Infiltrating CD8+ T Cells and IL15 Resistance. Cancer Immunol Res. 2016 Sep 2;4(9):799–811.
222. Pijnenborg R, Anthony J, Davey DA, Rees A, Tiltman A, Vercruysse L, et al. Placental bed spiral arteries in the hypertensive disorders of pregnancy. Br J Obstet Gynaecol. 1991 Jul;98(7):648–55.
223. Maynard SE, Min JY, Merchan J, Lim KH, Li J, Mondal S, et al. Excess placental soluble fms-like tyrosine kinase 1 (sFlt1) may contribute to endothelial dysfunction, hypertension, and proteinuria in preeclampsia. J Clin Invest. 2003 Mar 1;111(5):649–58.
224. Gonçalves-Rizzi VH, Nascimento RA, Possomato-Vieira JS, Dias-Junior CA. Sodium Nitrite Prevents both Reductions in Circulating Nitric Oxide and Hypertension in 7-Day Lead-Treated Rats. Basic Clin Pharmacol Toxicol. 2016 Mar;118(3):225–30.
225. Ahmad A, Dempsey SK, Daneva Z, Azam M, Li N, Li PL, et al. Role of Nitric Oxide in the Cardiovascular and Renal Systems. Int J Mol Sci. 2018 Sep 3;19(9):2605.
226. Lee J, Cho H, Kim J, Lim J, Kang Y, Kim WJ. Breaking barriers: Nitric oxide-releasing nanocomplexes for collagen degradation and enhanced αPD-L1 immunotherapy in deep tumor. J Control Release. 2025 May 10;381:113576.
227. Fondjo LA, Awuah EO, Sakyi SA, Senu E, Detoh E. Association between endothelial nitric oxide synthase (eNOS) gene variants and nitric oxide production in preeclampsia: a case–control study in Ghana. Sci Rep. 2023 Sep 7;13(1):14740.
228. Jiang R, Teng Y, Huang Y, Gu J, Ma L, Li M, et al. Preeclampsia serum-induced collagen I expression and intracellular calcium levels in arterial smooth muscle cells are mediated by the PLC-γ1 pathway. Exp Mol Med. 2014 Sep;46(9):e115–e115.
229. Lyall F, Robson SC, Bulmer JN. Spiral Artery Remodeling and Trophoblast Invasion in Preeclampsia and Fetal Growth Restriction. Hypertension. 2013 Dec;62(6):1046–54.

230. Fernandes NRJ, Reilly NS, Schrock DC, Hocking DC, Oakes PW, Fowell DJ. CD4+ T Cell Interstitial Migration Controlled by Fibronectin in the Inflamed Skin. Front Immunol. 2020 Jul 24;11:1501.
231. Spiecker M, Peng HB, Liao JK. Inhibition of endothelial vascular cell adhesion molecule-1 expression by nitric oxide involves the induction and nuclear translocation of IkappaBalpha. J Biol Chem. 1997 Dec 5;272(49):30969–74.
232. Seligman SP, Buyon JP, Clancy RM, Young BK, Abramson SB. The role of nitric oxide in the pathogenesis of preeclampsia. Am J Obstet Gynecol. 1994 Oct;171(4):944–8.
233. Bošanská L, Michalský D, Lacinová Z, Dostálová I, Bártlová M, Haluzíková D, et al. The influence of obesity and different fat depots on adipose tissue gene expression and protein levels of cell adhesion molecules. Physiol Res. 2010;59(1):79–88.
234. Haller H, Ziegler EM, Homuth V, Drab M, Eichhorn J, Nagy Z, et al. Endothelial adhesion molecules and leukocyte integrins in preeclamptic patients. Hypertension. 1997 Jan;29(1 Pt 2):291–6.
235. Kallikourdis M, Andersen KG, Welch KA, Betz AG. Alloantigen-enhanced accumulation of CCR5+ “effector” regulatory T cells in the gravid uterus. Proc Natl Acad Sci U S A. 2007 Jan 9;104(2):594–9.
236. Zhou W, Chen Y, Zheng Y, Bai Y, Yin J, Wu XX, et al. Characterizing immune variation and diagnostic indicators of preeclampsia by single-cell RNA sequencing and machine learning. Commun Biol. 2024 Jan 5;7(1):1–16.
237. Liu L, Callahan MK, Huang D, Ransohoff RM. Chemokine Receptor CXCR3: An Unexpected Enigma. In: Current Topics in Developmental Biology [Internet]. Academic Press; 2005 [cited 2025 Jul 7]. p. 149–81. Available from: https://www.sciencedirect.com/science/article/pii/S0070215305680064
238. Rosenkilde MM, Schwartz TW. The chemokine system – a major regulator of angiogenesis in health and disease. APMIS. 2004;112(7–8):481–95.
239. Lockwood CJ, Huang SJ, Chen CP, Huang Y, Xu J, Faramarzi S, et al. Decidual Cell Regulation of Natural Killer Cell–Recruiting Chemokines. Am J Pathol. 2013 Sep;183(3):841–56.
240. Gotsch F, Romero R, Friel L, Kusanovic JP, Espinoza J, Erez O, et al. CXCL10/IP-10: a missing link between inflammation and anti-angiogenesis in preeclampsia? J Matern Fetal Neonatal Med. 2007 Nov;20(11):777–92.
241. Hirsch K, Nolley S, Ralph DD, Zheng Y, Altemeier WA, Rhodes CJ, et al. Circulating Markers of Inflammation and Angiogenesis and Clinical Outcomes Across Subtypes of Pulmonary Arterial Hypertension. J Heart Lung Transplant. 2023 Feb;42(2):173–82.
242. Bodnar RJ, Yates CC, Wells A. IP-10 Blocks Vascular Endothelial Growth Factor–Induced Endothelial Cell Motility and Tube Formation via Inhibition of Calpain. Circ Res. 2006 Mar 17;98(5):10.1161/01.RES.0000209968.66606.10.
243. Wang Z, Ou Q, Liu Y, Liu Y, Zhu Q, Feng J, et al. Adipocyte-derived CXCL10 in obesity promotes the migration and invasion of ovarian cancer cells. Journal of Ovarian Research. 2024 Dec 19;17(1):245.
244. Montani JP, Carroll JF, Dwyer TM, Antic V, Yang Z, Dulloo AG. Ectopic fat storage in heart, blood vessels and kidneys in the pathogenesis of cardiovascular diseases. Int J Obes Relat Metab Disord. 2004 Dec;28 Suppl 4:S58-65.

245. Zhang X, Shen J, Man K, Chu ESH, Yau TO, Sung JCY, et al. Corrigendum to “CXCL10 plays a key role as an inflammatory mediator and a non-invasive biomarker of non-alcoholic steatohepatitis” [J Hepatol (2014) 61:1365-75]. J Hepatol. 2025 Sep;83(3):812–3.
246. He W, Wang H, Yang G, Zhu L, Liu X. The Role of Chemokines in Obesity and Exercise-Induced Weight Loss. Biomolecules. 2024 Sep 4;14(9):1121.
247. Sowers JR, Habibi J, Jia G, Bostick B, Manrique-Acevedo C, Lastra G, et al. Endothelial sodium channel activation promotes cardiac stiffness and diastolic dysfunction in Western diet fed female mice. Metabolism. 2020 Aug;109:154223.
248. Cote AT, Phillips AA, Harris KC, Sandor GGS, Panagiotopoulos C, Devlin AM. Obesity and Arterial Stiffness in Children. Arteriosclerosis, Thrombosis, and Vascular Biology. 2015 Apr;35(4):1038–44.
249. Koenen M, Hill MA, Cohen P, Sowers JR. Obesity, Adipose Tissue and Vascular Dysfunction. Circ Res. 2021 Apr 2;128(7):951–68.
250. Padilla J, Vieira-Potter VJ, Jia G, Sowers JR. Role of Perivascular Adipose Tissue on Vascular Reactive Oxygen Species in Type 2 Diabetes: A Give-and-Take Relationship. Diabetes. 2015 Jun;64(6):1904–6.
251. Wu P, Haththotuwa R, Kwok CS, Babu A, Kotronias RA, Rushton C, et al. Preeclampsia and Future Cardiovascular Health: A Systematic Review and Meta-Analysis. Circ Cardiovasc Qual Outcomes. 2017 Feb;10(2):e003497.
252. Parker VJ, Solano ME, Arck PC, Douglas AJ. Diet-induced obesity may affect the uterine immune environment in early–mid pregnancy, reducing NK-cell activity and potentially compromising uterine vascularization. Int J Obes. 2014 Jun;38(6):766–74.
253. Valentine Y, Nikolajczyk BS. T cells in obesity-associated inflammation: The devil is in the details. Immunol Rev. 2024 Jul;324(1):25–41.
254. Ahmed A, Singh J, Khan Y, Seshan SV, Girardi G. A New Mouse Model to Explore Therapies for Preeclampsia. PLoS One. 2010 Oct 27;5(10):e13663.
255. Mirabelli M, Misiti R, Sicilia L, Brunetti FS, Chiefari E, Brunetti A, et al. Hypoxia in Human Obesity: New Insights from Inflammation towards Insulin Resistance—A Narrative Review. Int J Mol Sci. 2024 Sep 11;25(18):9802.
256. Wang H, Flach H, Onizawa M, Wei L, McManus MT, Weiss A. Negative regulation of Hif1a expression and TH17 differentiation by the hypoxia-regulated microRNA miR-210. Nat Immunol. 2014 Apr;15(4):393–401.
257. Bruning U, Cerone L, Neufeld Z, Fitzpatrick SF, Cheong A, Scholz CC, et al. MicroRNA-155 Promotes Resolution of Hypoxia-Inducible Factor 1α Activity during Prolonged Hypoxia ▿ . Mol Cell Biol. 2011 Oct;31(19):4087–96.
258. Ginouvès A, Ilc K, Macías N, Pouysségur J, Berra E. PHDs overactivation during chronic hypoxia “desensitizes” HIFalpha and protects cells from necrosis. Proc Natl Acad Sci U S A. 2008 Mar 25;105(12):4745–50.
259. Krock BL, Skuli N, Simon MC. Hypoxia-induced angiogenesis: good and evil. Genes Cancer. 2011 Dec;2(12):1117–33.
260. Liao D, Johnson RS. Hypoxia: A key regulator of angiogenesis in cancer. Cancer Metastasis Rev. 2007 Jun 1;26(2):281–90.

261. Yang M, Mu Y, Yu X, Gao D, Zhang W, Li Y, et al. Survival strategies: How tumor hypoxia microenvironment orchestrates angiogenesis. Biomedicine & Pharmacotherapy. 2024 Jul 1;176:116783.
262. Sehgel NL, Vatner SF, Meininger GA. “Smooth Muscle Cell Stiffness Syndrome”—Revisiting the Structural Basis of Arterial Stiffness. Front Physiol. 2015 Nov 18;6:335.
263. Kim B, Zhao W, Tang SY, Levin MG, Ibrahim A, Yang Y, et al. Endothelial lipid droplets suppress eNOS to link high fat consumption to blood pressure elevation. J Clin Invest. 133(24):e173160.
264. Vanalderwiert L, Henry A, Wahart A, Carvajal Berrio DA, Brauchle EM, El Kaakour L, et al. Metabolic syndrome-associated murine aortic wall stiffening is associated with premature elastic fibers aging. Am J Physiol Cell Physiol. 2024 Sep 1;327(3):C698–715.
265. Tomasek JJ, Haaksma CJ, Schwartz RJ, Vuong DT, Zhang SX, Ash JD, et al. Deletion of smooth muscle alpha-actin alters blood-retina barrier permeability and retinal function. Invest Ophthalmol Vis Sci. 2006 Jun;47(6):2693–700.
266. Tighe RM, Liang J, Liu N, Jung Y, Jiang D, Gunn MD, et al. Recruited exudative macrophages selectively produce CXCL10 after noninfectious lung injury. Am J Respir Cell Mol Biol. 2011 Oct;45(4):781–8.
267. House IG, Savas P, Lai J, Chen AXY, Oliver AJ, Teo ZL, et al. Macrophage-Derived CXCL9 and CXCL10 Are Required for Antitumor Immune Responses Following Immune Checkpoint Blockade. Clin Cancer Res. 2020 Jan 15;26(2):487–504.

9. DECLARATION OF INDEPENDENT WORK

I hereby declare that I have written this thesis without unauthorized aid and without using sources other than those listed.
Data and concepts that have been taken directly or indirectly from other sources have been marked as such, citing the source. In particular, I have not used paid agency or advisory services (commercial advisers for doctoral degrees or others).
This thesis has so far never been submitted to another examination authority in Germany or abroad, neither in this form nor in a similar form.

Regensburg,

Place, date handwritten signature of the doctoral candidate